Effects of phylogeny, physiology, and function on bone microstructure in extant endothermic vertebrates

Maria de Boef
Department of Biology
McGill University, Montreal
July 2009

A thesis submitted to McGill University in partial fulfillment of the requirements of the degree of Doctor of Philosophy

For Hendrik and Anneke de Boef,
for nurturing and inspiring my love of living things.

Whether allowing me to observe all stages of life and death on the farm, giving me free reign to terrorize the frogs and snakes in our backyard or welcoming a mummified cat into your home, you never discouraged and always supported my interests.

This could not have been done without your support and confidence in me.

Thank you!

Table of Contents

Contribution of Authors

This thesis includes three manuscripts that have been or will be submitted to refereed journals for publication and one paper that has been published. For all papers I am listed as the first author, having been solely responsible for the collection and analysis of data and preparation of the manuscript. Also for all papers, Hans Larsson is listed as the second author, in recognition of his support and assistance with the development of each paper as my thesis advisor.

In addition, Andrew Biewener is listed as co-author for Chapter 4. This is in recognition of this support and assistance with the development of this chapter and for his assistance with several of the surgeries and data collection.

Abstract

A strong relationship between bone macrostructural morphology and bone mechanical function has been well documented and is an essential component of many vertebrate biomechanical studies. However, a vastly richer data set could be had if the relationship between bone microstructure and bone function were as well understood. This thesis enumerates the bone microstructure-function relationship in a statistically consistent manor in extant endotherms.

Phylogeny, physiology and function have been shown to independently contribute to bone microstructure morphology. However, rarely have two or more of these factors been examined in combination. In this work the author used various statistical and experimental techniques to quantify the contribution of each of these factors to bone microstructure.

This work is organized into four parts: First, a review of methods used to quantify bone microstructure is given and a new method for quantifying vascular orientation proposed. This method allows the researcher to observe vascular orientation as an unbiased continuous measure and therefore complete more extensive statistical testing. Second, an analysis of the use of skeletochronology for aging three species of extant carnivores is given. This technique, although rarely used in extant endotherms, is commonly used for aging specimens from palaeontological findings. Upon discovering a significant

discordance between organismal age and skeletochronology in the carnivorans studied here, I discuss the validity of its use in palaeontology. Third, using a sample of seven carnivoran species, the impact of phylogeny, function and physiology on bone microstructure was tested using a variance partitioning method. It was found that phylogeny has a large and significant impact on bone microstructural characteristics but only in conjunction with functional and physiological variables. When considering the effects of the three “pure” factors I found that physiological factors are the major drivers of bone microstructure. To further explore these findings, the final chapter presents an experimental study on the effects of biomechanical function and repeated loading on the humerus and tibiotarsus in Helmeted GuineaFowl. It was found that the type of strain and the repetition of strain from exercise both significantly impact bone microstructure but the relationship between tensile, compressive and shear strains to microstructure is complex with no obvious correlation.

Résumé

Il existe une forte relation entre la morphologie de la structure macroscopique des os et leurs caractéristiques fonctionnelles au niveau mécanique. Cette relation est bien documentée et est un aspect essentiel de plusieurs études sur la biomécanique des vertébrés. Cependant, un ensemble de données beaucoup plus étoffé serait disponible si la relation entre la morphologie de la microstructure des os et leur fonction était mieux comprise. La présente thèse comporte une énumération des relations entre la microstructure des os et leurs caractéristiques fonctionnelles chez certaines espèces actuelles d'endothermes, en suivant une approche statistique cohérente.

Il a été démontré que la phylogénie, la fonction et la physiologie contribuent séparément à la morphologie de la microstructure des os. Cependant, les effets combinés de deux ou plusieurs de ces facteurs ont rarement été examinés. Dans la présente étude, l'auteur a utilisé plusieurs méthodes statistiques et expérimentales afin de quantifier l'impact respectif de chacun de ces facteurs sur la microstructure des os.

Cette thèse est organisée en quatre parties. D'abord, une revue des méthodes utilisées pour quantifier la microstructure des os est présentée et une nouvelle méthode pour quantifier l'orientation vasculaire est proposée. Cette nouvelle méthode permet d'observer l'orientation vasculaire d'une

manière continue et non-biaisée, et permet donc une analyse statistique plus approfondie. Ensuite, l'utilisation de la squelettochronologie pour la détermination de l'âge de trois espèces de carnivores est analysée. Cette technique, bien que rarement utilisée pour déterminer l'âge chez les endothermes actuels, est communément employée pour les espèces paléontologiques. À la suite de la découverte d'une discordance significative entre l'âge des organismes et la squelettochronologie chez les carnivores étudiés ici, la validité de cette technique en paléontologie est discutée. En troisième partie, à partir d'un échantillon de sept espèces de carnivores et au moyen d'une analyse de partition de variance, l'impact de la phylogénie, de la fonction et de la physiologie sur la microstructure des os a été testé. Il a été découvert que la phylogénie avait un impact important sur la microstructure des os, mais seulement en conjonction avec les variables liées à la fonction et à la physiologie. Lorsque les effets des trois facteurs « purs » étaient considérés, la physiologie était le facteur qui contribuait le plus à la variabilité observée dans la microstructure des os. Afin d'examiner ces résultats plus en détail, le chapitre final présente une expérience investiguant les effets d'une charge répétée et de la fonction biomécanique sur l'humérus et le tibiotarse de la pintade de Numidie (*Numida meleagris*). Le type d'effort et la répétition de l'effort imposé par l'exercice avaient tous les deux un impact significatif sur la microstructure des os, mais les relations entre les forces de tension, de

compression et de cisaillement et la microstructure des os sont complexes et sans corrélation évidente.

Acknowledgements

Academic Support and Discussions Many thanks go to Hans Larsson for discussions, inspiration and leadership during this process. I could not have hoped for a more helpful, understanding and intellectually stimulating supervisor. I additionally benefitted from the guidance of my supervisory committee, Donald Kramer and Murray Humphries and would like to thank them both for their frank appraisals and useful suggestions. I would like to thank my "adopted supervisor", Andrew Biewener, for his guidance and teaching as I completed the fourth chapter. I would like to thank Lincoln Miara for help in writing the many Matlab scripts that were used in data collection and analysis. My graduate student and post doc. colleagues at both McGill and Harvard were of enormous help both academically and personally throughout this process. Specifically, I would like to acknowledge the support of Allison Arnold-Rife, Angela Berg, Jennifer Carr, Andrew Carroll, Stacey Combes, James Crall, Alex Dececchi, Carolyn Eng, Luke Harrison, Audrey Heppleston, Tim Higham, Erin Maxwell, Trond Sigurdson, Nadia (Stöcker) Fröbisch, Carlos Moreno, Chris Richards, Ivo Ros, Rui Tahara, Sylvie Tissandier, Matthew Vavrek and Edwin Yoo.

Specimen Access I would like to thank Bob McClymont from Alberta Fish & Wildlife Services, Kim Melton and Tom Jung from Yukon Environment and Kim Bennett from the Ontario Ministry of Natural resources for giving me access to their specimens.

Funding Funding for this project was provided by a Fonds de Recherche sur la Nature et les Technology (FQRNT) grant to me, as well as an NSERC Discovery Grant and Canada Research Chair to H. Larsson.

Fascilities and Equipment I would like to thank Andrew Biewener and the Concord Field Station of Harvard University for use of their fascilities and equipment. In particular I'd like to thank Pedro Ramirez for his assistance with the GuineaFowl, A. "Fuzz" Crompton for the use of his microscope and camera, Ken Wilcox for aid in construction of the setup, and Peg Hedstrom and Lisa Litchfield for administrative assistance.

Editorial Help I would like to thank Hans Larsson, Lincoln Miara, Jim Miara, Chris Miara and several anonymous reviewers of chapter 1 for improvements made to this thesis.

Personal Support The process of completing a Ph.D. is an emotional and very personal journey. I'd like to thank the following people who joined me on that journey. First of all, thanks to all of my friends and colleagues who supported me in so many ways. Many of these people have already been named but I'd like to acknowledge the support of Ed Hudson and all the members of the Cambridge Running Club. I thank my parents for supporting me throughout this process and limiting the number of times they asked when it would be complete. It is to them I have dedicated this work. Additional support was provided by Jim and Chris Miara, who have allowed me to enter their family and have supported me in many ways. To my beautiful daughter, Corrina, thank you for allowing me to escape this work physically and mentally when it was necessary, and inspiring me to keep going. My greatest supporter and the one to which I owe the most thanks is my finacé, Lincoln Miara. He supported me as I entered this program and supported me through every step in the process. He has been my motivator, cheerleader, editor, and therapist. This truly could not have been done without his help.

List of Tables

List of Figures

Introduction

This work examines the effects of evolutionary history (phylogeny), biomechanics (function) and growth rate (physiology) on bone microstructural morphology in endothermic vertebrates. In this work I will use the terms function and physiology to refer to locomotor behaviour and energetic respectively. Just as one can learn a great deal about an organism's diet, behavior, evolutionary history and individual life history by observing the macrostructural morphology of its bones, studies have found that bone microstructure varies predictably in response to a similar suite of variables (de Margerie 2002; de Margerie et al. 2004; Cubo et al. 2005; Cubo et al. 2008; Habib and Ruff 2008).

It is not necessarily intuitive that such variability would exist in bone microstructure. The bones in all vertebrates form using the same process and the same few structural elements (Hall 2005). The variety of functional and physiological demands placed on bone that would promote variability are offset by the common evolutionary origin of the tissue. The evolutionary history of bone is long but also well understood. Being a mineralized tissue, bone fossilizes remarkably well and scientists have traced its origin back more than 450 million years ago (Carroll 1988). It is believed that bone did not originate as a protective or structural tissue. Instead, calcium phosphate, the mineral component of bone, evolved to act as a phosphate reserve and an

insulator of electrosensory organs in fish. Once formed however, the protective capabilities of this tissue would have promoted the evolution of a full body exoskeleton. Over time, the exoskeleton would become an internal endoskeleton, giving structural and biomechanical advantages to subsequent species. Today, bone is present in a wide variety of taxa and has a wide variety of specialized physiological and biomechanical characteristics (Hall 2005). As a result, phylogenetic history could plausibly explain some of the variability found in bone microstructure. The most obvious function of bone is as a structural element. Bone provides the framework on which muscles and tendons act to move the body. This ingenious system has allowed organisms to evolve the ability to swim, walk, run, jump, climb, dig, and fly. All of these motions produce different mechanical loads, and bones have evolved the macro- and microstructural properties needed to perform them. While the relationship between bone macrostructural properties and this wide range of biomechanical demands has been well mapped (Currey 2006), the structure-function relationship in bone microstructure is just beginning to be examined.

Another, less obvious but equally important, function of bone is as a physiologically active tissue. Bone acts as a store of calcium and phosphorous in the body and equilibrates the levels of these two minerals in the blood stream. As a result, deposition and resorption rates of bone are highly dependent on the physiological state of the animal. Further, bone

microstructural morphology is closely linked to rates of bone deposition. As a result, bone microstructure can vary over time as a result of differences in physiology between taxa, between individuals or even within an individual.

Undoubtedly, the relationships between phylogeny, function and physiology in an organism can be complex and can result in a concomitantly complex pattern when we examine its bones under the microscope. It is the goal of this thesis to isolate the effects of each of these three factors and determine how they act individually to produce variability in bone microstructure. The thesis also examines the combined effects of these factors.

To undertake such an analysis it was first necessary to create a method by which to quantify one of the major bone microstructure characteristics: the orientation of bone vasculature. Previous studies have focused on qualitative descriptions of bone microstructure or over-simplified measures that cannot be easily incorporated into statistical tests and as a consequence are prone to subjective interpretations. Moreover, they are unable to detect slight differences in vascular orientation. Chapter One includes a description of a new, more rigorous method for examining bone microstructure and instructions for its use.

It was noted that growth marks, visible as part of bone microstructure, are commonly used to age extinct vertebrates and extant ectotherms. The

underlying assumption of such methodology, known as skeletochronology, is that these marks are deposited on an annual basis. This assumption additionally allows researchers to estimate growth rates from intervals between marks. While the annual nature of growth marks has been sufficiently supported for ectothermic species, there has been little research on its validity in endothermic species. Chapter Two tests the applicability of this assumption to endothermic species by comparing the number of growth marks visible in samples of three carnivoran species to their known ages.

The complex relationship between phylogeny, physiology and function and the resulting bone microstructure is difficult to study. In most cases, previous studies examined one or two of these factors. Studies in which all three factors and their interactions are examined are rare. Chapter Three focuses on bone microstructure, quantifying samples of seven carnivoran species. A variance partitioning method is then used to quantify the proportion of the variance in bone microstructure that can be explained by each of the three factors and their interactions. Additionally, as bone microstructure has not been previously described in these seven species, a detailed description of both qualitative and quantitative characteristics is included.

As an animal moves, it places stress on its bones which can cause compressive, tensile or shear strain. Many biomechanical studies have

mapped how and when such strains occur (Biewener et al. 1986; Swartz et al. 1992; Biewener and Dial 1995; Main and Biewener 2004). Other studies generalized these loading patterns and correlated them with bone microstructure characteristics (de Margerie 2002; de Margerie et al. 2005; Skedros et al. 2007; Habib and Ruff 2008). Chapter Four, the final chapter, describes a study in which bone strain is measured and compared directly to bone microstructure in flying and running Helmeted Guinea Fowl (*Numida meleagris)*. This study also examined the effects of repeated loading from daily exercise to determine the plasticity of this morphological characteristic.

In summary, this thesis provides an in depth analysis of the individual and combined effects of phylogeny, function and physiology on the bone microstructure in endotherms. It provides new methods for the quantification of bone microstructure, examines the assumption that bone growth marks are annually deposited, presents the first study in which individual and combined effects of phylogeny, function and physiology are statistically tested and offers the first study in which bone microstructure is mapped directly with measures of bone strain.

Literature Cited

Biewener, A. A., and K. P. Dial. 1995. In Vivo Strain in the Humerus of Pigeons (*Columba livia)* During Flight. Journal of Morphology 225:61-75.

Biewener, A. A., S. M. Swartz, and J. E. A. Bertram. 1986. Bone Modeling During Growth: Dynamic Strain Equilibrium in the Chick Tibiotarsus. Calcified Tissue International 39:390-395.

Carroll, R. L. 1988. Vertebrate paleontology and evolution. W. H. Freeman and Company, New York.

Cubo, J., P. Legendre, A. de Ricqles, L. Montes, E. de Margerie, J. Castanet, and Y. Desdevises. 2008. Phylogenetic, functional, and structural components of variation in bone growth rate of amniotes. Evolution & Development 10:217-227.

Cubo, J., F. Ponton, M. Laurin, E. de Margerie, and J. Castanet. 2005. Phylogenetic Signal in Bone Microstructure of Sauropsids. Systematic Biology 54:562-574.

Currey, J. D. 2006. Bones: Structure and Mechanics. Princeton University Press, Princeton, NJ.

de Margerie, E. 2002. Laminar bone as an adaptation to torsional loads in flapping flight. Journal of Anatomy 201:521-526.

de Margerie, E., J. Robin, D. Verrier, J. Cubo, R. Groscolas, and J. Castanet. 2004. Assessing a relationship between bone microstructure and growth rate: a fluorescent labelling study in the king penguin chick (*Aptenodytes patagonicus*). Journal of Experimental Biology 207:869-879.

de Margerie, E., S. Sanchez, J. Cubo, and J. Castanet. 2005. Torsional Resistance as a Principal Component of the Structural Design of Long Bones: Comparative Multivariate Evidence in Birds. The Anatomical Record Part A 282A:49-66.

Habib, M. B., and C. B. Ruff. 2008. The effects of locomotion on the structural characteristics of avian limb bones. Zoological Journal of the Linnean Society 153:601-624.

Hall, B. K. 2005. Bones and Cartilage: Developmental Skeletal Biology. Academic Press, St. Louis, MO.

Main, R. P., and A. A. Biewener. 2004. Ontogenetic patterns of limb loading, in vivo bone strains and growth in the goat radius. The Journal of Experimental Biology 207:2577-2588.

Skedros, J. G., S. M. Sorenson, and N. H. Jenson. 2007. Are distributions of secondary osteon variants useful for interpreting load history in mammalian bones? Cells Tissues Organs 185:285-307.

Swartz, S. M., M. B. Bennett, and D. R. Carrier. 1992. Wing bone stresses in free flying bats and the evolution of skeletal design for flight. Nature 359.

Literature Review

Current Knowledge and uses of Bone Microstructure

This thesis touches on a wide range of biological disciplines including development, evolution, morphology, biomechanics, ecology, palaeontology and physiology (a term used here to mean energetics). The following review attempts to identify the key pieces of knowledge from each of these fields that are important for the understanding of this work.

Bone Development

The formation of bone is a well understood process. Intermediate bone is formed directly under a membrane. When formed by the replacement of a cartilage precursor, bone is referred to as endochondral. In both cases bone formation occurs when osteoblasts, bone forming cell, deposit a protein matrix called osteoid. Osteoid consists mainly of type I collagen which later becomes mineralized with hydroxyapatite (Currey 2006). This process is the same, with only slight variations, in all species that contain bone (Hall 2005). As this two-phase collagen-crystal matrix is formed vascular canals and osteoblasts may become encorporated into the bone tissue. Osteoblasts that undergo this process change in morphology and function and are known as osteocytes. While all bone is made of these three components - a collagen

hydroxyapatite matrix, vascular canals and osteocytes - there is a great deal of variability in their organization between and within species. This variability is due to differences in density and organization of the vascular canals, osteocytes and collagen fibers (de Ricqlès et al. 1991). Much of the work on bone microstructure in paleontology and zoology focuses on the elongated bones of the appendicular skeleton. In particular, there is much work done on the compact bone that comprises the outer ring of the midshaft, or diaphysis, of these bones. In this thesis I examine vascular canal orientation and osteocyte density in cortical bone as measures of bone microstructure.

Bone microstructural characteristics and growth rates

Collagen fiber orientation has been found to vary predictably with growth rate. Bone that is deposited more quickly has a less organized collagen matrix than bone that is deposited more slowly (Smith 1960; de Ricqlès et al. 1991; Currey 2006). Vascular orientation has also been found to vary depending on growth rate. De Margerie and colleagues (2004) characterized bone vascular orientation in King Penguin chicks that were growing at different rates. Specifically they discovered that bone which was deposited quickly tended to incorporate vascular canals such that they radiated outwards from the medullary (internal) surface toward the periosteal (external) surface. Vascular canals in slower growing bone was oriented parallel to the outer surface of the bone in a laminar arrangement. The results

of this study are supported by reports of changing vascular canal orientation throughout ontogeny with bone that was deposited during the fast, growing early stages of life having different vascular orientation than bone that was deposited after growth had slowed (Castanet et al. 2000; Erickson et al. 2001). The relationship between osteocyte density and growth rate has not been studied but it can be hypothesized that such a relationship may exist. Osteocytes are former osteoblasts which in turn are responsible for bone formation. Increased rates of bone formation indicates increased numbers of osteoblasts and possibly increased numbers of osteocytes within the resulting bone matrix. The rate of bone growth is a product of the animal's physiology as determined by its genome and environment. The impact of an organisms physiology on the bone microstructure that develops is one of the three relationships that is examined in this thesis.

Bone microstructural characteristics and function

It has been well established that bone macroscopic morphology is tightly linked to bone function (Currey 2006). This correlation has been vital in vertebrate paleontological studies, particularly in those attempting to ascertain the biomechanics of an extinct species (Carrano 1998; Rayfield et al. 2001; Hutchinson 2004; Carpenter and Wilson 2008; Hutchinson and Allen 2009). This structure-function relationship is often referred to as Wolff's law after Julius Wolff who first proposed that bone trabeculae are oriented in

order to provide the best structural support for the bone's functional demands. This law is often extended to include microstructural characteristics of bone (Pearson and Lieberman 2004; Ruff et al. 2006). However, the structure-function relationship at this level is somewhat less clear. Two recent studies in bird bone microstructure have found significant differences in vascular orientation between skeletal elements. It has been noted in isolated cases that bones which experience high levels of torsion such as the humerus and ulna tend to have vascular canals that are oriented laminarly while bones that experience higher tensile and compressive stresses tend to have vascular canals that are oriented longitudinally (de Margerie 2002; Habib and Ruff 2008). Neither of these studies measured the bone strain in species they studied but instead correlate bone vascular orientation with their known locomotor behavior and postulate on the type of strain that behavior would produce. An extremely interesting approach to the study of vascular canal orientation and bone function was reported recently by de Margerie and colleagues (2006). This group used an evolutionary algorithm and finite element modeling to develop an *in silico* organization of vascular canals that would best resist mechanical loads. While their model was not consistent with structure-function relationships found in living organisms they did produce realistic bone phenotypes.

Bone microstructural characteristics and phylogeny

While all vertebrate bone is formed from the same basic elements, its structure can vary greatly. It would seem likely that as with most morphological characters, bone microstructure, would be influenced by evolutionary history. However, it seems that phylogeny has very little, if any, influence on bone microstructural characteristics such as vascular canal orientation. Cubo and colleagues found that there is no effect of phylogeny on this trait in sauropsids (2005). This is further supported by work done by Habib and Ruff (2008) who found that in avian species that had recently evolved new locomotor functions such as swimming with their forelimbs, vascular canal orientation was more similar to distantly related species with similar locomotor behavior than to closely related species with different behavior. However, it has also been recently shown that phylogeny can have a significant effect on bone growth rate (Cubo et al. 2008). While growth rate can have a large effect on bone vascular orientation and it is possible that evolutionary history can impact bone microstructure through its impact on physiology, de Buffrénil and colleagues (2008)found that in varanid lizards vascular orientation is independent of both phylogeny and growth rate.

Quantifying bone microstructure

Vascular canals are cylindrical structures that move through three dimensions within a bone (Cooper et al. 2003). However, much of bone microstructural analysis takes place through the use of two-dimensional cross

sections. The characterization of this three-dimensional structure from two-dimensional visualizations can be difficult. Historically vascular canals have been described qualitatively (de Ricqlès et al. 1991). While this method is sufficient for broad-scale comparisons between widely different samples it is difficult to detect small differences in orientation using this method. Also, as with all qualitative measures, this leaves room for subjectivity and irregularity. Methods to quantify vascular orientation have been proposed recently. De Margerie and colleagues (2002) proposed the use of a laminarity index that quantifies the proportion of vascular canals that are oriented laminar to the bone layers. However, this index does not detect differences between vascular canals that are oriented longitudinally or radially. An analysis of this method and a comparison between it and a newly proposed method are presented here in the first chapter.

Osteocyte density is measured as a single value for the whole bone cross section in the vast majority of studies (Mullender et al. 1996; Vashishth et al. 2000; Dai et al. 2004; Skedros 2005; Ma et al. 2008). This method yields only one data point per section which often results in one data point per individual. This is useful when asking questions about differences in osteocyte density between species or between treatment groups. However, some studies in bone microstructure have interest in the patterns of variability within regions of bone within a species. Bone osteocyte densities may be

variable throughout the bone in relation to the dynamic properties of bone biomechanics and growth rates.

To relate osteocyte density with bone strain patterns measures of bone strain must be taken in vivo. This can be done using strain gauges surgically glued to the bone (Biewener 1992). Limb bones used in locomotion experience loading patterns that vary between different surfaces of the bone (medial, lateral, anterior, posterior, etc) and at different points in the stride cycle (Main and Biewener 2004). This allows us to correlate osteocyte density with bone strain. Such correlations can be used to make predictions about the bone strain experienced by extinct species. From this we can make further predictions about the locomotor behaviour of these species.

There are several methods that can be employed to correlate osteocyte density with bone growth rate. The first method uses the assumption at as an animal grows primary bone is deposited on the outer surface of the bone only. This leaves a chronological history of the animals growth much as the rings in a tree trunk do for a tree. In general growth rates decrease as animals age and so a gradient in bone deposition rates can be found moving from quickly deposited bone at the endosteum to slowly deposited bone at the periosteum. However, growth rates are highly dependent on environmental variables such as stress and nutrition. Therefore, unless detailed measures of growth rate are taken throughout an animal's life,

equating osteocyte density with growth rate in this way are rough estimates at best and misleading at worst.

A far superior method of determining bone deposition rate uses fluorescent markers such as tetracycline or calcein . These products can be safely injected into or ingested by most vertebrates. They enter the blood stream and are incorporated into all mineralized tissue including bone and teeth. When bone sections are viewed post-mortem using fluorescence microscopy any bone that was deposited while the marker was in the animals system fluoresces. By giving fluorescent markers of different colour to the animal days or even weeks apart we can measure the volume of bone deposited between doses and thus calculate growth rate . The number of osteocytes between fluorescent markers can also be measured and in this way the relationship between growth rate and osteocyte density can be much more accurately measured. Further, since these markers are safe, easy to administer and work in most animals this method provides standardized comparisons within and between species.

In addition to vascular orientation and osteocyte density, changes in bone deposition patterns that are related to deposition rates can leave marks in the bone lamellae (de Ricqlès et al. 1991). These marks are often associated with life history events such as birth or hatching, weaning, hibernation, reproduction or seasonal changes (Klevezal and Mina 1990; Castanet 2006).

When these marks occur on an annual basis, as they have been found to do in many ectotherms, they can be used to age animals and estimate growth curves (Millar and Zwickel 1972; Erickson and Brochu 1999; Misawa and Matsui 1999; Erickson and Tumanova 2000; Horner et al. 2000; Erickson et al. 2001; Padian et al. 2001; Horner and Padian 2004).

With improvements in microtomography (microCT) the visualization and quantification of bone microstructural properties will be greatly improved. This also gives a nondestructive way to view bone microstructure. Both synchrotron and non synchrotron Xrays can be used, although the results from synchrotron X rays are much more detailed (Weiss et al. 2005; Tafforeau and Smith 2008). The methods for quantifying vasculature and osteocyte distributions using such three dimension views have yet to be developed but may be built on existing methods from two dimension analyses.

Current uses of bone microstructure

Bone microstructure, as a method for examining function, phylogeny or physiology, is often driven by work in the field of palaeontology and anthropology. The fossilization process preserves microstructure in bone remarkably well and gives researchers in these fields additional data on which to hypothesize about the lives of the extinct species (Enlow and Brown 1956, 1957, 1958; Horner et al. 2000; de Ricqlès et al. 2003). Often it is scientists from these same two fields who study the microstructure in extant species,

usually in order to apply what they learn back to the fossil record (Lieberman 1993; Starck and Chinsamy 2002; Habib and Ruff 2008). In fact, rarely is bone microstructural characteristics observed in extant species for specifically zoological purposes. This does not mean, however, that information gleaned from such studies is not useful for zoology. In fact, the use of skeletal growth marks to age and study growth rates, is a method that has been useful in both paleontological and zoological studies (Morris 1972; Horner et al. 1999; Misawa and Matsui 1999; Barker et al. 2003; Erickson et al. 2004; Steyer et al. 2004).

Conclusions

It is obvious from the many studies on the topic, that bone microstructure can give a wealth of information on a wide variety of biologically significant factors. The influence of phylogeny, function and physiology on many bone microstructure parameters is evident but the magnitude of this influence and degree to which these factors interact is just beginning to surface.

Literature Cited

Barker, J., R. Boonstra, and A. Schulte-Hostedde. 2003. Age determination in yellow-pine chipmunks (*Tamias amoenus*): a comparison of eye lens masses and bone sections. Canadian Journal of Zoology 81:1774-1779.

Biewener, A. A. 1992. In vivo measurement of bone strain and tendon force. Pp. 123-147 *in* A. A. Biewener, ed. Biomechanics:Structures and Systems. A Practical Approach. Oxford University Press, Oxford.

Buffrénil, V. d., A. Houssaye, and W. Böhme. 2008. Bone Vascular Supply in Monitor Lizards (Squamata:Varanidae): Influence of Size, Growth, and Phylogeny. Journal of Morphology 269.

Carpenter, K., and Y. Wilson. 2008. A new species of *Camptosaurus* (Ornithopoda : Dinosauria) from the morrison formation (Upper Jurassic) of dinosaur national monument, Utah, and a biomechanical analysis of its forelimb. Annals of Carnegie Museum 76:227-263.

Carrano, M. 1998. Locomotion in Non-Avian Dinosaurs: Integrating Data from Hindlimb Kinematics, in Vivo Strains, and Bone Morphology. Paleobiology 24:450-469.

Castanet, J. 2006. Time recording in bone microstructures of endothermic animals; functional relationships. Comptes Rendus Biologies 5:629-636.

Castanet, J., K. Curry Rogers, J. Cubo, and J.-J. Boisard. 2000. Periosteal bone growth rates in extant ratites (ostrich and emu). Implications for assessing growth in dinosaurs. Comptes Rendus de l'Academie des Sciences Serie III-Sciences de la vie-Life Sciences 323:543-550.

Cooper, D. M. L., A. L. Turinsky, C. W. Sensen, and H. B. 2003. Quantitative 3D Analysis of the Canal Network in Cortical Bone by Micro-Computed

Tomography. The Anatomical Record (Part B: New Anatomy) 274B:169-179.

Cubo, J., P. Legendre, A. d. Ricqlès, L. Montes, E. d. Margerie, J. Castanet, and Y. Desdevises. 2008. Phylogenetic, functional, and structural components of variation in bone growth rates of amniotes. Evolution & Development 10:217-227.

Cubo, J., F. Ponton, M. Laurin, E. de Margerie, and J. Castanet. 2005. Phylogenetic Signal in Bone Microstructure of Sauropsids. Systematic Biology 54:562-574.

Currey, J. D. 2006. Bones: Structure and Mechanics. Princeton University Press, Princeton, NJ.

Dai, R.-C., E.-Y. Liao, C. Yang, X.-P. Wu, and Y. Jiang. 2004. Microcracks: an alternative index for evaluating bone biomechanical quality. Journal of Bone and mineral metabolism 22:215-223.

de Margerie, E. 2002. Laminar bone as an adaptation to torsional loads in flapping flight. Journal of Anatomy 201:521-526.

de Margerie, E., J. Cubo, and J. Castanet. 2002. Bone typology and growth rate: testing and quantifying 'Amprino's rule' in the mallard (*Anas platyrhynchos)*. Comptes Rendus Biologies 325:225-230.

de Margerie, E., J. Robin, D. Verrier, J. Cubo, R. Groscolas, and J. Castanet. 2004. Assessing a relationship between bone microstructure and growth rate: a fluorescent labelling study in the king penguin chick

(*Aptenodytes patagonicus*). Journal of Experimental Biology 207:869-879.

de Margerie, E., P. Tafforeau, and L. Rakotomanana. 2006. *In silico* evolution of functional morphology: a test on bone tissue biomechanics. Journal of the Royal Society Interface 3:678-687.

de Ricqlès, A., F. Meunier, J. Castanet, and H. Francillon-Vieillot. 1991. Comparative microstructure of bone. Pp. 1-78 *in* B. Hall, ed. Bone. CRC Press.

de Ricqlès, A., K. Padian, J. Horner, E. Lamm, and N. Myhrvold. 2003. Osteohistology of *Confuciusornis sanctus* (Theropoda : Aves). Journal of Vertebrate Paleontology 23:373-386.

Enlow, D., and D. Brown. 1956. A comparative histological study of fossil and recent bone tissues. Part I. Texas Journal of Science 8:403-443.

Enlow, D., and D. Brown. 1957. A comparative histological study of fossil and recent bone tissues. Part II. Texas Journal of Science 9:185-214.

Enlow, D., and D. Brown. 1958. A comparative histological study of fossil and recent bone tissues. Part III. Texas Journal of Science 10:187-230.

Erickson, G., and C. Brochu. 1999. How the 'terror crocodile' grew so big. Nature 398:205-206.

Erickson, G., K. Curry Rogers, and S. Yerby. 2001. Dinosaurian growth patterns and rapid avian growth rates. Nature 412:429-432.

Erickson, G., P. Makovicky, P. Currie, M. Norell, S. Yerby, and C. Brochu. 2004. Gigantism and comparative life-history parameters of tyrannosaurid dinosaurs. Nature 430:772-775.

Erickson, G., and T. Tumanova. 2000. Growth curve of *Psittacosaurus mongoliensis* Osborn (Ceratopsia : Psittacosauridae) inferred from long bone histology. Zoological Journal of the Linnean Society 130:551-566.

Habib, M. B., and C. B. Ruff. 2008. The effects of locomotion on the structural characteristics of avian limb bones. Zoological Journal of the Linnean Society 153:601-624.

Hall, B. K. 2005. Bones and Cartilage: Developmental Skeletal Biology. Academic Press, St. Louis, MO.

Horner, J., A. de Ricqlès, and K. Padian. 1999. Variation in dinosaur skeletochronology indicators: implications for age assessment and physiology. Paleobiology 25:295-304.

Horner, J., A. de Ricqlès, and K. Padian. 2000. Long bone histology of the hadrosaurid dinosaur *Maiasaura peeblesorum*: Growth dynamics and physiology based on an ontogenetic series of skeletal elements. Journal of Vertebrate Paleontology 20:115-129.

Horner, J., and K. Padian. 2004. Age and growth dynamics of *Tyrannosaurus rex*. Proceedings. Biological sciences 271:1875-1880.

Hutchinson, J. R. 2004. Biomechanical modeling and sensitivity analysis of bipedal running ability. II. Extinct taxa. Journal of Morphology 262:441-461.

Hutchinson, J. R., and V. Allen. 2009. The evolutionary continuum of limb function from early theropods to birds. Natuwissenschaften 96:423-448.

Klevezal, G. A., and M. V. Mina. 1990. Daily layers and hibernation marks in incisor dentin of *Sicista pseudonapaea* and some biological remarks. Acta Theriologica 35:345-356.

Lieberman, D. E. 1993. Life history variables preserved in dental cementum microstructure Science 261:1162-1164.

Ma, Y.-L., R.-C. Dai, Z.-F. Sheng, Y. Jin, Y.-H. Zhang, L.-N. Fang, H.-J. Fan, and E.-Y. Liao. 2008. Quantitative associations between osteocyte density and biomechanics, microcrack and microstructure in OVX rats vertebral trabeculae. Journal of Biomechanics 41:1324-1332.

Main, R. P., and A. A. Biewener. 2004. Ontogenetic patterns of limb loading, in vivo bone strains and growth in the goat radius. The Journal of Experimental Biology 207:2577-2588.

Millar, J. S., and F. C. Zwickel. 1972. Determination of age, age structure, and mortality of the pika, Ochotona princeps(Richardson). Canadian Journal of Zoology 50:229-232.

Misawa, Y., and M. Matsui. 1999. Age determination by skeletochronology of the Japanese salamander *Hynobius kimurae* (Amphibia, Urodela). Zoological science 16:845-851.

Morris, P. 1972. A review of mammalian age determination methods. Mammal Review 2:69-104.

Mullender, M. G., D. D. v. d. Meer, R. Huiskes, and P. Lips. 1996. Osteocyte Density Changes in Aging and Osteoporosis. Bone 18:109-113.

Padian, K., A. de Ricqlès, and J. Horner. 2001. Dinosaurian growth rates and bird origins. Nature 412:405-408.

Pearson, O. M., and D. E. Lieberman. 2004. The Aging of Wolff's "Law": Ontogeny and Responses to Mechanical Loading in Cortical Bone. Yearbook of Physical Anthropology 47:63-99.

Rayfield, E. J., D. B. Norman, C. C. Horner, J. R. Horner, P. M. Smith, J. J. Thomason, and P. Upchurch. 2001. Cranial design and function in a large theropod dinosaur. Nature 409:1033-1037.

Ruff, C., B. Holt, and E. Trinkaus. 2006. Who's Afraid of the Big Bad Wolff?: "Wolff's Law" and Bone Functional Adaptation. American Journal of Physical Anthropology 129:484-489.

Skedros, J. 2005. Osteocyte lacuna population densities in sheep, elk and horse calcanei. Cells Tissues Organs 181:23-27.

Smith, J. W. 1960. Collagen fibre patterns in mammalian bone. Journal of Anatomy 94:329-344.

Starck, J., and A. Chinsamy. 2002. Bone microstructure and developmental plasticity in birds and other dinosaurs. Journal of Morphology 254:232-246.

Steyer, J., M. Laurin, J. Castanet, and A. de Ricqlès. 2004. First histological and skeletochronological data on temnospondyl growth: palaeoecological and palaeoclimatological implications. Palaeogeography, palaeoclimatology, palaeoecology 206:193-201.

Tafforeau, P., and T. M. Smith. 2008. Nondestructive imaging of hominoid dental microstructure using phase contrast X-ray synchrotron microtomography. Journal of Human Evolution 54:272-278.

Vashishth, D., O. Verborgt, G. Divine, M. B. Schaffler, and D. P. Fyhrie. 2000. Decline in osteocyte lacunar density in human cortical bone is associated with accumulation of microcracks with age Bone 26:375-380.

Weiss, P., D. L. Nihouannen, C. Rau, P. Pilet, E. Aguado, O. Gauthier, A. Jean, and G. Daculsi. 2005. Synchrotron and non synchrotron X-ray microtomography threedimensional representation of bone ingrowth in calcium phosphate biomaterials. European Cells and Materials 9:48-49.

Chapter 1

New Methods in Bone Microstructure Analysis

Bridging Text

This chapter was published as a peer-reviewed article in the Canadian Journal of Zoology (de Boef and Larsson 2007). It provides a metric that is used in subsequent chapters and would be useful in other palaeontological or zoological studies.

Abstract

Bone microstructure often preserves a temporal record of the life history of the animal to which it belongs. Previously used bone microstructure metrics to differentiate between primary bone types are reviewed and tested with a broad sample of bone types. Two new metrics, the radial index and longitudinal index, are developed to quantitatively differentiate bone types based on bone vascular orientation in three dimensions. All previously used metrics described the bone microstructure in a non-linear pattern and were unable to separate bone types satisfactorily. The Radial Index and Longitudinal Index effectively differentiated bone types and described bone microstructure within a linear continuum. The continuous nature of the range of vascular orientation in bone microstructure necessitates a quantitative approach rather than the commonly used qualitative classifications. The Radial Index and Longitudinal Index, which objectively detect small differences in vascular orientation in three dimensions, are therefore preferable to other metrics for inter- and intra-specific comparisons of bone microstructure. These metrics offer novel methods to facilitate examinations of the relationship between primary bone type and ontogeny, biomechanics, and phylogeny.

Introduction

The microstructure of cortical bone can be used in palaeontological and zoological studies for assessing the life histories of the animals of which it

belongs. Phylogenetic, ontogenetic and functional signals have all been found when different bone types and their patterns of deposition (Wolff 1892; Amprino 1947; Castanet et al. 2000; Currey 2002; Cubo et al. 2005) have been examined. The study of these signals in bone microstructure is highly dependent on the ability of the observer to identify and differentiate between different bone types. Bone tissue types have been divided into several discrete categories (de Ricqlès et al. 1991) that are sometimes difficult to differentiate objectively. Additionally, bone tissues appear to cover a continuous range of variability making some bone type assessments problematic when using discrete categories.

Different types of cortical bone, characterized by differing collagen fibril and vascular canal orientations, have been associated with differing rates of bone deposition (de Ricqlès et al. 1991; Castanet et al. 1993); a relationship first recognized by Amprino (1947) and now commonly referred to as Amprino's rule. Slowly deposited bone, at a rate less than 1 µm per day, tends to organizes collagen fibrils into sheets, a structure reminiscent of plywood (Boyde 1980). Such bone is referred to as lamellar bone. Quickly deposited bone, at a rate greater than 4 µm per day, is associated with haphazardly organized collagen fibrils and is aptly termed woven bone (Currey 2002). Intermediate rates of bone deposition are commonly associated with intermediate collagen fibril orientations. This type of bone is called parallel-

fibered bone with collagen fibrils oriented in the same general orientation and relatively parallel to one another.

A study of king penguin chicks (*Aptenodytes patagonicus* Miller, 1778*)* has further supported this relationship between bone structure and growth rate. Decreased growth rates in this species is associated with a change in vascular canal orientation (de Margerie et al. 2004). Vascular canals in bone formed during rapid growth were predominantly oriented radially, or orthogonal to the long axis of the bone and radiating from the cortex outward to the periosteum (Figure 1-1). Vascular canals in bone formed at intermediate rates of growth were predominately oriented longitudinally or parallel to the long axis of the bone. Finally, vascular canals in bone formed at slower growth rates were oriented laminarly, or parallel to the circumference of the bone and orthogonal to its long axis. The terms radial, longitudinal and laminar are used to describe both the orientation of vascular canals as well as the bone types that contain a majority of vascular canals in these orientation (Enlow and Brown 1956; de Ricqlès et al. 1991). In addition, bone which shows a variety of vascular canal orientations with no dominant type is commonly referred to as reticular bone (de Ricqlès et al. 1991; de Margerie et al. 2004).

While the evidence for Amprino's rule has been mounting there also exists support for a theory known as Wolff's law (1892) which states that variation in bone microstructure is in response to variation in bone function and corresponding mechanical stresses. It has been found in both sheep and

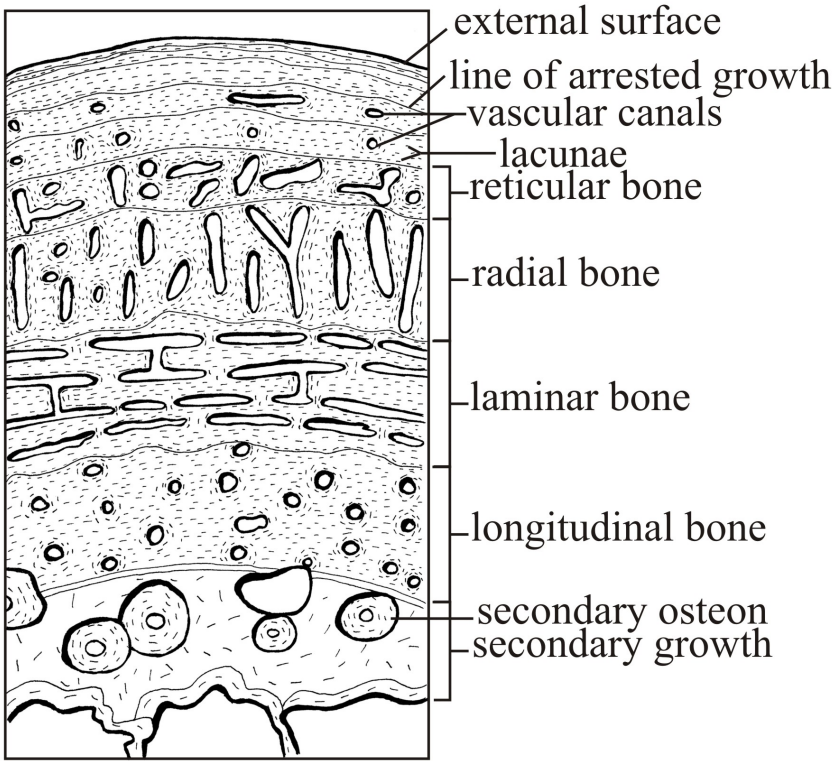

FIGURE 1-1. A schematic sketch of cortical fibrolamellar bone histology. Each of the four major bone types are shown separated by lines of arrested growth. Note that such separation of bone types, variety of bone types in one sample and clarity of lines of arrested growth are not typically seen and are represented here for illustrative purposes only.

dogs that the radius carries greater osteon remodeling on the caudal aspect which receives a greater compression strain than on the cranial aspect which receives a greater tensile strain (Lanyon and Baggot 1976; Carter et al. 1980). Studies of the long bones of adult mallards (*Anas platyrhynchos*, L. 1758*)* found that orientation of vascular canals within the bone is independent of growth rate (de Margerie et al. 2002) and that the proportion of laminar vascular canals (those oriented parallel to the bone wall and orthogonal to the long axis of the bone) is higher in those exposed to a high torsional load (de Margerie 2002). Additional studies in other bird species have supported this functional interpretation of variation in not only vascular orientation but also other structural characteristics of long bones (de Margerie et al. 2005).

Phylogenetic constraints have been hypothesized to also explain bone type, in addition to Amprino's rule and Wolff's law. This relationship was first recognized by Quekett (1849) when he began to use the microstructure of bone to identify fragments of fossil bone. While studied exclusively in a palaeontological context a relationship between phylogeny and bone microstructure has since been identified in extinct birds (Houde 1987) and reptiles (Cubo et al. 2005).

The strong relationship between bone microstructure, growth rate, function, and phylogeny offers an important research avenue to examine life histories of animals with bones. However, if we are to successfully tease apart these complex relationships it is important that we are consistent and

objective in our designation of bone types. Differentiating between different bone types based on collagen fibril orientation or on vascular orientation can be quite straightforward when the bone in question clearly has only one or another bone types. What becomes more difficult is when the bone contains the intermediate levels of fibril or vascular orientation between more obvious bone types. It is at this point when categorizing bone becomes extremely subjective. For this reason we believe that a quantitative metric measuring and differentiating bone vascular orientation will be useful. Such a metric would ideally allow small differences between bone tissue types to be detected to provide higher resolutions between the relationships of bone microstructure, growth rates, function, and phylogeny.

Some quantitative methods have been developed to assess bone microstructure. Botha and Chinsamy (2000) measured the percentage of the section area occupied by vascular canals in the midcortical regions of limb bones, a morphometry referred to as porosity. They suggest that more extensively vascularized bone (i.e. higher percent vascularization) is indicative of a faster growth rate and higher energy demand. This parameter, while useful for measuring relative differences is inappropriate for characterizing bones by their canal orientations. A similar metric created by Girondot and Laurin (2003) measures the compactness of bone using specialize software, Bone Profiler. A third metric that was used in conjunction with percent vascularization is average canal size, defined as the total area of all vascular

canals divided by their number (Starck and Chinsamy 2002). Stark and Chinsamy (2002) reject all relationships between vascularization, average canal size and bone deposition rate because variation in vascularization is exceeded by variation in bone deposition rates. Additionally canal diameter decreases with continuous bone deposition over post-natal development making it difficult to accurately compare bone deposition rates between individuals of different ages.

The low correlation between bone growth and microstructures such as canal diametres suggests the most accurate way to describe rates of bone growth is through cortical bone type as defined by vascular orientation (de Margerie et al. 2004). De Margerie (2002) proposed such an index to describe vascular orientation but its purpose was to distinguish laminar bone from other types and thus is not as complete as would be desired. We hypothesize that a metric that quantitatively describes how vascular canals are oriented in three-dimensional space will allow for a more accurate interpretation of differences between bone types, even when these differences are small. Here we describe a new method for distinguishing between bone types in a quantifiable manner and will compare our methods to the previous methods mentioned above. A comparison of the three previously used metrics mentioned above was performed in order to test their ability at differentiating between longitudinal, radial, laminar and reticular bone as described by (de Ricqlès et al. 1991) (Figure 1-1).

Materials and Methods

Fifty previously published images of bone microstructure were measured and analyzed from the literature (Castanet et al. 2000; Erickson and Tumanova 2000; Sander 2000; Padian et al. 2001; de Margerie 2002; de Ricqlès et al. 2003; de Margerie et al. 2004; Horner and Padian 2004; Ray and Chinsamy 2004; Steyer et al. 2004; Tutken et al. 2004) (Appendix 1). The images were chosen blindly and include a wide range of taxa and skeletal elements and included both fossilized and unfossilized bone. The samples are expected to include longitudinal, radial, laminar bone and reticular (as they were identified by some of the authors). The sampling is an attempt to assemble a random and even sample of bone types. Thus a metric that is capable of measuring this range would be expected to behave linearly between bone types without subjective identification or false weighting.

Assessment of previously used Indices

Porosity, average canal size, and de Margerie's (2002) laminarity index were calculated for all 50 images. The laminarity index was defined by de Margerie (2002) to be the ratio of the area of the laminar canals to total vascular area. Laminar canals were defined as those lying in the plane of cross-section approximately parallel ($0 \pm 22.5°$) to the bone wall. The laminarity index is calculated as a quotient of the total area of laminar canals divided by

the sum of all canal areas. This metric is, incidentally, somewhat auto correlated as the area of laminar canals are both in the numerator and denominator. The value of each of the metrics was calculated for each image included in this study. The values of the images for each metric were skree plotted (Figure 1-2) to assess their ability to isolate visually identified bone types.

The Longitudinal and Radial Indices

We recognized that a simple function would be needed to create the desired linear metric for measuring bone microstructure. By assessing the merits and weaknesses of de Margerie's index (2002) , we decided that vascular area was best removed from the metric as bone type is determined mainly by vascular canal orientation. Area and other metrics such as the previously used porosity index could be included as a complement to the metrics developed here.

We also recognized the need for canal measurement to be repeatable. For bone cross-sections, we achieve consistent canal measurements by approximating the largest ellipse into the canal areas (Figure 1-3). These measurements give major and minor axes that can be readily used for the metric calculations. If canals bend or branch, they will require two or more ellipses, to accommodate the canal shape. While this does increase the number of canals considered it should have no effect on the metrics as each is

an average of all canals considered. If the orientation of the vascular canal is reflective of the bone's growth rate or biomechanical use the different branches of such vascular canals may be important and thus it is important that they be considered in isolation. The use of ellipses makes the assumption that canals are roughly cylindrical in shape, an assumption justified by micro-CT reconstructions (Cooper et al. 2003). The approximation of largest ellipse, its orientation and its major and minor axes were all measured using the freeware program Scion Image (Scion Corp., Fredrick, Maryland, USA).

From the ellipse measurement data, we isolated two indices. The first identifies radial canals and we term it the Radial Index. The Radial Index is calculated by the average of all angles between the major axis of the ellipse and the vector tangent to the outer surface of the bone cross-section that is closest to the centroid of the vascular canal.(Figure 1-3, Figure 1-4A). Therefore, vascular canals running parallel to the radius of the bone cross section are assigned angles of 90° to give higher values to radially oriented canals. Laminar canals will have angles approaching 0°. For simplicity, all angles are transformed to gradians, a unit of measure where 90° is equal to 100. The use of gradians is not required to use this metric however and users may prefer degrees or radians. A threshold parameter is required for the Radial Index. If the canal is nearly circular in cross-section (indicating a parallel canal) the ellipse measurement method will still assign a major and minor axis to the canal. The canal will either not be absolutely circular or the

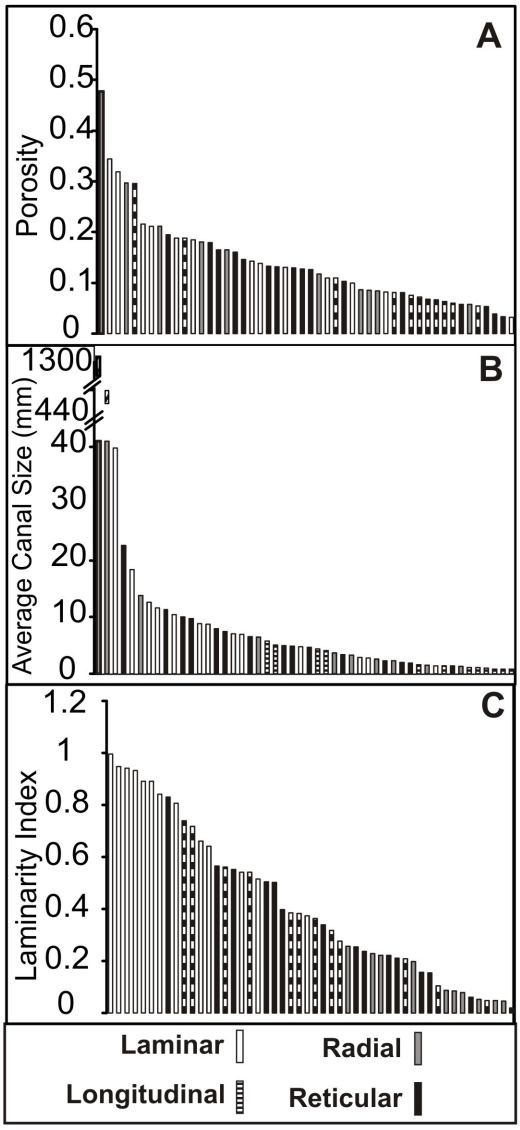

FIGURE 1-2. Discrete plots of the values found for fifty published images of bone histology using three previously used metrics. Bone types were assigned qualitatively according to de Ricqlès et al. (1991). A, Porosity B, Average Canal size C, Laminarity Index as developed by de Margerie (2002).

measurement of both axes will not be equal. A series of longitudinal canals will then be expected to result in a Radial Index of 50 gradians because the measured angles will vary stochastically between 0 and 100. To solve this issue, we introduce a threshold value that can be modified by the user. We choose to assign a Radial Index of 0 to canals that have their minor axis (b) within 5% of the value of the major axis (a).

Only one further index is required to assess all canal types in three-dimensions. The Longitudinal Index is calculated from the average angles of the long axes of the canals from the cross sectional plane. The major and minor axes of each ellipse are used to calculate the angle each canal lies to this axis – again, assuming roughly cylindrical canals (Figure 1-4C). The resultant formula to calculate the angle in gradians between the long axis of the canals from the radial plane is $\sin^{-1}(b/a)$. This angle in gradians gives a maximum for angles approaching the parallel axis of the bone. The extremes of each index describes radial and parallel bone. The intersection the indices describes laminar bone. Therefore, the two indices can describe the essential properties of longitudinal, radial, and laminar canalled bone.

It should be noted that while mean values of RI and LI were take for each bone cross section it is possible and may be desirable to compare RI and LI for regions of bone cross sections (medial vs. lateral for instance) or even individual vascular canals.

These indices were experimented with an array of possible canal orientations (Figure 1-5). The range of canal orientations extended fromthe extremes of having only one type of primary canal orientation to combinations of all. These 'simulations' suggest that all possible combinations of primary canal orientations can be accounted by these indices and the indices behave predictably. The gradian angle data was also trigonometrically transformed to give weight to angles near 0 and 90 degrees. This transformation was done to assess the impact of weighting angles according to a sine function to distinguish bone types. All data were skree-plotted for each index for the gradian (Figure 1-6) and trigonometrically transformed data (not shown).

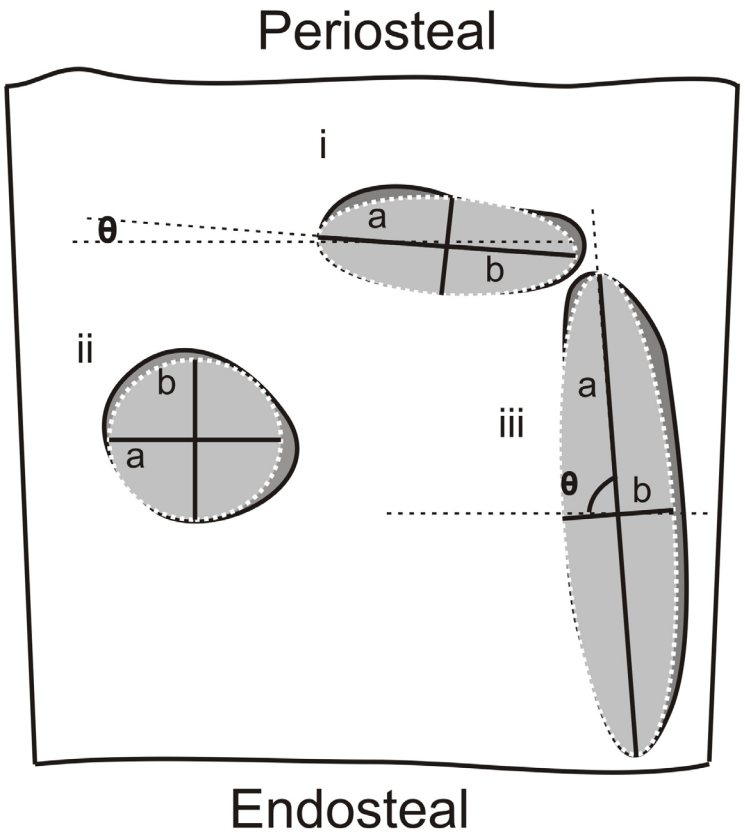

	Radial Index			Longitudinal Index
vascular canal	θ**	**a***	**b***	**sin-1 (b/a)**
i	**1.2**	**27.2**	**10.3**	**6.2**
ii	**0.0**	**13.4**	**12.8**	**20.2**
iii	**23.8**	**57.4**	**13.3**	**3.7**
Average	8.3			10.0

FIGURE 1-3. Method of measuring bone vascular orientation: ellipses are approximated into each vascular space on a bone cross section and the major axes (a), minor axes (b), and the angle between the major axis of the ellipse and a vector tangent to the outer surface of the bone cross are measured. These values are used to calculate the Radial Index and Longitudinal Index for each vascular canal as well as the section as a whole. i. laminar vascular canal, ii. longitudinal vascular canal, iii. radial vascular canal. * in arbitrary units ** when the minor axis is greater than 95% of the minor axis the vascular canal is assumed to be circular and assigned a radial index value of 0.

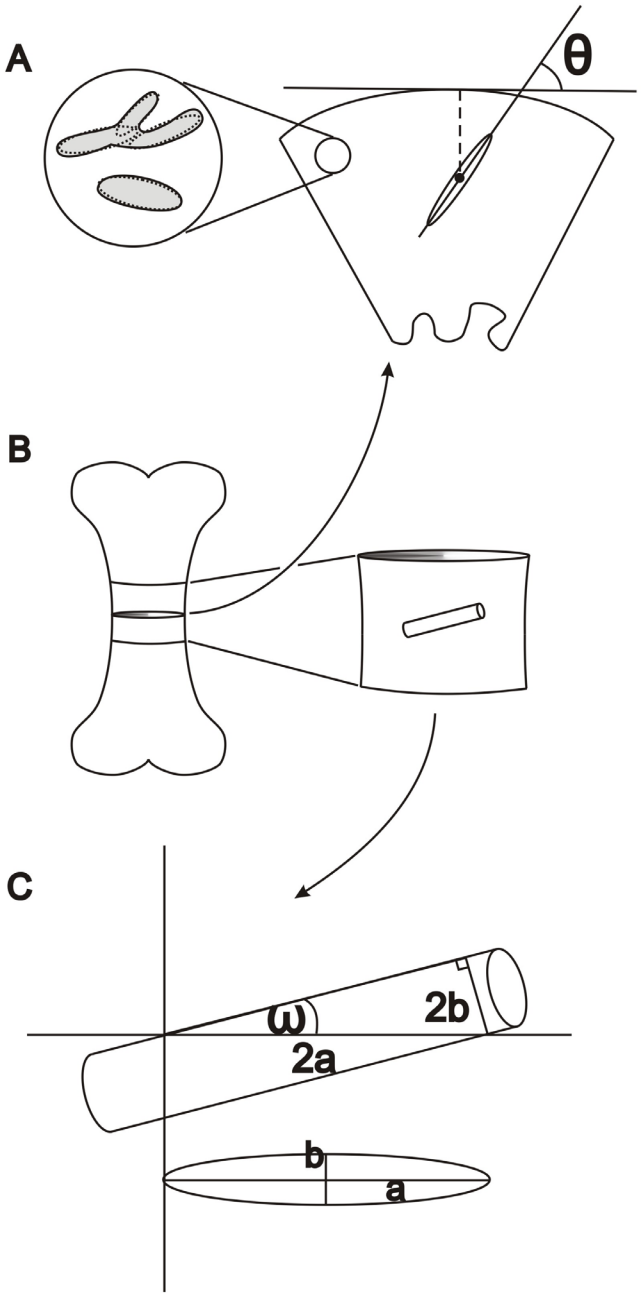

FIGURE 1-4. **(A).** The Radial Index is measured as the average of all angles between the major axis of the ellipse and the vector tangent to the outer surface of the bone cross-section that is closest to the centroid of the vascular canal., θ **(B).** The Longitudinal Index is measured as the average of all angles of the canals' long axis to the cross sectional plane of section, ω **(C).**

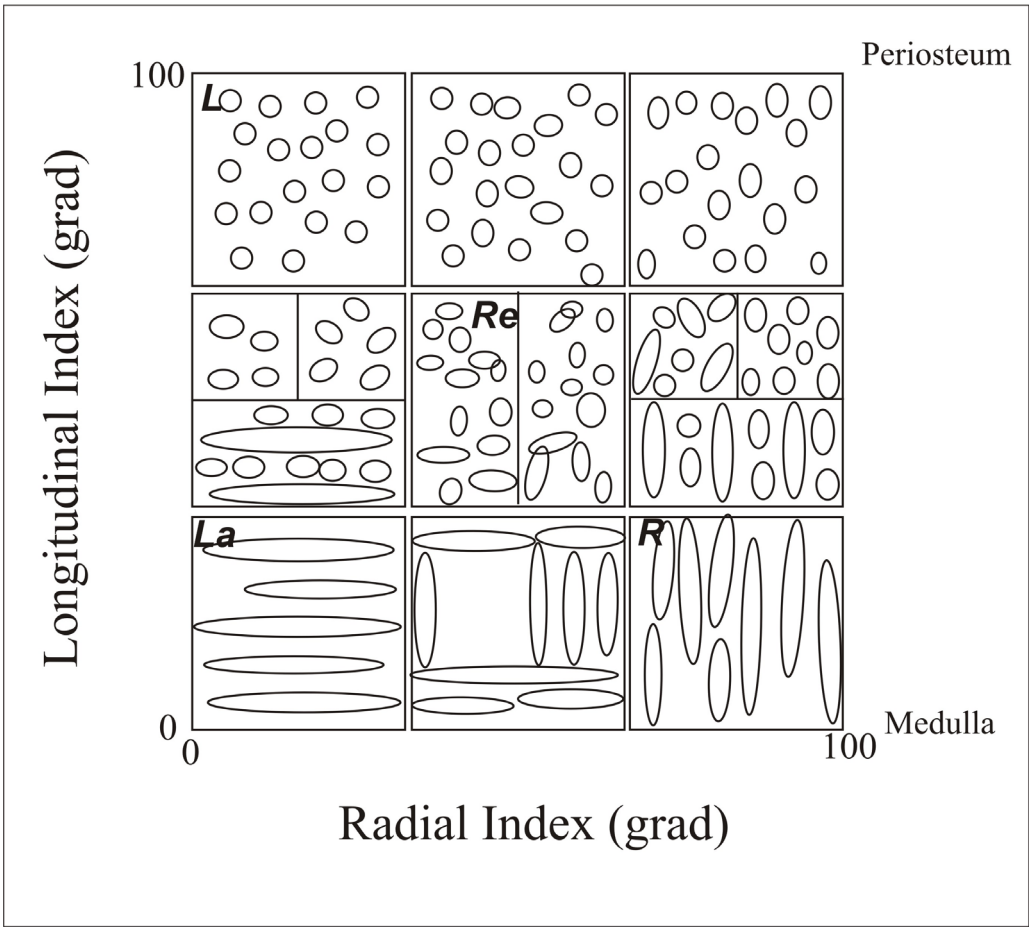

FIGURE 1-5. A schematic sketch showing hypothetical bone types fitting within the two dimensional framework of the longitudinal and radial indices La – laminar; L –longitudinal; R –radial; Re – reticular.

Results

When each image is analyzed using both the previously described bone microstructure metrics and those formulated here it becomes evident that bone tissue type is indeed a continuous character (Figures 1-2 and 1-5). The skree plots show all bone types intermingled and no separation between visually identified bone types. The range of values obtained for each of the metrics was large however suggesting that a significant amount of variability does exist between bone types for each of the metrics measured.

All three indices described the bone microstructure in a non-linear pattern and were unable to separate bone types satisfactorily (Figure 1-2). The porosity metric, while behaving the most linear of the three, was unable to isolate bone by type. All four bone types were present throughout the full range of values calculated for this metric. The average vascular canal area was able to isolate laminar bone to some degree but was non-linear and had some very extreme outliers. Again, all four bone types were present throughout the full range of values calculated. As expected, de Margerie's (2002) laminarity index produced highest values for the images of laminar bone. This index isolated bone type on one axis allowing us to distinguish between laminar and radial bone that have a majority of canals oriented parallel to the plane of section. However, this index is unable to isolate bone that has a majority of

canals running longitudinal to the bone and perpendicular to the plane of section (longitudinal bone).

The new metrics presented here can much more effectively differentiate between bone types. The longitudinal index is able to separate longitudinal bone from all other types of bone (Figure 1-6). The radial index is able to differentiate between radial bone and laminar bone; the former showing high values and the later low values. Both the untransformed (Figure 1-6) and trigonometrically transformed (not shown) versions of the Longitudinal Index and Radial Index plot a near linear progression of values through the entire bone section sample. The near linear progression of values suggests the metrics are not giving excess weight to any particular bone type, assuming a random selection of bone types.

The utility of the indices becomes clearer with bi-plots (Figure 1-7). The gradian angle values present the bone types within the expected regions of the plot with some overlap at their boundaries. Laminar bone occupies the region of relatively low Radial Index and Longitudinal Index. Radial bone occupies a region with similar Longitudinal Index values as laminar bone but with higher Radial Index values. Longitudinal bone occupies a region of intermediate Radial Index values than laminar and radial bone but with higher Longitudinal Index values. As expected, reticular bone values appear intermediate to all extremes and overlap the boundaries of the three major bone types.

Bone identified as longitudinal bone with the largest values on the longitudinal index also have high values on the radial index. The combination of longitudinal and radial canals is relatively common and often identified as longitudinal or radial by authors. The trigonometric transformations appear to have the largest effect on bones with high Longitudinal Index and Radial Index values and, as expected, appear to skew these highest values (not shown). We suggest that the unadjusted indices should be used to evaluate bone type to avoid the skewing of the extreme values of the indices. However, in some cases, researches may wish to use the transformations in order to emphasize small differences between intermediate values.

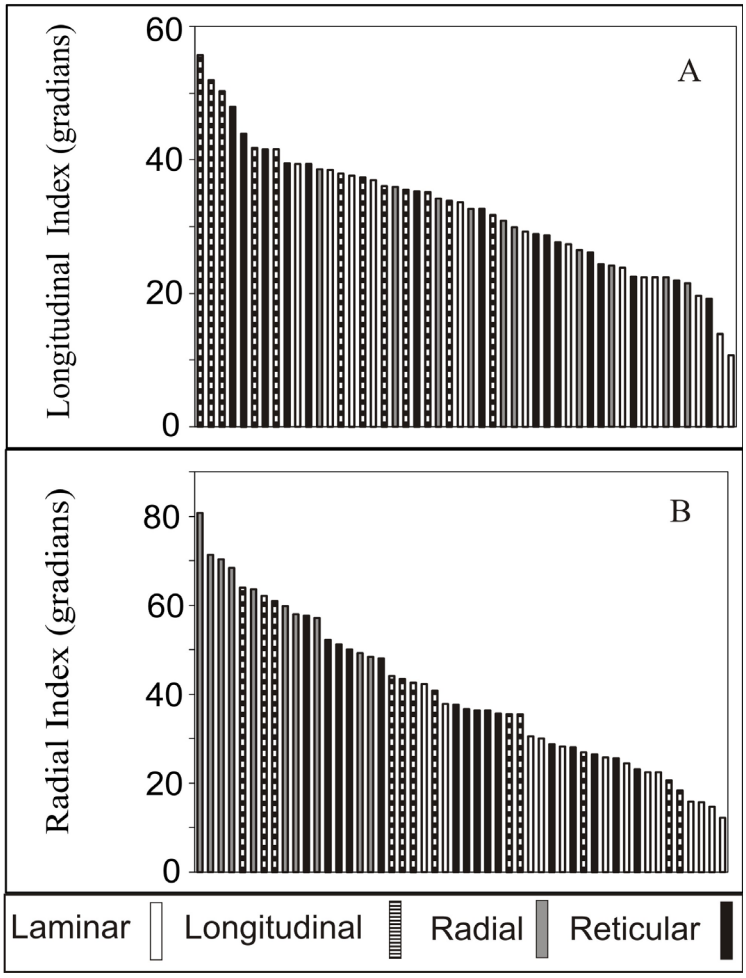

FIGURE 1-6. Discrete plots of the values found for the fifty published images of bone histology using the two new metrics designed to measure average canal orientation. Bone types (by vascular orientation) were assigned qualitatively according to de Ricqlès et al. (1991). **A**, The longitudinal index that measures average vascular canal orientation with respect to the long axis of the bone. **B,** The radial index that measures average vascular canal orientation with respect to an axis perfectly radial to the bone surface.

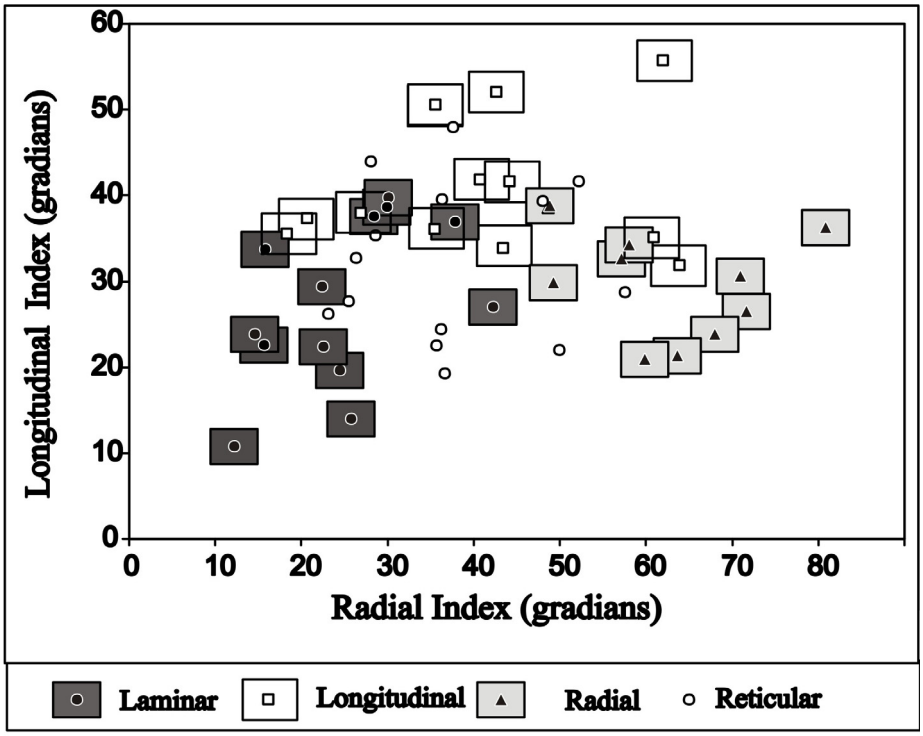

FIGURE 1-7. An x-y plot of the values found for the fifty published images of bone histology using the two new metrics designed to measure average canal orientation. Bone types were assigned qualitatively according to de Ricqlès et al. (1991). Boxes surrounding laminar, longitudinal and radial bone types represent 95% confidence intervals.

Discussion

Recent authors have suggested a number of quantitative metrics to apply to internal bone structure. Laurin and colleagues (2004) applied metrics to address the issue of bone density to assess ecological lifestyle of fossil taxa. Others have examined bone microstructure by quantifying relative porosities of bone sections (Botha and Chinsamy 2000). Other authors have developed metrics to assess relative contributions of laminar vasculature within bone (de Margerie et al. 2002). Here, we present a new quantitative metric to describe bone vascular orientations from transverse cross-sections. This metric is demonstrated to be sensitive to all possible vascular orientations. The results highlight the non-discrete nature of the variation of bone microstructure (Figure 1-6). While the terminologies presented by earlier workers are useful to qualitatively describe extreme ranges of cortical bone vascular orientation, they do not capture the continuum found in nature (Figure 1-2). The overlap between the reported bone types is large and highlights the subjective assignment of bone types by authors. A clear example of this subjectivity can be found in bones identified as radial bones. In most cases, radial canals are often divided by a row of longitudinal canals. The larger number of longitudinal canals within the section overrides the identification of the section as representing a radial bone. If we are to successfully evaluate the importance of ontogeny, biomechanics, or phylogeny on bone microstructure it is important that we be able to correctly assess differences between bone

types. This can most accurately be done if the metric used is able to evaluate changes in this continuous character. For vascular orientation we believe this can most effectively be done with the metric presented here. Metrics used by previous authors, while useful for assessing the qualities of bone microstructure for which they were designed, are unable to differentiate between all bone types.

The measurement of porosity, calculated as the percentage of the section area occupied by vascular canals in the midcortical region of bones, can tell us a great deal about how much vascularization exists within a bone (Botha and Chinsamy 2000). However, as there appears to be no relationship between the amount of vascularization and vascular orientation, this metric does not allow us to differentiate between bone types (Figure 1-2a). The measurement of average canal size, calculated as the total area occupied by all vascular canals divided by their number, may also contain signals about ontogeny, biomechanics or phylogeny of bone tissue. However, as with porosity, there appears to be no relationship between this metric and vascular orientation (Figure 1-2b). De Margerie's (2002) laminarity index is the only previously used index of the three tested that was designed to assess vascular orientation. The relative abundance of laminarly oriented vascular canals was determined by calculating the ratio of the area of the laminar canals to total vascular area. This metric was designed to distinguish laminar (sometimes termed laminar) bone from all other types but cannot distinguish between

other bone types (Figure 1-2c). Additionally, while it is able to distinguish between laminar bone and other bone types it is subjective in its definition of laminar canals by identifying them as lying within 22.5° from the plane of the bone surface. Finally, this metric could potentially give inaccurate results if laminar canals are of significantly different size than other types of vascular canals, although this has yet to be tested.

As hypothesized the radial index and longitudinal index are a much more atisfactory way of differentiating between bone types than either of the three previously used indices (Figure 1-6). The Radial Index and Longitudinal Index allow us to quantitatively evaluate the orientation of vascular canals in a three dimensional framework. This is preferable to all previously used indexes which analyze bone microstructure in a two dimensional framework based upon cross sections. It is possible that signals found in bone related to ontogeny, biomechanics, or phylogeny are only evident when bone microstructure can be evaluated using three dimensions. If this were the case then a set of three-dimensional indices are required, such as the Radial Index and Longitudinal Index. While it is necessary to include a small subjective correction in the Radial Index to ensure that longitudinal canals are given low values this correction has no visible effect on assessment of bone type (Figures 1-5 and 1-6). The objectivity of the indices and the simplicity in their use are also attractive for those who desire to do large studies of bone microstructure involving many specimens.

The new indices we present here do encompass the entire range of possibilities of canal orientations predictably. The findings presented here show that although the study of bone histology has been hindered by many overlapping and even conflicting terminologies, it is possible to obtain objective, qualitative data. Such numerical data can be valuable for those wishing to test statistically hypotheses about life histories. This is particularly true for those studying extinct species where bones may offer the only signatures of life histories. Bone microstructure can improve our understanding of growth patterns, physiology, age, bone biomechanics, sexual morphs, and phylogeny in species that we only recognize by fossil remains.

The continuous format of the metrics allow for direct inter- and intraspecific comparisons with no ambiguity of the degree of qualitative interpretation of bone types. They even allow for transect comparisons within the same bone section (de Boef et al. in prep). These transect measurements can incorporate previously created metrics, such as porosity and canal size.

Literature Cited

Amprino, R. 1947. La structure du tissu osseux envisagée comme expression de différences dans la vitesse de l'accroissement. Archives de biologie 58:315-330.

Botha, J., and A. Chinsamy. 2000. Growth patterns deduced from the bone histology of the cynodonts *Diademodon* and *Cynognathus*. Journal of Vertebrate Paleontology 20:705-711.

Boyde, A. 1980. Electron Microscopy of the mineralizing front. Metabolic bone disease and related research 2 (suppliment):69-78.

Carter, D. R., D. J. Smith, D. M. Spengler, C. H. Daly, and V. H. Frankel. 1980. Measurement and analysis of *in vivo* bone strains on the canine radius and ulna. Journal of Biomechanics 13:27-38.

Castanet, J., K. Curry Rogers, J. Cubo, and J.-J. Boisard. 2000. Periosteal bone growth rates in extant ratites (ostrich and emu). Implications for assessing growth in dinosaurs. Comptes Rendus de l'Academie des Sciences Serie III-Sciences de la vie-Life Sciences 323:543-550.

Castanet, J., H. Francillon-Vieillot, F. Meuner, and A. Ricqles de. 1993. Bone and individual aging. Pp. 245-283 *in* B. Hall, ed. Bone. CRC Press.

Cooper, D. M. L., A. L. Turinsky, C. W. Sensen, and H. B. 2003. Quantitative 3D Analysis of the Canal Network in Cortical Bone by Micro-Computed Tomography. The Anatomical Record (Part B: New Anatomy) 274B:169-179.

Cubo, J., F. Ponton, M. Laurin, E. de Margerie, and J. Castanet. 2005. Phylogenetic Signal in Bone Microstructure of Sauropsids. Systemactic Biology 54:562-574.

Currey, J. D. 2002. Bones: Structure and Mechanics. Princeton University Press, Princeton.

de Boef, M., and H. C. E. Larsson. 2007. Bone Microstructure: quantifying bone vascular orientation. Canadian Journal of Zoology 85:63-70.

de Margerie, E. 2002. Laminar bone as an adaptation to torsional loads in flapping flight. Journal of Anatomy 201:521-526.

de Margerie, E., J. Cubo, and J. Castanet. 2002. Bone typology and growth rate: testing and quantifying 'Amprino's rule' in the mallard (*Anas platyrhynchos)*. Comptes Rendus Biologies 325:225-230.

de Margerie, E., J. Robin, D. Verrier, J. Cubo, R. Groscolas, and J. Castanet. 2004. Assessing a relationship between bone microstructure and growth rate: a fluorescent labelling study in the king penguin chick (*Aptenodytes patagonicus*). Journal of Experimental Biology 207:869-879.

de Margerie, E., S. Sanchez, J. Cubo, and J. Castanet. 2005. Torsional Resistance as a Principal Component of the Structural Design of Long Bones: Comparative Multivariate Evidence in Birds. The Anatomical Record Part A 282A:49-66.

de Ricqlès, A., F. Meunier, J. Castanet, and H. Francillon-Vieillot. 1991. Comparative microstructure of bone. Pp. 1-78 *in* B. Hall, ed. Bone. CRC Press.

de Ricqlès, A., K. Padian, J. Horner, E. Lamm, and N. Myhrvold. 2003. Osteohistology of *Confuciusornis sanctus* (Theropoda : Aves). Journal of Vertebrate Paleontology 23:373-386.

Enlow, D., and D. Brown. 1956. A comparative histological study of fossil and recent bone tissues. Part I. Texas Journal of Science 8:403-443.

Erickson, G., and T. Tumanova. 2000. Growth curve of *Psittacosaurus mongoliensis* Osborn (Ceratopsia : Psittacosauridae) inferred from long bone histology. Zoological Journal of the Linnean Society 130:551-566.

Girondot, M., and M. Laurin. 2003. Bone Profiler: A tool to quantify, model, and statistically compare bone-section compactness profiles. Journal of Vertebrate Paleontology 23:458–461.

Horner, J., and K. Padian. 2004. Age and growth dynamics of *Tyrannosaurus rex*. Proceedings. Biological sciences 271:1875-1880.

Houde, P. 1987. Histological Evidence for the Systematic Position of *Hesperornis* (Odontornithes, Hesperornithiformes). Auk 104:125-129.

Lanyon, L., and D. Baggot. 1976. Mechanical function as an influence on the structure and form of bone. Journal of bone and joint surgery 58B:436-443.

Laurin, M., M. Girondot, and M.-M. Loth. 2004. The evolution of long bone microanatomy and lifestyle in lissamphibians. Paleobiology 30:589-613.

Padian, K., A. de Ricqlès, and J. Horner. 2001. Dinosaurian growth rates and bird origins. Nature 412:405-408.

Quekett, J. 1849. On the intimate structure of bone as composing the skeleton in the four great classes of animals viz., mammals, birds, reptiles and fishes, with some remarks on the great value of the knowledge of such structure in determining the affinities of minute fragments of organic remains. . Trans.R.Micr.Soc.Lond. 2:46-58.

Ray, S., and A. Chinsamy. 2004. Diictodon feliceps (Therapsida, Dicynodontia): Bone histology, growth, and biomechanics. Journal of vertebrate paleontology 24:180-194.

Sander, P. 2000. Longbone histology of the Tendaguru sauropods: implications for growth and biology. Paleobiology 26:466-488.

Starck, J., and A. Chinsamy. 2002. Bone microstructure and developmental plasticity in birds and other dinosaurs. Journal of Morphology 254:232-246.

Steyer, J., M. Laurin, J. Castanet, and A. de Ricqlès. 2004. First histological and skeletochronological data on temnospondyl growth: palaeoecological and palaeoclimatological implications. Palaeogeography, palaeoclimatology, palaeoecology 206:193-201.

Tutken, T., H. Pfretzschner, T. Vennemann, G. Sun, and Y. Wang. 2004. Paleobiology and skeletochronology of Jurassic dinosaurs: implications from the histology and oxygen isotope compositions of bones. Palaeogeography, Palaeoclimatology, Palaeoecology 206:217-238.

Wolff, J. 1892. Das Gesetz der Transformation der Knochen. A. Hirshwald, Berlin.

Chapter 2

Aging through Skeletochronology: A study in Carnivora and commentary on its use in Endotherms

Bridging Text

This chapter is in manuscript format in preparation for its submission to a peer-reviewed journal. In continuation of the first chapter this chapter analyses a second metric commonly used in bone microstructure analyses. Here I test the method of using bone growth marks, skeletochronology, to age three Carnivorans.

Abstract

Skeletochronology is the method by which vertebrates are aged using growth marks present in compact bone. The method is commonly used to age ectothermic vertebrates, such as fishes, reptiles and amphibians and has been occasionally used in endothermic mammals and birds. This study reports on counts of bone growth marks in three species of carnivorans – raccoons (*Procyon lotor*), red foxes *(Vulpes vulpes*) and striped skunks (*Mephitis mephitis)* and compares these to known ages. Growth marks were found in all three species, but while these marks were more abundant in older individuals, the marks to not correspond directly to age and could not be used as accurate predictors for age. It is suggested that skeletochronology be used in endothermic species only where a strong relationship between growth mark counts and age has been previously established.

Introduction

The use of skeletal growth marks to age an animal, known as skeletochronology, is a common practice in ichthyological, herpetological and paleontological studies. In much the same way that dendrochronology uses annual rings in the trunks of trees to estimate age, skeletochronology is based

on the assumption that growth lines in bone are formed annually. Growth lines visible in bone can vary a great deal in both structure and appearance and have a similarly confusing array of names. The terms: line of arrested growth (LAG), annulus, zone, resorption line, growth line, growth ring, hibernation mark, hematoxylinophilic line, resting line (RL), Harris line, outer circumferential layer (OCL) and external fundamental system (EFS) have all been assigned to growth marks found in bone (Klevezal and Mina 1990; Castanet et al. 1993; Horner et al. 1999; Misawa and Matsui 1999; Barker et al. 2003). While an excellent review by Castanet (2006) clearly defines some of the above terms, it is clear that there is still some disagreement about which terms to use and when (Morris 1972; Klevezal and Mina 1990).

The confusion surrounding the nomenclature of the marks may be due, in part, to a lack of understanding regarding their cause. It is generally thought that these marks indicate a change in physiology, specifically a slowing in the deposition of bone. For instance, in ectothermic animals the appearance of these marks has been linked to seasonal changes in metabolism related to colder temperatures or dryer conditions (Castanet 1985a, b; Misawa and Matsui 1999). In many of these cases organisms hibernate or experience periods of torpor during these periods, and it is postulated this inactivity has led to the formation of a growth mark. However, annual marks have also been found where seasonality is absent either naturally (Chinsamy et al. 1995) or

artificially (Castanet et al. 2004). In these latter cases it is thought that photoperiodicity triggers the formation of a growth mark. Certainly, physiological changes caused by stressful events, including hatching, weaning and starvation (Castanet et al. 1993; Castanet 2006), can cause a growth mark to form in the bone as has been documented for teeth (Smith and Tafforeau 2008). Dental growth marks have been well studied and the various types of growth marks visible in tooth enamel and their causes have been well defined (Smith and Tafforeau 2008) and used extensively to age individuals in anthropological settings. Growth marks in tooth cementum or dentin is frequently used in modern zoological research to age wild-caught individuals (Allen 1974; Garshelis 1984; Jenks et al. 1984; Driscoll et al. 1985; Klevezal and Mina 1990). Tooth enamel is deposited daily and slight changes in deposition rates over a daily cycle allow for the visualization of daily lines. However, it is more prominent marks that are deposited annually are those that are usually used for aging. The biochemical process that lead to the deposition of these growth marks in teeth is poorly understood although there is some evidence that changes in diet can lead to changes in tooth enamel composition thus leaving a growth mark (Wright and Schwarcz 1998; Humphrey et al. 2008)

In modern species, skeletochronology is most commonly used in ectothermic species. Fish are commonly aged using their otoliths and scales, and the age from both tissues are considered quite accurate (Machias et al. 2002; Roberson et al. 2005). Many amphibian species are aged from toe- and

longbone sections, although counts sometimes only represent ages post-metamorphosis (Leclair and Castanet 1987; Misawa and Matsui 1999). All major groups of reptiles, including snakes, turtles and lizards, have been successfully aged using counts of bone growth marks (Castanet 1985a, b). Skeletochronology in endothermic species is less common and considered unreliable in most cases (Castanet 2006). However, there are a few exceptions. The validity of using skeletochronology to age birds was first suggested by Klevezal (1972). This was further validated by Klomp and Furness (1992) who found that skeletochronology was able to correctly age 13 species of birds that were of known age and was unreliable for only one species. Skeletochronology is rarely used in mammals. Morris (1972) suggested bone growth marks were a potentially useful method for aging mammals. Studies of marine mammals found a laminar structure in seal, whale, manatee and even polar bear bone that contained what were thought to be annual marks (Laws 1953; Laws 1960; Chinsamy and Dodson 1995; Marmontel et al. 1996). Costain and Verts (1982) found that Belding's ground squirrels could be accurately aged using stained lines in their mandibles. The mandible was also able to correctly measure age in the Altai gray birch mouse (Klevezal and Mina 1990) and the pika (Millar and Zwickel 1972). The yellow-pine chipmunk could be aged as accurately from growth lines as it could from using the more traditional methods of eye lens mass or size (Barker et al. 2003). Most recently Castanet and colleagues (2004)

reported growth lines in the primate *Microcebus murinus* and found they were deposited annually.

While there is evidence that skeletochronology can be used to accurately determine age in some mammals species, there are cases where the method may not be as accurate (Morris 1972; Castanet 2006). A universal application of skeletochronology would clearly be a valuable tool of great benefit to ecological and life history studies of vertebrates. While tooth cementum lines are known to be accurate, teeth are not always available for analysis. This is particularly true in palaeontological samples. In this study I will look at the ability of bone growth lines to correctly measure the age in three terrestrial carnivores: red fox (*Vulpes vulpes*), raccoon (*Procyon lotor)* and striped skunk (*Mephitis mephitis)*. Two of these species, the skunk and raccoon, experience periods of torpor during the winter. Since growth lines are thought to be caused by slowed or stopped growth it was thought that growth lines might be visible only in the raccoon and skunk in this study. These three species were chosen for the ease of access to tooth-aged samples.

While Laws (1953) found that skeletochronology is possible in one species of carnivoran, the elephant seal, this is an aquatic species and the types of environmental factors that cause the formation of growth marks may be different from terrestrial carnivorans. For instance, it has been suggested that aquatic ecosystems are more prone to trophic cascades (Strong 1992).

Such cascades would be likely to result in the formation of a growth mark as growth rate increases or decreases in response to dietary changes. Also, with so few studies of bone growth marks in mammalian species, the addition of data from three additional species may be highly valuable. In this study, the number of growth marks in the bone will be compared to the ages of each individual determined from cementum growth marks. The use of cementum growth marks in carnivorans is common and accurate (Linhart and Knowlton 1967; Allen 1974; Garshelis 1984; Jenks et al. 1984; Root and Payne 1984; Driscoll et al. 1985).

Occasionally, when all other markers of age are absent, size measures, such as bone length, are used to estimate age. However, using size measures to estimate age are unreliable and may introduce significant biases into typical analyses (Halliday and Verrell 1988; McRoberts et al 1998; Cooch et al 1999). In this study we will compare the known-age (from tooth cementum marks) to bone length to examine the validity of the use of length measures in the three species examined here.

Materials and Methods

Humeri and femora of three species of carnivorans, the raccoon (*Procyon lotor)*, red fox (*Vulpes vulpes)* and striped skunk (*Mephitis mephitis)*, were obtained from the Ministry of Natural Resources in Ontario. All animals

had been sacrificed as part of a rabies research program. All were captured in mid-latitude Ontario between 48 and 49.7 degrees North. The longitudinal range for the individuals is unknown, but the climate at this latitude is fairly similar across Ontario. They were also all captured in the fall and as these species are habitually born in the spring they were all six months old or six months past their most recent birthday. All muscle and connective tissues were removed and the bones were allowed to dry in a fume hood for at least one week. Bones were then embedded in an epoxy resin (Buehler Epothin) and sectioned transversely at the midshaft using a precision saw with a diamond bit blade (Isomet 1000, Buehler, Lake Bluff, Illinois, USA). The resulting sections were bonded to a glass slide using a cyanoacrylate adhesive. These sections were viewed under 40x magnification under a compound light microscope (Nikon Optiphot, Japan). While the sections were photographed using a digital camera for a separate study (Chapter3), the counts of growth marks were taken using the microscope (Figure 2-1). Differences in bone texture and colouration, which often define a growth mark, are more easily visible when viewed through a microscope than from a digital image. All individuals were aged by the Ministry of Natural Resources in Trent, Ontario through counts of cementum layers in the canines of the animals which were viewed using polarized light microscopy. Counts of growth marks in the bones of the animals were taken blind to the counts of growth marks in the canines. Also, counts of growth marks in one skeletal element (humerus) were taken blind to the

counts of growth marks in another skeletal element from the same individual (femur). Comparisons between the number of growth marks in the bone (hereafter referred to as “bone-age”), the number of growth marks in the teeth (hereafter referred to as “tooth-age”) and bone length were conducted using a Spearman’s rank correlation. The analysis was performed using the “rcorr” function in the “Hmisc” package of R (R Development Core Team, Vienna, Austria).

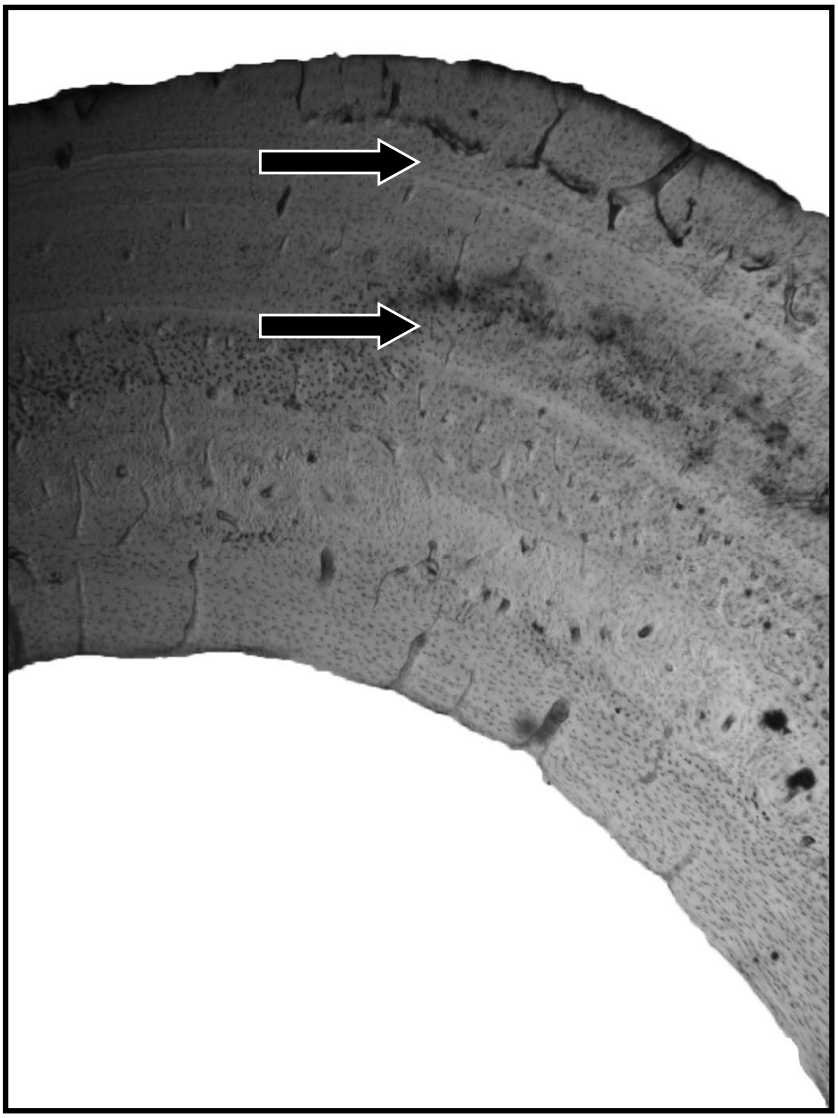

Figure 2-1: Part of a transverse, mid-diaphyseal section. Growth marks are indicated by arrows.

Results

Bone lengths, tooth-ages and bone-ages are found in Appendix 1. A summary of the relationships between the age measures and their levels of significance are found in Table 2-1.

Tooth-age and length

Figure 2-2 depicts the relationship between bone length and age as measured by layers in tooth cementum. In all cases bone length did not correlate well with tooth-age. In both skunk femora and humeri, bone length was found to have a slightly negative relationship with tooth-age but the variance surrounding this relationship was high. The variance was also high in the bones of fox and raccoon but the relationship was near zero in the bones of the former and positive in the bones of the later.

Tooth-age and bone-age

Figure 2-3 depicts the relationship between bone-age and tooth-age. A general linear model using a Poisson distribution found that the growth rings in the skunk humeri and femora were positively related to tooth-age ($p<0.001$ and $p=0.002$, respectively). A similar pattern was found for the raccoon and fox humeri and femora ($p<0.001$ for each).

Length and bone-age

The relationships between bone-age and length were generally non-significant (Table 2-1). The exception to this was a significantly positive relationship between raccoon femur length and bone-age (ρ=0.41, p=0.0285).

TABLE 2-1: Results of statistical analyses testing the relationships between bone length and toothage and boneage and toothage for three species of carnivore. P values represent Spearman's rank coeffiecient. Values in brackets represent statistical significance.

Species	Element	Sample Size	Mean Length	P length~bone.age	P length~tooth.age	P bone.age~tooth.age
Fox	Humerus	15	131.77	-0.13 (0.6603)	0.08 (0.7956)	0.85 (<0.001*)
	Femur	17	125.02	-0.17 (0.5125)	<0.01 (0.9979)	0.83 (<0.001*)
Raccoon	Humerus	15	102.56	0.29 (0.33)	0.34 (0.2591)	0.85 (<0.001*)
	Femur	17	99.98	0.41 (0.0285*)	0.35 (0.0609)	0.90 (<0.001*)
Skunk	Humerus	24	66.77	-0.24 (0.2621)	-0.24 (0.2780)	0.64 (<0.001*)
	Femur	24	58.69	0.17 (0.4261)	-0.04 (0.8496)	0.60 (0.002*)

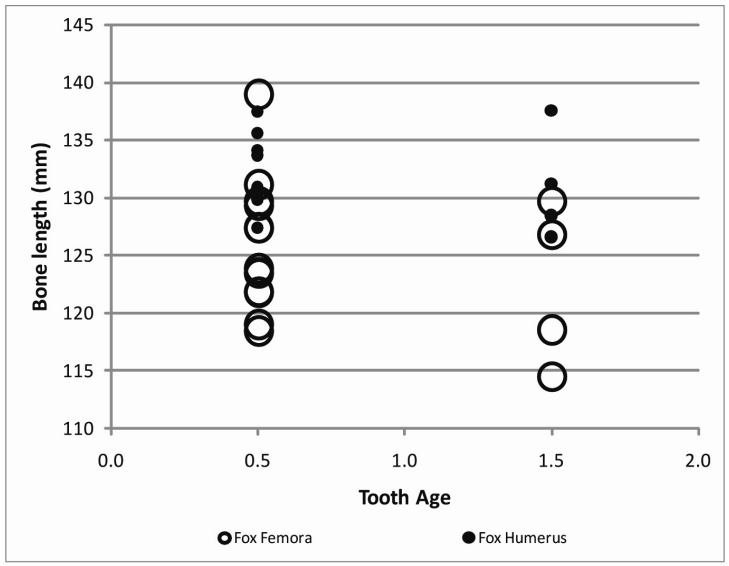

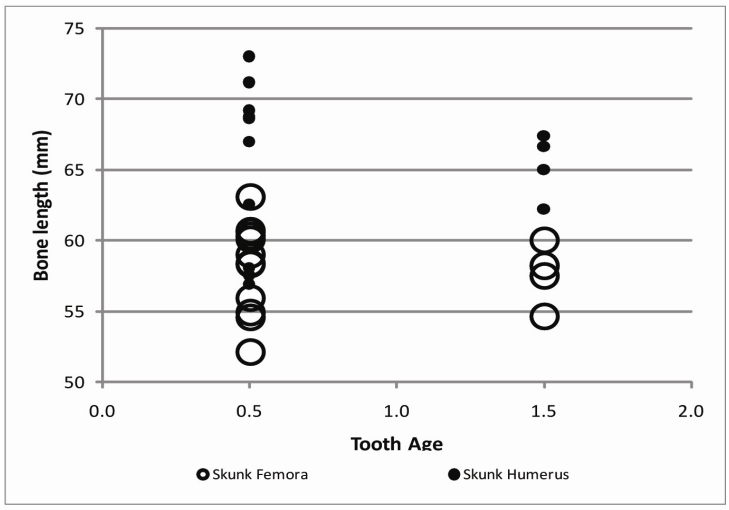

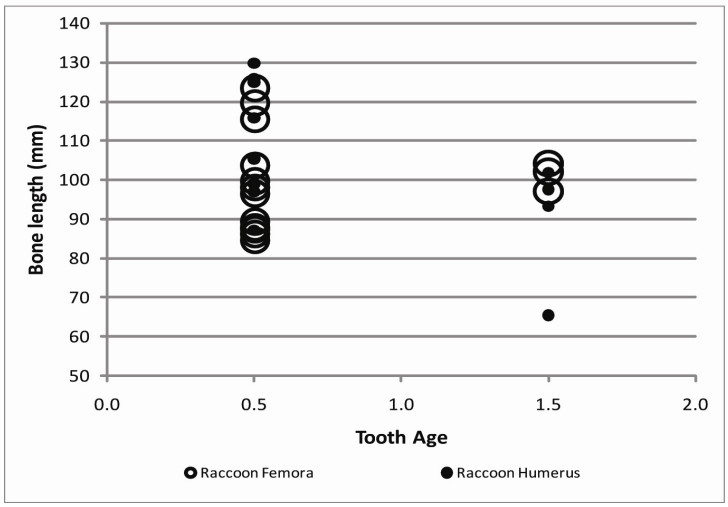

Figure 2-2: Plots of bone length to tooth-age as measured by counts of growth marks in the cementum teeth.

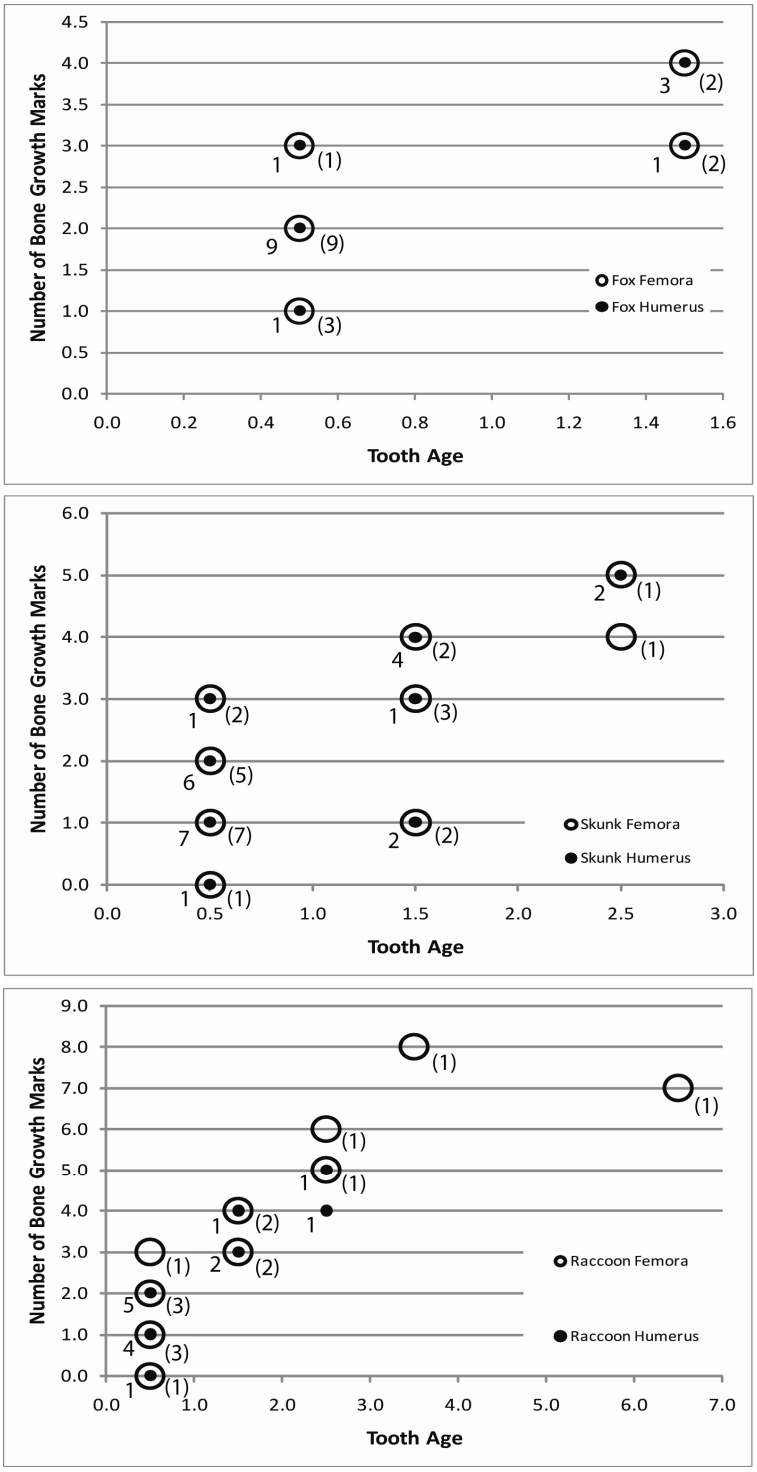

Figure 2-3: Plots of bone-age, as measured by counts of growth marks in compact bone, to tooth-age, as measured by counts of growth marks in the cementum of teeth. Numbers to the right and in brackets of each point represent samples size in femora. Numbers to the left represent sample size in humerii.

Discussion

Using size to estimate age

The relationship between bone length and tooth-age is nonsignificant and any trend that does exist is negative. Assuming tooth-age to be an accurate measure of age (Linhart and Knowlton 1967; Allen 1974; Garshelis 1984; Jenks et al. 1984; Root and Payne 1984; Driscoll et al. 1985), this suggests that, in these three species, using animal size as a method to estimate age can be highly inaccurate. This was not an unanticipated result as previous studies have found size to be a "rough guide" at best for age determination (Morris 1972; Catling et al. 1991). All species show some level of variability in linear measures of size, and often the largest of one age class can be larger than the smallest of older age classes. Such variability can occur both between and within populations and is amplified by environmental differences including diet, climate and habitat. Therefore it seems unlikely that these three species are unique among carnivorans and use of length measures to estimate age should be used only as a last resort.

Using bone growth marks to estimate age

A significant positive relationship between bone growth marks and tooth marks was found in the humerus and the femur for all species, with the fox humerus as the only exception. It was hypothesized that bone growth marks

would be deposited on an annual basis in a similar manner to growth marks found in tooth cementum. However, bone growth marks were deposited more frequently than those in tooth cementum. In nearly all cases, individuals that were aged at half a year old expressed one or more growth marks. Only the humerus and femur of one skunk and raccoon had no growth lines although these were from different individuals. Most foxes at half a year of age had two growth marks while most skunks and raccoons of this age had approximately equal numbers of one and two growth marks. At one and a half years of age, foxes had between two and three growth marks, skunks had three to four (although two individuals had only one), and raccoons had three to four. Skunks at two and a half years of age had between four and five growth marks while raccoons had between four and six. The largest variance in growth mark number occurs at half a year of age for all species. This variance may be due to the sensitivity of young individuals to their nutritional and environmental conditions. Although the sample sizes are too small to analyze, variance in bone growth marks appears to decrease with age, suggesting that more mature individuals may be more resilient to bone growth interruptions.

All individuals were captured in the late fall or early winter, and young were born in the spring. The first few months of growth may have at least two factors influencing bone growth marks. Birth may be traumatic enough for these mammals to induce a growth mark in newborns. The earliest period of

growth is nurtured from their mother's milk and would be expected to not stress the young to deposit a growth mark. The late summer to early fall season is generally dry in this region of Ontario and may influence the formation of a growth mark due to the relatively poorer nutrition during this time. Thus, we could hypothesize that two growth marks would be relatively common in half-year olds. This pattern is found in nearly all the foxes and about half of the skunks and raccoons. Subsequent years of growth generally add one growth mark to each species and may be attributable to the harsh winters of the region and its impact on diet and physiology. One exception is a six and a half year old raccoon femur with only seven growth marks. This may be due to secondary remodeling of the bone's medullary surface that may have erased earlier growth marks. It is also possible that bone growth marks are also deposited in mothers as a consequence of gestation, birth, and nursing.

Two of the three species studied here, raccoons and skunks, undergo periods of torpor. It seems likely that such behavior may contribute to the formation of growth marks. However, the relationship between growth marks and age did not vary greatly between the foxes and the skunks and raccoons. Therefore, it seems that torpor behavior may not be the only trigger that causes growth marks.

Ultimately, skeletochronology may still be somewhat useful as a measure to age carnivorans and other mammals. However, it is clear that the relationship between the age of an animal and the number of growth lines visible in its longbones is not simply a one-to-one correspondence. The best that such measures could be used for in the three species that have been studied here is a comparison between populations. For instance, by measuring growth marks in two different populations of animals it would be possible to say if one population was, on average, older than the other. Such information can be valuable for ecological or palaeontological studies that compare assemblages of bones from large die-offs such as those that occur at river crossings to the general population of that species. Additional studies, particularly ones that include captive animals or capture-recapture methods, would allow better understanding of what the ratio may be and how robust it is between different species and populations. The use of skeletochronology in extant mammalian studies is not common, and those that do use it, do so with caution. However, it is still a commonly-used method in palaeontological studies (Chinsamy et al. 1994; Chinsamy and Dodson 1995; Chinsamy et al. 1998; Erickson et al. 2004; Horner and Padian 2004; Ray and Chinsamy 2004). It has been suggested that many non-avian dinosaurs had endotherm-like physiologies (Chinsamy and Dodson 1995; Schweitzer and Marshall 2001). If this is the case, then perhaps the use of skeletochronology in these species may not be as reliable as it is sometimes assumed to be.

Literature Cited

Allen, S. H. 1974. Modified techniques for aging red fox using canine teeth. . Journal of Wildlife Management 38.

Barker, J., R. Boonstra, and A. Schulte-Hostedde. 2003. Age determination in yellow-pine chipmunks (*Tamias amoenus*): a comparison of eye lens masses and bone sections. Canadian Journal of Zoology 81:1774-1779.

Castanet, J. 1985a. Skeletochronology in Reptiles. 1. Experimental-data about the signification of the skeletal growth marks among lizards and turtles. Annales des Sciences Naturelles. Zoologie et Biologie Animale 7:23-40.

Castanet, J. 1985b. Skeletochronology in Reptiles. 2. Experimental data about the signification of the skeletal growth marks among snakes.Comments on growth and longevity of Asp viper. Annales des Sciences Naturelles. Zoologie et Biologie Animale 7:41-62.

Castanet, J. 2006. Time recording in bone microstructures of endothermic animals; functional relationships. Comptes Rendus Biologies 5:629-636.

Castanet, J., S. Croci, F. Aujard, M. Perret, J. Cubo, and E. de Margerie. 2004. Lines of arrested growth in bone and age estimation in a small primate: *Microcebus murinus*. Journal of Zoology 263:31-39.

Castanet, J., H. Francillon-Vieillot, F. Meuner, and A. Ricqles de. 1993. Bone and individual aging. Pp. 245-283 *in* B. Hall, ed. Bone. CRC Press.

Catling, P. C., L. K. Corbett, and M. Westcott. 1991. Age Determination in the Dingo and Crossbreeds. Wildlife Research 18:75-83.

Chinsamy, A., L. M. Chiappe, and P. Dodson. 1994. Growth rings in Mesozoic birds. Nature 368:196-167.

Chinsamy, A., and P. Dodson. 1995. Inside a Dinosaur Bone. American Scientist 83:174-180.

Chinsamy, A., S. A. Hanrahan, R. M. Neto, and M. Seely. 1995. Skeletochronological Assessment of Age in Angolosaurus skoogi, a Cordylid Lizard Living in an Aseasonal Environment. Journal of Herpetology 29:457-460.

Chinsamy, A., L. Martin, and P. Dodson. 1998. Bone microstructure of the diving *Hesperornis* and the volant *Ichthyornis* from the Niobrara Chalk of western Kansas. Cretaceous Research 19:225-235.

Cooch, E. G., A. Dzubin, and R. F. Rockwel. 1999. Using body size to estimate gosling age. Journal of Field Ornithology 70:214-229.

Costain, D. B., and B. J. Verts. 1982. Age determination and age-specific reproduction in Belding's ground squirrels. Northwest Science 59:230-235.

Driscoll, K. M., G. S. Jones, and F. Nichy. 1985. An efficient method by which to determine age of carnivores, using dentine rings. Journal of Zoology 205:309-313.

Erickson, G., P. Makovicky, P. Currie, M. Norell, S. Yerby, and C. Brochu. 2004. Gigantism and comparative life-history parameters of tyrannosaurid dinosaurs. Nature 430:772-775.

Garshelis, D. L. 1984. Age Estimation of Living Sea Otters. The Journal of Wildlife Management 48:456-463.

Halliday, T. R., and P. A. Verrell. 1988. Body size and age in amphibians and reptiles. Journal of Herpetology 22:253-265.

Horner, J., A. de Ricqlès, and K. Padian. 1999. Variation in dinosaur skeletochronology indicators: implications for age assessment and physiology. Paleobiology 25:295-304.

Horner, J., and K. Padian. 2004. Age and growth dynamics of *Tyrannosaurus rex*. Proceedings. Biological sciences 271:1875-1880.

Humphrey, L.T., W. Dirks , M. C. Dean, and T.E. Jeffries. 2008. Tracking dietary transitions in weanling baboons (*Papio hamadryas anubis*) using strontium/calcium ratios in enamel. Folia Primatologica 79:197–212.

Jenks, J. A., R. T. Bowyer, and A. G. Clark. 1984. Sex and age-class determination for fisher using radiographs of canine teeth. The Journal of Wildlife Management 48:626-628.

Klevezal, G. A. 1972. Determination of age in birds by layers in the periosteal bone. Zoologicheskii Zhurnal 57:917–922.

Klevezal, G. A., and M. V. Mina. 1990. Daily layers and hibernation marks in incisor dentin of *Sicista pseudonapaea* and some biological remarks. Acta Theriologica 35:345-356.

Klomp, N. I., and R. W. Furness. 1992. A technique which may allow accurate determination of the age of adult birds. IBIS 134:245-249.

Laws, R. 1960. Laminated Structure of Bones from Some Marine Mammals. Nature 187:338-339.

Laws, R. M. 1953. The elephant seal (Mirounga leonina Linn.). H.M. Stationery Offices, London.

Leclair, R., and J. Castanet. 1987. A skeletochronological assessment of age and growth in the frog *Rana pipiens* Schreber (Amphibia, Anura) from Southwestern Quebec. American Society of Ichthyologists and Herpetologists 1987:361-369.

Linhart, S. B., and F. F. Knowlton. 1967. Determining age of coyotes by tooth cementum layers. The Journal of Wildlife Management 31:362-365.

Machias, A., E. Maraveyia, M. Pavlidis, S. Somarakis, and P. Divanach. 2002. Validation of annuli on scales and otoliths of common dentex (*Dentex dentex)*. Fisheries Research 54:287-294.

Marmontel, M., T. J. O'Shea, H. I. Kochman, and S. R. Humphrey. 1996. Age determination in manatees using growth-layer-group counts in bone. Marine Mammal Science 12:54-88.

McRoberts, R. E., R. T. Brooks, and L. L. Rogers. 1998. Using nonlinear mixed effects models to estimate size-age relationships for black bears. Canadian Journal of Zoology 76:1098-1106.

Millar, J. S., and F. C. Zwickel. 1972. Determination of age, age structure, and mortality of the pika, *Ochotona princeps* (Richardson). Canadian Journal of Zoology 50:229-232.

Misawa, Y., and M. Matsui. 1999. Age determination by skeletochronology of the Japanese salamander *Hynobius kimurae* (Amphibia, Urodela). Zoological science 16:845-851.

Morris, P. 1972. A review of mammalian age determination methods. Mammal Review 2:69-104.

Ray, S., and A. Chinsamy. 2004. *Diictodon feliceps* (Therapsida, Dicynodontia): Bone histology, growth, and biomechanics. Journal of Vertebrate Paleontology 24:180-194.

Roberson, N. E., D. K. Kimura, D. R. Gunderson, and A. M. Shimada. 2005. Indirect validation of the age-reading method for Pacific cod (*Gadus macrocephalus)* using otoliths from marked and recaptured fish. Fishery Bulletin 103:153-160.

Root, D. A., and N. F. Payne. 1984. Evaluation of Techniques for Aging Gray Fox. The Journal of Wildlife Management 48:926-933.

Wright, L.E., and H.P. Schwarcz. 1998. Stable carbon and oxygen isotopes in human tooth enamel: identifying breastfeeding and weaning in prehistory. American Journal of Physical Anthropology 106:1–18.

Schweitzer, M. H., and C. L. Marshall. 2001. A molecular model for the evolution of endothermy in the theropod- bird lineage. Journal of Experimental Zoology (Molecular Development and Evolution) 291:317-338.

Smith, T. M., and P. Tafforeau. 2008. New visions of dental tissue research: tooth development, chemistry, and structure. Evolutionary Anthropology 17:213-226.

Strong, D. R. 1992. Are trophic cascades all wet? Differentiation and donor-control in speciose ecosystems. Ecology 73:747-754.

Chapter 3

The effects of Phylogeny, Function and Physiology in Carnivoran bone microstructure

Bridging Text

This chapter is in manuscript format in preparation for its submission to a peer-reviewed journal. This chapter aims to evaluate the role that phylogeny, function and physiology play in the formation of bone microstructure. Using seven species from the order Carnivora, a variance partitioning method is used to determine the effects of each of these factors.

Abstract

The structure of bone is influenced by the physiological and functional demands placed upon it as well as the organism's phylogenetic history. These three factors do not act independently, however; the shared influence of the three factors further influence bone structure. In this study, the long bone microstructure was described for seven species of carnivore, a group for which bone microstructure has not been previously described. The variance in the observed microstructural characteristics was then partitioned among the three influencing factors - phylogeny, function and physiology - and their shared influence. It was found that while phylogeny has a significant impact on bone microstructural characteristics its effect is mainly through shared variance between function and physiology. The effects of function and physiology were smaller but also highly shared. The factor with the largest "pure" effect was physiology.

Introduction

Bone is a complex tissue that has both biomechanical and physiological functions. It is also the product of many years of evolutionary history. It is not surprising then that bone structure is affected by the biomechanical function it

has, the physiological environment it experiences and the evolutionary history of the organism in which it was formed.

The structuring of bone in response to functional demands was first identified by Julius Wolff (1892) and is therefore often referred to as "Wolff's law." Wolff described the relationship in terms of macrostructural changes in bone shape in response to repetitive strain. However, many think of his "law" in broader terms that encompass all aspects of bone micro and macrostructure. Evidence for Wolff's law has been found in a wide variety of species, from sheep to humans (Chamay and Tschantz 1972; Woo et al. 1981; Frost 2003; Lieberman et al. 2003; Habib and Ruff 2008). However, Wolff's law is anything but a simple structure-function relationship as there are many other factors that can influence how a bone responds, or whether it responds at all, to a functional demand (Pearson and Lieberman 2004; Ruff et al. 2006).

The physiological environment in which a bone forms is also of importance to bone structure. It has been shown that the microstructure of bone, particularly the orientation of collagen fibers and vasculature, can change depending upon the rate at which it was deposited (de Ricqlès et al. 1991; de Margerie et al. 2002; de Margerie et al. 2004). This relationship was first described by Amprino in 1947 and for that reason is often referred to as "Amprino's rule." However, like Wolff's law, Amprino's rule is not completely consistent in all situations. Different skeletal elements observed within the

same individual can show vastly different arrangements of vascular canals and collagen fibers while presumably the overall growth rate was consistent throughout the entire animal (de Margerie 2002; Habib and Ruff 2008).

The third factor that may influence bone micro- and macro-structure is the evolutionary history of the organism in which the bone is formed. While not given the designation of a "law" or "rule" it has been found that bone microstructure characteristics can be mapped to phylogeny, at least in sauropsids (Cubo et al. 2005). However, as with functional and physiological influences, phylogeny alone does not dictate bone structure. Cubo and colleagues (2008) found that bone growth rate has a significant phylogenetic signal but that this signal is strongly influenced by functional and structural characteristics of the bone.

It seems that while we can confidently claim that phylogeny, function and physiology can all impact bone structure individually, the impacts of shared variance between these factors are unknown.

In this study we look at microstructural and macrostructural characteristics in seven species of mammalian carnivores and use variation partitioning to determine the fraction of the variation in these characteristics that is explained by phylogeny, function, physiology and their shared variance. Also, as bone microstructure has been characterized in very few mammals and not

at all for any of the species studied here, an extensive description of their bone microstructure is also included.

Materials and Methods

Bone sectioning and observation

The humerii and femora of seven species of carnivorans were obtained from the Ministry of Natural Resources in Ontario, the Ministry of Sustainable Resource Development in Alberta and the Ministry of the Environment in the Yukon. All animals had been sacrificed as part of a fur trapping program or as part of a rabies research program. All muscle and connective tissues were removed and the bones were allowed to dry in a fume hood for at least one week. One strand of copper wire (20 gauge) was adhered to the cranial and medial surfaces of the bone, while two strands were adhered to the caudal surfaces to facilitate bone section orientation. Bones with attached wires were then embedded in an epoxy resin (Buehler Epothin) and sectioned transversely at the midshaft using a precision saw with a diamond bit blade (Isomet 1000, Buehler, Lake Bluff, Illinois, USA). Bone bone sections were taken at the midshaft because this is the region of long bones that experience peak stress *in vivo* (Lanyon et al. 1979). If bone microstructure is associated with bone biomechanics, the midshaft region of long bones is expected to be better associated with bone microstructure than other regions, such as the

epiphyses. The resulting sections were bonded to a glass slide using a cyanoacrylate adhesive. The sections were viewed under 40x magnification under a compound light microscope (Nikon Optiphot, Japan) and photographed using a digital camera (QICAM Fast 1394, QImaging, Surrey BC, Canada). The photos did not image a full cross section of the bone so several overlapping photos were taken of each sample and combined in Adobe Photoshop (Adobe Systems Inc., USA) manually.

From these magnified cross-sections, measures of cross-sectional area, maximum and minimum second moment of area (Imax and Imin) and polar moment of inertia(J) were calculated in Image J (National Institutes of Health, USA) using a custom macro. These were all corrected for animal size by dividing by bone length squared. The second moments of area are an estimation of the bone's ability to resist bending along the axis in question. The polar moment of inertia is an estimation of the bone's ability to resist torsion.

Bone Microstructure Measures

The orientation of the vasculature was measured using the radial index (RI) and longitudinal index(LI) (de Boef and Larsson 2007) which give a quantitative measure of each vascular canal's orientation within the plane of section and perpendicular to the plane of section respectively. These indices are in gradians which, for RI, gives a value of 100 for a vascular canal oriented

perpendicular to the periosteal surface and a value of 0 for a vascular canal oriented parallel to it. Similarly, LI gives a value of 100 for a vascular canal oriented perpendicular to the plane of section and a value of 0 for a vascular canal oriented parallel to the plane of section. These two indices were measured for every vascular canal in each bone section using a custom program in MATLAB.

The density of osteocytes was measured for each quadrant of the bones: cranial, caudal, medial and lateral (dorsal and ventral in the humerus). Images of each were imported into ImageJ and osteocyte lacunae were counted using the analyze particles function.

Statistical Analysis

The method of variation partitioning used by Cubo et al. (2008) and described by Desdevises (2003) was used here. This method partitions the total variation found in a dependent variable into the components explained by two or more explanatory variables. In this case we used three such variables: phylogeny, function and physiology (Figure 3-1). Both the dependent and the explanatory variables can consist of a vector or a matrix of values. Here, the following three dependent variables were examined in separate analyses:

Y1-Vascular Orientation

Vascular orientation was examined as a matrix of RI and LI values.

Y2-Osteocyte Density

Osteocyte density was examined as a vector.

Y3-Bone geometry

Bone geometry was examined as a matrix of Imax, Imin, J and cross sectional area values.

The following three explanatory variables were used in each analysis:

X1-Phylogeny

A matrix of the phylogenetic relationships between the species is expressed as principal coordinates. These values are obtained by performing a principal coordinate analysis (PCoA: Gower 1966) using a phylogenetic distance matrix. The distance matrix employed was calculated using the branch lengths and phylogenetic relationships presented by Fulton and Strobeck (2006) and the "cophenetic.phylo" function in the "ape" library for R (R Development Core Team, Vienna, Austria). This function computes the pairwise distances between the pairs of tips from a phylogenetic tree using its branch lengths. The principal coordinates were then calculated using the "pcoa" function in the "PCNM" library. This function takes the input matrix giving dissimilarities between pairs of items and outputs a coordinate matrix whose configuration minimizes a loss function. It does this by computing the eigenvectors corresponding to all eigenvalues, positive and negative, using matrix algebra.

The resulting distance matrix gives the was found to be Euclidean, giving only positive eigen values in the PCoA and therefore no correction was necessary.

X2-Function

Two components were included into the function matrix: a discrete variable for climbing behavior and a numerical value of home range. Home range data was collected from Muñoz-Garcia and Williams (2005), while data on climbing behavior was derived from Gittleman and Harvey (1982) and Gittleman (1986).

X3-Physiology

Two components were included into the physiology matrix: a discrete variable for hibernation or winter torpor behavior and a numerical value of basal metabolic rate. Hibernation or torpor behavior was derived from various sources (Johnson 1931; Banci 1981; Harris and Ogan 1997) as was basal metabolic rate (Davison et al. 1978; Knudsen and Jr. 1990; Muñoz-Garcia and Williams 2005).

Variation partitioning was performed three times (once for each dependent variable) using the "varpart" function in the "vegan" library for R. The resulting adjusted residual (R_a^2) values represent the proportion of variance in the dependent variable explained by the fractions of the explanatory variables as seen in Figure 3-1. Some of these R_a^2 can be tested for

significance using the “rda” and “anova” functions as explained in the “varpart” help file.

Results

Descriptions of the bone macrostructural and microstructural characteristics for each of the seven species studied are included below. Descriptions of vascular orientation follow the nomenclature outlined in de Ricqlès *et al.* (1991). All quantitative values presented below refer to the mean value for all samples of each species followed by the standard deviation. The descriptions are followed by a summary of results of the statistical analyses that were outlined in the materials and methods and which describe the relationships between the various explanatory variables and the bone morphology metrics.

Bone Descriptions

Wolverine Bone Description

The mean length of the femora of wolverines used in this study was 141.8±9.6mm. Transverse sections at midshaft were fairly circular with an average mediolateral diameter of 13.7mm (Figure 3-2). There was some evidence of periodic growth marks with one individual having 5 such marks,

but all others evinced few or none. The age of the animals was not known and thus it cannot be determined if these growth marks are related to annual cessation or slowing of growth or some other factor. There was no evidence of secondary reconstruction in wolverine femora. The bones were highly vascularized, and both the size and orientation of the vascular canals showed a great degree of variation within individuals. In general, the layer of bone closest to the medullary cavity contained radially oriented vascular canals. Moving away from the medullary surface, vascular canals became more laminar and then more longitudinal. The outer most layer of bone, that closest to the periosteal surface, was often avascular or contained a small number of laminar vascular canals. This vascular canal organization was quantified as having an average RI of 36.5±2.8 gradians and an average LI of 27.7±3.1 gradians. The mean cortical area of the wolverine femora observed here was 72.5±3.5mm^2. The mean maximum and minimum second moment of area measured were 705±108mm^4 and 577±94mm^4 respectively. The corresponding mean polar moment of inertia was recorded as 1282±188mm^4. Osteocyte density was highly variable with a mean of 1212 osteocytes*mm^{-2} but a standard deviation of 980 osteocytes*mm^{-2}.

The mean length of the wolverine humerii used in this study was 143.7±25.5mm. Transverse sections at midshaft showed a protuberance on the cranio-lateral surface which corresponded to the deltoid tuberosity (Figure

3-2). Bones often showed a great number and complex arrangement of trabecular struts in the medulla although these were sometimes lost as part of the sectioning process. Growth marks were often present with up to 6 being visible in one individual while others did not show any evidence of growth marks. Some specimens showed evidence of secondary reconstruction, particularly on the medullary surface directly across from the protuberance on the cranio-lateral surface. The bones were highly vascularized and both the size and orientation of the vascular canals showed a great degree of variation within individuals. In general, vascular canals had a highly reticulate organization near the medullary surface and became more longitudinally organized near the periosteal surface. On the cranial surface vascular canals were nearly entirely longitudinal. This vascular canal organization was quantified as having a RI of 42.6±2.7 gradians and a LI of 29.2±1.0 gradians. The mean cortical area of the wolverine humeri observed here was 79.4±14.3mm^2. The mean maximum and minimum second moment of area measured were 1065±234mm^4 and 928±299mm^4 respectively. The corresponding mean polar moment of inertia was recorded as 1994±393mm^4. Osteocyte density was both very large and highly variable having a mean of 5886 osteocytes*mm^{-2} but a standard deviation of 5055 osteocytes*mm^{-2}.

Red Fox Bone Description

The mean length of the fox femora used in this study was 125.0±5.9mm. Transverse sections at midshaft were fairly circular (Figure 3-3) with a small extension on the latero-caudal surface likely corresponding to the location of the linea aspera. Most individuals had growth marks. The relationship of these to the age of the animals (as measured using tooth cementum annuli) is discussed in Chapter 2. There was no evidence of secondary reconstruction in fox femora. The bones were vascularized and usually in a reticular arrangement. Often the caudal region of the bone had a series of radial canals radiating from the medullary surface and an arrangement of laminar vasculature on the cranial region closest to the medullary cavity. This vascular canal organization was quantified as having a RI of 41.1±2.1 gradians and a LI of 17.0±2.1 gradians. The mean cortical area of the fox femora observed here was 31.2±0.8mm^2. The mean maximum and minimum second moment of area measured were 245±9mm^4 and 173±1mm^4 respectively. The corresponding mean polar moment of inertia was recorded as 418±19mm^4. Osteocyte density was highly variable, having a mean of 311 osteocytes*mm^{-2} and a standard deviation of 351 osteocytes*mm^{-2}.

The mean length of the fox humeri used in this study was 131.7±4.3mm (Figure 3-3). Growth marks were often present and the relationship between these and the age of the animal is discussed in Chapter 2. None of the individuals studied here showed evidence of secondary

reconstruction in this element. The bones were vascularized with the orientation varying a great deal over the cross-section of the bone. In general, vascular canals had a highly radial organization in the region of the bone nearest to the medullary surface. Between the medullary and periosteal surface the vascular canals were organized in a highly reticular manner. In the cranio-medial region the vascular canals became more laminar near the periosteum. The entire bone section showed somewhat avascular bone with sparse radial canals in the region closest to the periosteum. This vascular canal organization was quantified as having a RI of 40.3±2.5 gradians and a LI of 17.6±2.9 gradians. The mean cortical area of the fox humerii observed here was 34.3±1.5mm^2. The mean maximum and minimum second moment of area measured were 275±17mm^4 and 212±16mm^4 respectively. The corresponding mean polar moment of inertia was recorded as 488±32mm^4. Osteocyte density was found to be 8002±886 osteocytes*mm^{-2}.

Raccoon Bone Description

The mean length of the raccoon femora used in this study was 100.0±11.9mm. Transverse sections at midshaft were fairly circular (Figure 3-4). Most individuals had growth marks and the relationship of these to the age of the animals (as measured using tooth cementum annuli) is discussed in Chapter 2. There was some evidence of secondary reconstruction in near the medullary cavity in these bones. The numerous vascular canals of raccoon

femora are quite uniformly arranged throughout the bone section showing a reticular pattern with a high concentration of radial canals. This vascular canal organization was quantified as having a RI of 51.6±1.5 gradians and a LI of 19.2±1.9 gradians. The mean cortical area of the raccoon femora observed here was 37.4±7.6mm^2. The mean maximum and minimum second moment of area measured were 426±180mm^4 and 260±105mm^4 respectively. The corresponding mean polar moment of inertia was recorded as 687±284mm^4. Osteocyte density was very high, with a mean of 3031 osteocytes*mm^{-2} and a standard deviation of 1867 osteocytes*mm^{-2}.

The mean length of raccoon humeri used in this study was 102.6±17.9mm (Figure 3-4). The section was ovoid in shape, being elongate along the craniomedial-caudolateral axis and narrowing towards the craniomedial portion of the section. Growth marks were often present and the relationship between these and the age of the animal is discussed in Chapter 2. None of the individuals studied here showed evidence of secondary reconstruction in this element. The bone was relatively avascular at both the medullary and the periosteal surfaces. The region between these areas showed a relatively uniform reticular organization of the vascular canals. This vascular canal organization was quantified as having a RI of 55.6±2.9 gradians and a LI of 13.7±0.4 gradians. The mean cortical area of the raccoon humeri observed here was 35.3±3.8mm^2. The mean maximum and minimum second

moment of area measured were 222±36mm^4 and 106±21mm^4 respectively. The corresponding mean polar moment of inertia was recorded as 328±49mm^4. Osteocyte density was found to be 309±256 osteocytes*mm^{-2}.

Striped Skunk Bone Description

The mean length of the skunk femora used in this study was 58.7±3.7mm. Transverse sections at midshaft showed an extensive protuberance on the caudal surface likely corresponding to the linea aspera (Figure 3-5). Most individuals had growth marks and the relationship of these to the age of the animals (as measured using tooth cementum annuli) is discussed in Chapter 2. The bone tissue near and in the protuberance was highly disorganized and the few vascular canals within were large and longitudinally arranged. The remainder of the bone was highly avascular, although the bone nearest the periosteal surface showed several radially arranged canals. This vascular canal organization was quantified as having a RI of 59.4±0.8 gradians and a LI of 24.3±2.9 gradians. The mean cortical area of the skunk femora observed here was 23.2±3.0mm^2. The mean maximum and minimum second moment of area measured were 81±7mm^4 and 53±6mm^4 respectively. The corresponding mean polar moment of inertia was recorded as 134±12mm^4. Osteocyte density was very high with a mean of 1074 osteocytes*mm^{-2} and a standard deviation of 719 osteocytes*mm^{-2}.

The mean length of skunk humeri used in this study was 66.8±6.0mm. (Figure 3-5). The section was extremely ovoid in shape with the long axis along the cranial-caudal axis and narrowing towards the cranial portion of the section. A prominent protuberance was located slightly lateral of the caudal margin of the section. Growth marks were often present and the relationship between these and the age of the animal is discussed in Chapter 2. None of the individuals studied showed evidence of secondary reconstruction in this element. The medullary cavity showed evidence of many trabeculae; however, many of these were lost during the sectioning process and cannot be accurately described here. The bone was quite disorganized at both the cranial and caudal surfaces. Both regions were quite avascular although the caudal region was less so, with the protuberance on this surface showing many longitudinal vascular canals. The lateral portion of the bone sections contained many radially organized vasculature while those on the medial surface were arranged longitudinally. This vascular canal organization was quantified as having a RI of 51.5±2.1 gradians and a LI of 19.7±2.1 gradians. The mean cortical area of the raccoon humerii observed here was 23.6±2.1mm^2. The mean maximum and minimum second moment of area measured were 117±13mm^4 and 53±4mm^4 respectively. The corresponding mean polar moment of inertia was recorded as 170±15mm^4. Osteocyte density was found to be 1165±746 osteocytes*mm^{-2}.

Ermine Bone Description

The mean length of the ermine femora used in this study was 31.4±1.5mm. Transverse sections at midshaft were nearly circular (Figure 3-6). Several individuals were found to have growth marks; however, the age of these animals was unknown. Whether it would be possible to age these animals using skeletochronology is not known. The bones had few vascular canals, and those that were present were nearly all oriented radially from the medullary cavity outwards. This vascular canal organization was quantified as having a RI of 76.9±2.3 gradians and a LI of 10.8±0.9 gradians. The mean cortical area of the ermine femora observed here was 2.0±0.5mm^2. The mean maximum and minimum second moment of area measured were 1.1±0.4mm^4 and 0.8±0.3mm^4 respectively. The corresponding mean polar moment of inertia was recorded as 1.8±0.6mm^4. Osteocyte density had a mean of 1016 osteocytes*mm^{-2} and a standard deviation of 773 osteocytes*mm^{-2}.

The mean length of ermine humeri used in this study was 30.1±1.7mm. (Figure 3-6). The midshaft transverse cross-section was ovoid in shape, being elongate along the craniolateral-caudomedial axis and narrowing towards the caudomedail portion of the section. Growth marks were present in a few individuals. None of the individuals studied here showed evidence of secondary reconstruction in this element. Vascular canals were sparse throughout the bone, with the few vascular canals that were present showing

a primarily radial orientation. This vascular canal organization was quantified as having a RI of 61.2±3.7 gradians and a LI of 12.0±3.7 gradians. The mean cortical area of the ermine humerii observed here was 1.9±0.2mm^2. The mean maximum and minimum second moment of area measured were 0.74±0.1mm^4 and 0.50±0.05mm^4 respectively. The corresponding mean polar moment of inertia was recorded as 1.2±0.1mm^4. Osteocyte density was found to be 922±783 osteocytes*mm^{-2}.

Fisher Bone Description

The mean length of the fisher femora used in this study was 102.0±7.2mm. Transverse sections at midshaft were nearly circular (Figure 3-7). Nearly all individuals showed growth marks but without knowing the age of the animal we were unable to determine if these represent annual marks or something else. The vasculature was oriented mainly radially particularly in regions close to the medullary surface. There were some laminar and reticular vascular canals but few longitudinal canals. Bone adjacent to the periosteal surface was often avascular. This vascular canal organization was quantified as having a RI of 49.7±2.2 gradians and a LI of 16.2±1.9 gradians. The mean cortical area of the fisher femora observed here was 28.9±1.7mm^2. The mean maximum and minimum second moment of area measured were 158.4±12.6mm^4 and 265.6±54.4mm^4 respectively. The corresponding mean polar moment of inertia was recorded as 424.0±57.3mm^4. Osteocyte density

had a mean of 1207 osteocytes*mm^{-2} and a standard deviation of 1085 osteocytes*mm^{-2}.

The mean length of fisher humerii used in this study was 92.7±6.9mm. (Figure 3-7). The midshaft transverse cross-section was ovoid in shape, being elongate along the cranial-caudal axis with a slight point on the cranial surface. Growth marks were present in most individuals but independent measures of age were unavailable and thus it is not known if these are annual marks. The region of bone closest to the medullary surface had few vascular canals and those that were present had a radial orientation. This region of low vascular density was thicker on the cranio-lateral region. The remainder of the bone showed a very dense network of reticular vascular canals. This vascular canal organization was quantified as having a RI of 47.1±1.9 gradians and a LI of 13.8±0.4 gradians. The mean cortical area of the fisher humerii observed here was 29.5±10.0mm^2. The mean maximum and minimum second moment of area measured were 210.0±10mm^4 and 137.4 ±4.5mm^4 respectively. The corresponding mean polar moment of inertia was recorded as 1.2±0.1mm^4. Osteocyte density was found to be 1082±764 osteocytes*mm^{-2}.

American Marten Bone Description

The mean length of the marten femora used in this study was 65.9±4.0mm. Transverse sections at midshaft were nearly circular (Figure 3-8) but had a small protuberance near the caudal surface and likely corresponded

to the linea aspera. Growth marks were faint when present but were generally rare. Vasculature was sparse and mainly oriented longitudinally with the occasional radial or laminar vascular canal. This vascular canal organization was quantified as having a RI of 43.1±1.6 gradians and a LI of 27.2±2.6 gradians. The mean cortical area of the marten femora observed here was 7.7±0.1mm^2. The mean maximum and minimum second moment of area measured were 12.8±0.4mm^4 and 9.7±0.25mm^4 respectively. The corresponding mean polar moment of inertia was recorded as 22.5±0.6mm^4. Osteocyte density had a mean of 630 osteocytes*mm^{-2} but varied extensively with a standard deviation of 624 osteocytes*mm^{-2}.

The mean length of the humerii of the marten used in this study was 59.6±3.8mm (Figure 3-8). The midshaft transverse cross-section was nearly circular in shape with a slight extension and roughening near the periosteum on the cranio-lateral surface. This feature also showed evidence of secondary reconstruction which was not evident elsewhere in the bone. Growth marks were present in most individuals but independent measures of age were unavailable and thus it is not known if these are annual marks. The region of bone closest to the medullary surface had relatively few vascular canals, and those present were mainly oriented radially. In the remainder of the bone, vascular canals were equally sparse but oriented in a more reticular pattern. Near the protuberance on the cranio-lateral surface the vascular canals

became somewhat more longitudinally oriented. This vascular canal organization was quantified as having a RI of 41.3±2.0 gradians and a LI of 21.6±0.8 gradians. The mean cortical area of the fisher humerii observed here was 8.1±0.7mm^2. The mean maximum and minimum second moment of area measured were 8.7±1.3mm^4 and 6.7 ± 0.9mm^4 respectively. The corresponding mean polar moment of inertia was recorded as 15.4±2.1mm^4. Osteocyte density was as varied as the femora and found to be 570±669 osteocytes*mm^{-2}.

Statistical Analyses

The explanatory variables used in the functional and physiological explanatory matrices (X2 and X3 respectively) are summarized in Table 3-1. A summary of means and standard deviations of the metrics used to quantify bone micro- and macro-structure is shown in Table 3-2. A full list of all measures for all individuals is found in Appendix 2.

Bone Vascular Orientation

Table 3-3 shows the relative contributions of phylogenetic history, physiological traits and functional demands on the orientation of bone vasculature as measured by RI and LI. Much of the variation in the vascular orientation between these groups can be explained by the three explanatory matrices (phylogeny, physiology and function) leaving only 5% of the variation

unexplained. However, much of the fraction of the variation explained by the three matrices is attributable to various combinations of these factors. In the humerus, the purely phylogenetic fraction accounts for a small portion of the variation (R_a^2=0.1455, p≤0.005), while the purely functional and physiological fractions do not explain any of the variation seen in this element. In the femur, a large portion of variation is explained by purely physiological factors (R_a^2=0.23384, p≤0.005), a small component by pure phylogenetics (R_a^2=0.07932, p≤0.005) and very little by purely functional factors (R_a^2=0.01260, p≤0.005). Clearly, the shared variance between the phylogenetic, functional and physiological factors has a much greater impact on vascular orientation than any of these components individually.

Osteocyte density

Table 3- 4 shows the relative contributions of phylogenetic history, physiological traits and functional demands on the density of osteocytes found in the cortex of the bone cross sections studied. Very little of the variation seen in osteocyte density can be explained by the explanatory matrices used here (R_a^2=0.11782, p=0.01 in the humerus, R_a^2=0.29171, p≤0.005 in the femur). In both skeletal elements, phylogeny alone explained around 6% of the variation. In the humerus, neither the purely functional nor purely physiological fractions contributed to the total variation. In the femur, however, purely physiological factors explained a large portion of the variation

(R_a^2=0.21938, p≤0.005). Unlike vascular orientation, the shared variance between phylogeny, function and physiology did not explain a significant portion of the variation (no greater than R_a^2=0.11782 in the humerus, R_a^2=0.29171 in the femur).

Bone geometry

Table 3-5 shows the relative contributions of phylogenetic history, physiological traits and functional demands on the measures of bone geometry taken for this sample. The explanatory factors explain all but 7%of the variation in the humerus and all but 17% in the femur. In the humerus, individual factors explain very little of the variation alone, with the purely phylogenetic fraction explaining 4%, the physiological and functional fractions explaining none of the variation. In combination, however, the three factors explain most of the variation (R_a^2=0.93315, p≤0.005). In the femur the contributions of the purely phylogenetic and purely physiological factors are larger (R_a^2=0.18917, p≤0.005 and R_a^2=0.22319, p≤0.005 respectively). The shared variance between the factors is larger in the humerus with all of the variation explained by these elements being related to an shared variance.

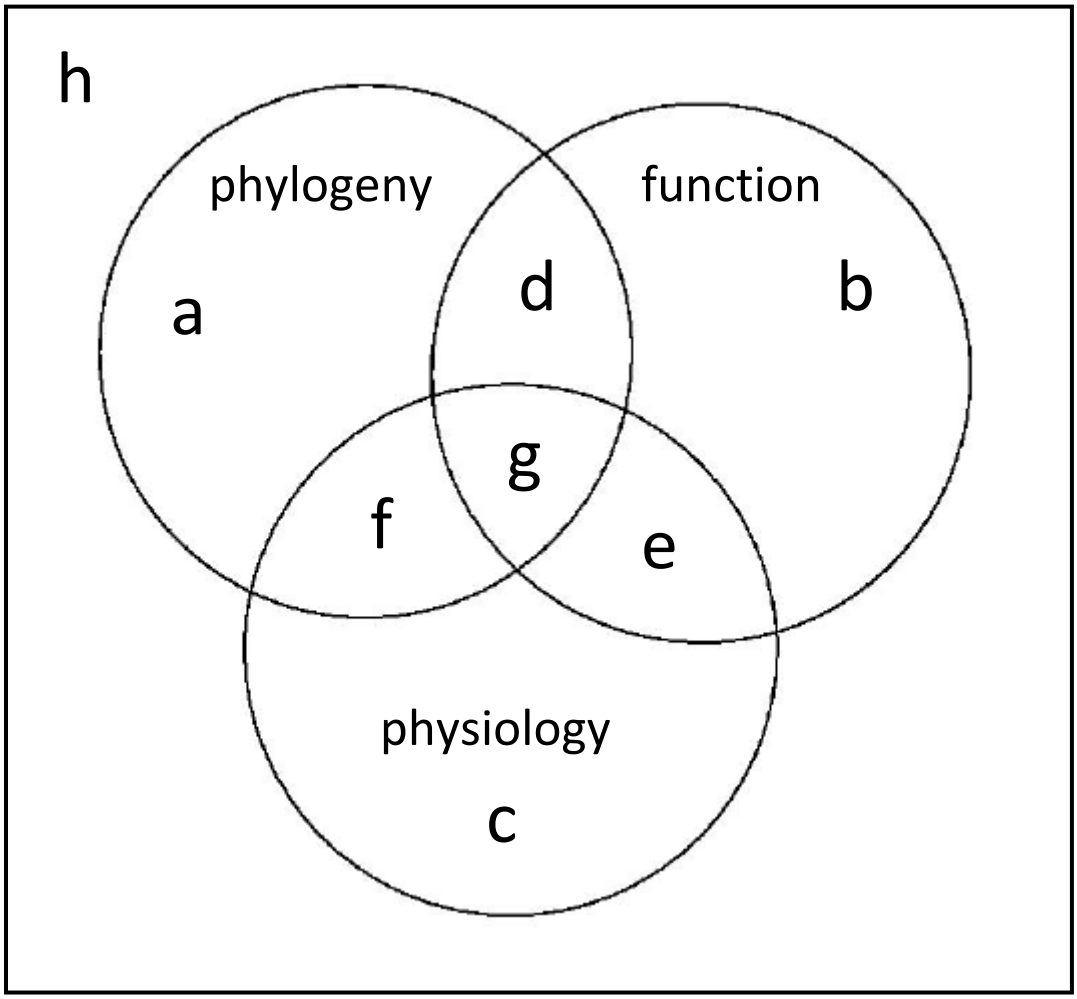

Figure 3-1: A schematic of the partitions assigned to each explanatory variable in the partitioning analysis. Total variation is represented by the outer box. The variation explained by phylogeny is represented by region (a+d+f+g) with the variation explained by "pure" phylogeny (no effect of function or physiology) represented by region (a). The variation explained by function is represented by region (b+d+e+g) with the variation explained by "pure" function (no effect of phylogeny or physiology) represented by region (b). The variation explained by physiology is represented by region (c+e+f+g) with the variation explained by "pure" physiology (no effect of phylogeny or function) represented by region (c). The unexplained variation is represented by region (h).

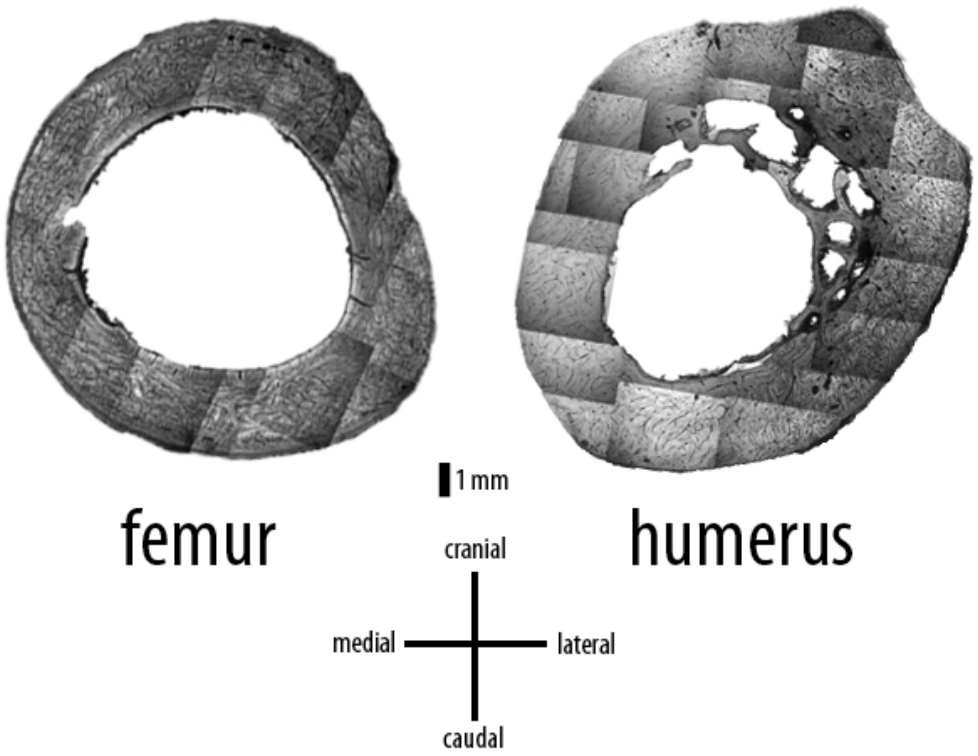

Figure 3-2: Representative mid-diaphyseal transverse cross-sections of the femur and humerus of a wolverine (*Gulo gulo)*

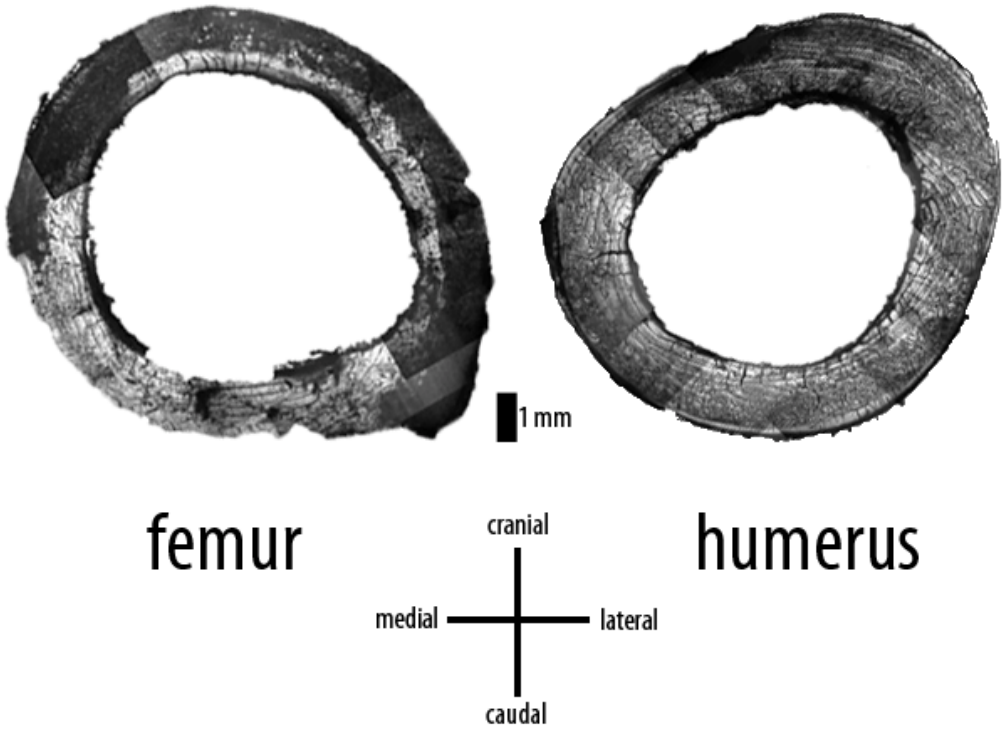

Figure 3-3: Representative mid-diaphyseal transverse cross-sections of the femur and humerus of a fox (*Vulpes vulpes*)

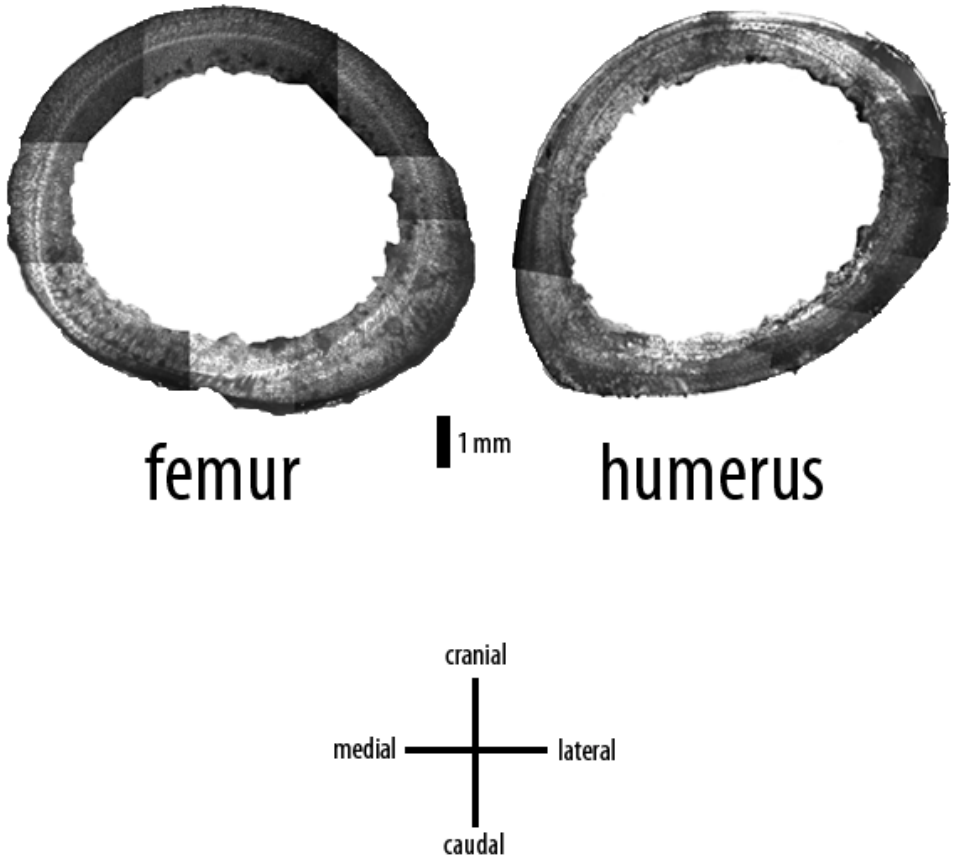

Figure 3-4: Representative mid-diaphyseal transverse cross-sections of the femur and humerus of a raccoon (*Procyon lotor*)

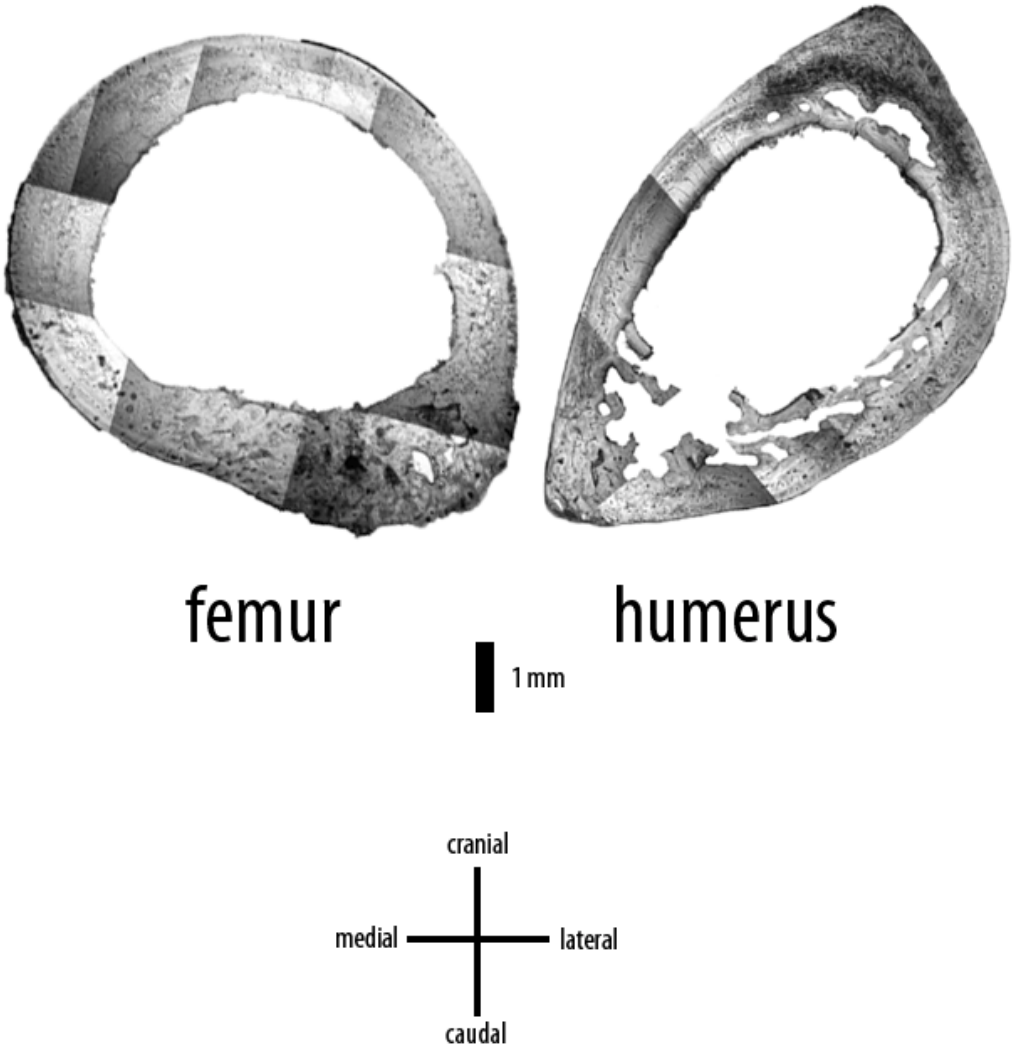

Figure 3-5: Representative mid-diaphyseal transverse cross-sections of the femur and humerus of a skunk (*Mephitis mephitis*)

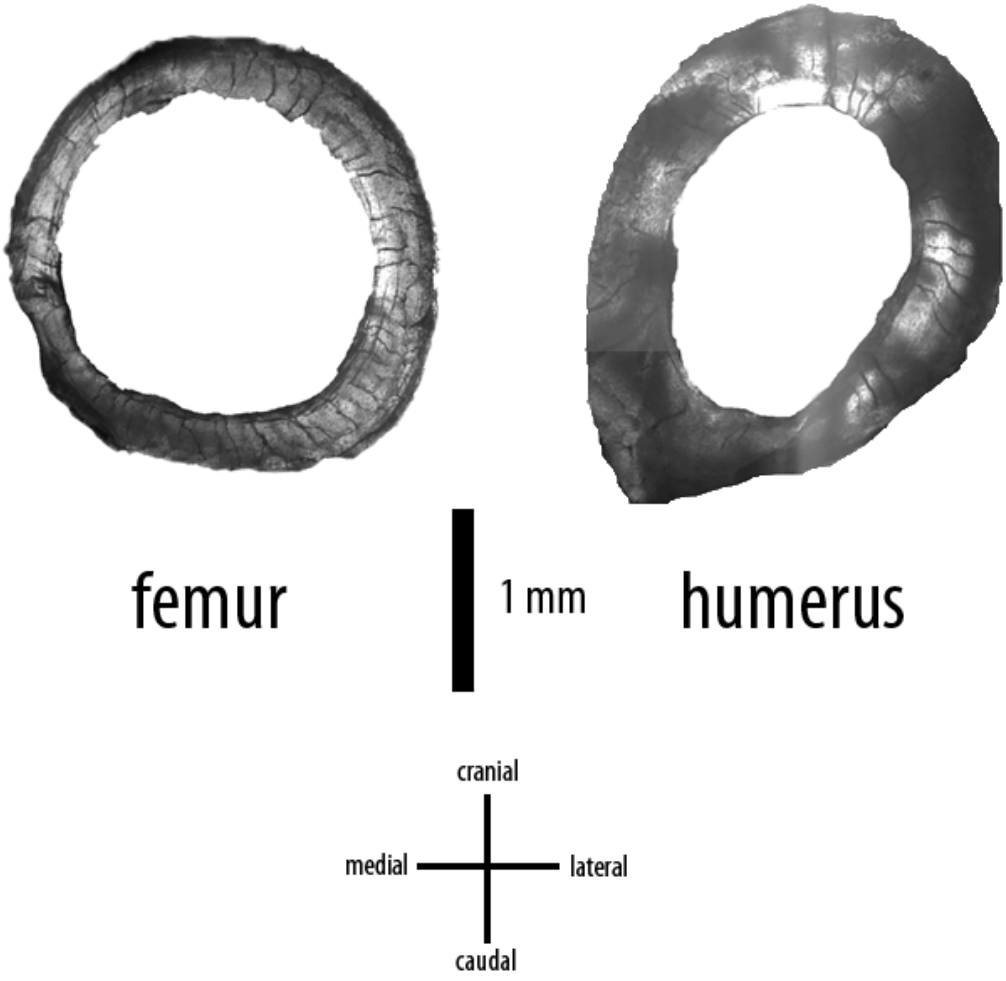

Figure 3-6: Representative mid-diaphyseal transverse cross-sections of the femur and humerus of a ermine (*Mustela erminea*)

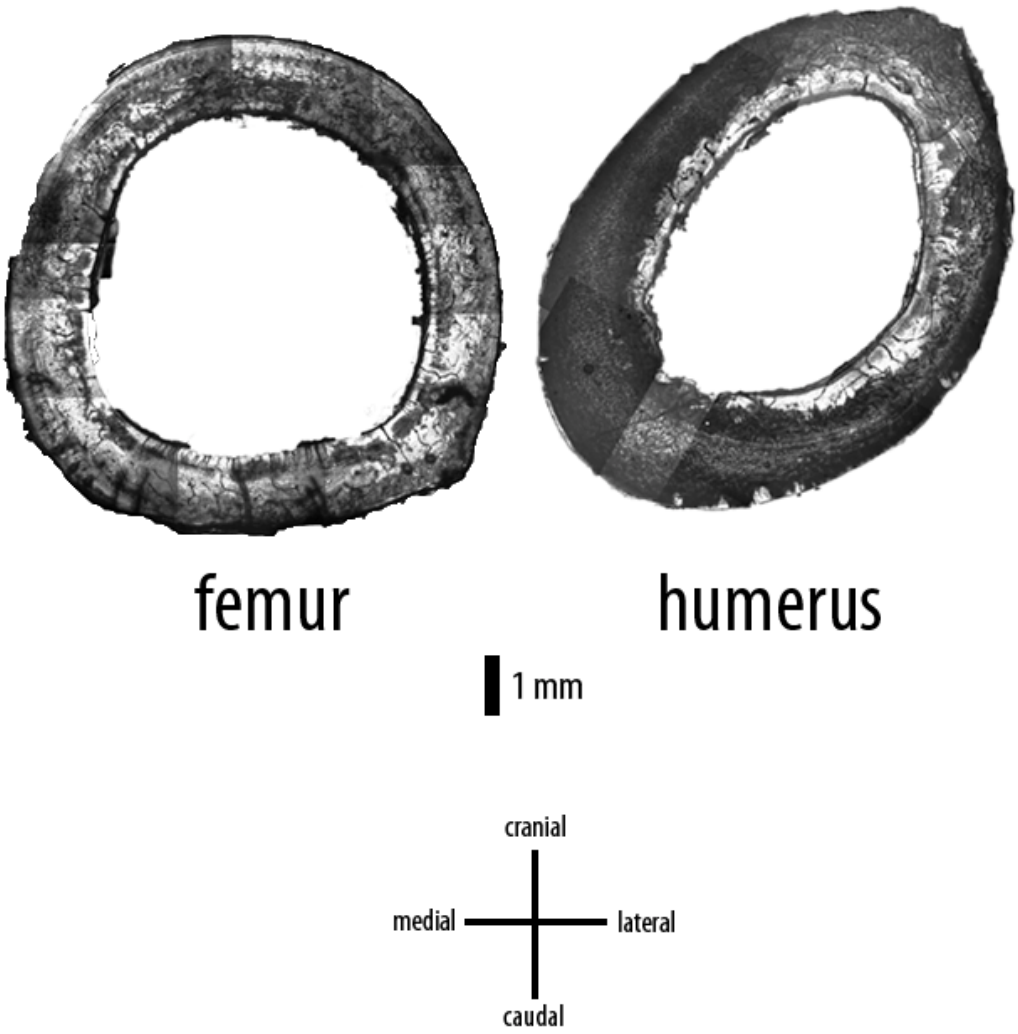

Figure 3-7: Representative mid-diaphyseal transverse cross-sections of the femur and humerus of a fisher (*Martes pennanti*)

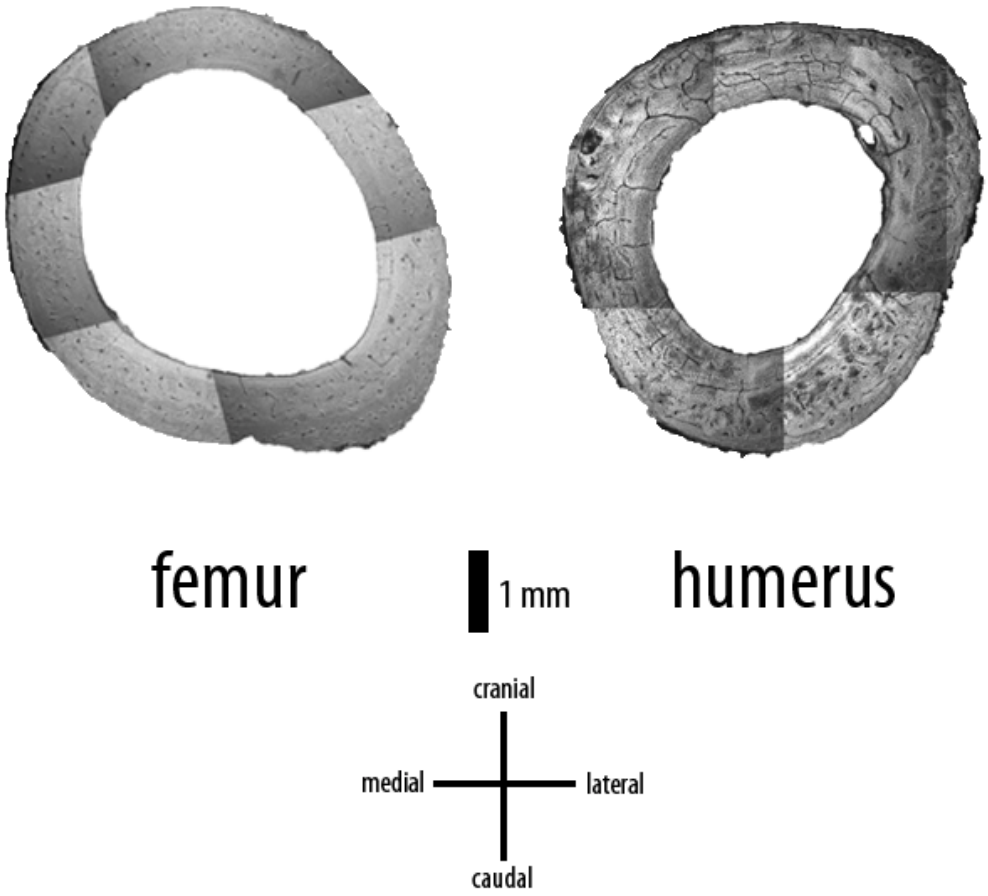

Figure 3-8: Representative mid-diaphyseal transverse cross-sections of the femur and humerus of a American marten (*Martes americana*)

Species	Functional Component		Physiology	
	Climbing Behaviour	Home Range (ha)	Basal Metabolic Rate (KJ/kg/d)	Hibernation or torpor behaviour
Gulo gulo	No	207.5	197.3	No
Martes pennanti	Yes	25.9	517.4	No
Mephitis mephitis	No	0.04	279.2	Yes
Mustela americana	Yes	15.15	317.3	No
Mustela ermine	Yes	0.04	862.3	No
Procyon lotor	Yes	1.10	153.1	Yes
Vulpes vulpes	No	4.12	253.0	No

Table 3- 1: Values of explanatory variables used in the variation partitioning analyses.

Table 3-2 : Means and standard deviations of bone macrostructural and microstructural metrics.

Species	Element	Length (mm)	RI (gradians)	LI (gradians)	OD (mm^{-2})	Imax (mm^4)	Imin (mm^4)	J (mm^4)	Area (mm^2)
Gulo gulo	Humerus (n=25)	143.7±25.5	42.6±2.7	29.2±1.0	5886±5055	1066±235	928.5±300.0	1994.0±393.3	79.4±14.3
	Femur (n=25)	141.8±9.6	36.5±2.8	27.7±3.1	1212±980	705.3±107.5	577.1±93.6	1282.4±187.6	72.5±3.5
Martes pennanti	Humerus (n=19)	92.7±6.9	47.1±1.9	13.8±0.4	1082±764	210.1±10.0	137.4±4.5	347.5±11.4	29.5±10.0
	Femur (n=17)	102.0±7.2	49.7±2.2	16.2±1.9	1207±1085	158.4±12.6	265.6±54.3	424.0±57.3	28.9±1.7
Mephitis mephitis	Humerus (n=23)	66.8±6.0	51.5±2.1	19.7±0.9	1165±746	117.7±13.0	52.7±3.6	170.4±15.5	23.6±2.1
	Femur (n=24)	58.7±3.7	59.4±0.8	24.4±2.9	1074±719	80.8±6.8	52.8±5.9	133.7±11.8	23.2±3.0
Mustela americana	Humerus (n=27)	59.6±3.8	41.3±2.0	21.6±0.8	571±669	8.7±1.3	6.7±0.9	15.4±2.1	8.1±0.7
	Femur (n=27)	65.9±4.0	43.2±1.6	27.3±2.6	630±625	12.8±0.4	9.7±0.3	22.5±0.6	7.7±0.1
Mustela ermine	Humerus (n=22)	30.1±1.7	61.2±3.7	12.0±0.9	922±784	0.7±0.1	0.5±0.1	1.2±0.1	1.8±0.2
	Femur (n=20)	31.4±1.5	76.9±2.3	10.8±0.9	1016±773	1.1±0.4	0.8±0.3	1.8±0.6	2.0±0.5
Procyon lotor	Humerus (n=13)	102.6±17.9	55.6±2.9	13.7±0.4	309±257	222.1±36.3	106±21.9	328.0±48.9	35.3±3.8
	Femur (n=16)	100.0±11.9	51.6±1.5	19.2±1.9	3031±1867	426.8±180.5	260.3±105.8	687.1±284.7	37.5±7.6
Vulpes vulpes	Humerus (n=15)	131.1±4.3	40.3±2.5	17.7±2.9	802±886	275.9±16.6	212.2±16.0	488.1±31.8	34.3±1.5
	Femur (n=17)	125.0±5.9	41.1±2.1	17.0±1.4	311±352	244.9±9.4	173.3±10.7	418.2±19.4	31.2±0.8

Table 3-3: Results of variation partitioning of bone vascular orientation among phylogenetic, functional and physiological components.

	Humerus		Femur	
Fraction	**Adjusted R_a^2**	**P**	**Adjusted R_a^2**	**P**
Phylogenetic (a+d+f+g)	0.92709	≤0.005*	0.63126	≤0.005*
Functional (b+d+e+g)	0.50888	≤0.005*	0.28312	≤0.005*
Physiological (c+e+f+g)	0.72384	≤0.005*	0.86115	≤0.005*
Phylogenetic +Functional (a+b+d+e+f+g)	0.94887	≤0.005*	0.71574	≤0.005*
Functional + Physiological (a+c+d+e+f+g)	0.94887	≤0.005*	0.93697	≤0.005*
Phylogenetic + Physiological (b+c+d+e+f+g)	0.80337	≤0.005*	0.87026	≤0.005*
Phylogenetic+Functional+Physiological (a+b+c+d+e+f+g)	0.94887	≤0.005*	0.94958	≤0.005*
Purely Phylogenetic (a)	0.14550	≤0.005*	0.07932	≤0.005*
Purely Function(b)	0	Cannot be tested	0.01260	≤0.005*
Purely Physiological (c)	0	Cannot be tested	0.23384	≤0.005*
Residual (h)	0.05113	Cannot be tested	0.05042	Cannot be tested

Table 3-4: Results of variation partitioning of bone osteocyte density among phylogenetic, functional and physiological components

	Humerus		Femur	
Fraction	**Adjusted R_a^2**	**P**	**Adjusted R_a^2**	**P**
Phylogenetic (a+d+f+g)	0.12277	≤0.005*	0.04898	0.034*
Functional (b+d+e+g)	0.01036	0.14	0.01526	0.12
Physiological (c+e+f+g)	0.03915	0.031*	0.10158	≤0.005*
Phylogenetic +Functional (a+b+d+e+f+g)	0.11782	≤0.005*	0.07233	0.015*
Functional + Physiological (a+c+d+e+f+g)	0.11782	≤0.005*	0.25773	≤0.005*
Phylogenetic + Physiological (b+c+d+e+f+g)	0.05244	0.025*	0.23195	≤0.005*
Phylogenetic+Functional+Physiological (a+b+c+d+e+f+g)	0.11782	0.01*	0.29171	≤0.005*
Purely Phylogenetic (a)	0.06538	0.015*	0.05976	≤0.005*
Purely Function(b)	0	Cannot be tested	0.03397	≤0.005*
Purely Physiological (c)	0	Cannot be tested	0.21938	≤0.005*
Residual (h)	0.88218	Cannot be tested	0.70829	Cannot be tested

Table 3-5: Results of variation partitioning of bone geometry among phylogenetic, functional and physiological components.

	Humerus		Femur	
Fraction	**Adjusted R_a^2**	**P**	**Adjusted R_a^2**	**P**
Phylogenetic (a+d+f+g)	0. 91591	≤0.005*	0. 53142	≤0.005*
Functional (b+d+e+g)	0. 88382	≤0.005*	0. 48863	≤0.005*
Physiological (c+e+f+g)	0. 30884	≤0.005*	0. 29794	≤0.005*
Phylogenetic +Functional (a+b+d+e+f+g)	0. 93315	≤0.005*	0. 60995	≤0.005*
Functional + Physiological (a+c+d+e+f+g)	0. 93315	≤0.005*	0. 81521	≤0.005*
Phylogenetic + Physiological (b+c+d+e+f+g)	0. 89229	≤0.005*	0. 64397	≤0.005*
Phylogenetic+Functional+Physiological (a+b+c+d+e+f+g)	0. 93315	≤0.005*	0. 83314	≤0.005*
Purely Phylogenetic (a)	0.04	≤0.005*	0.18917	≤0.005*
Purely Function(b)	0	Cannot be tested	0.01793	≤0.005*
Purely Physiological (c)	0	Cannot be tested	0.22319	≤0.005*
Residual (h)	0. 06685	Cannot be tested	0. 16686	Cannot be tested

Discussion

The statistical tests were conducted such that each dependent variable (vascular orientation, osteocyte density and bone geometry) was tested independently for the effects of the three explanatory variables (phylogeny, function and physiology), and the results were therefore reported in the same way. However, it may be of greater interest to the reader to consider the overall effects of each explanatory variable independently. It is in this format, then, that we discuss the results.

Phylogeny

The effect of phylogeny on bone microstructural characteristics in sauropsids has been described by Cubo and colleagues (2005). These workers reported that phylogeny explained much of the variation in bone size and cortical thickness, two measures of bone geometry. However, phylogeny had a much smaller influence on microstructural traits such as vascular density, vascular orientation and Haversian remodeling. In this study, we also found a large effect of phylogeny on bone geometry measures, an effect that was stronger in the humerus than in the femur. However, unlike in sauropsids, phylogeny had a strong effect on vascular orientation. Again, this effect was stronger in the humerus than in the femur. The difference between the two studies may be due to a stronger effect of phylogeny in mammals than in

sauropsids. Additionally, the relationship may be present at small phylogenetic scales, such as within mustelids, but not be as significant when looking at large phylogenetic scales, such as Sauropsida. Finally, the more refined manner in which vascular orientation was measured in this study may have allowed for the identification of patterns not evident previously.

Function

The effect of function on bone macro- and micro-structure has been studied in depth. In birds, it was found that bone geometry measures are strongly related to bone function. This is true even in species recently adapted for locomotor behaviours different from their sister taxa (Habib and Ruff 2008). Similarly, vascular orientation has also been linked to function in birds(de Margerie et al. 2005) with bones experiencing high degrees of torsion showing a more laminar arrangement of vascular canals, thinner cortices, and more oblique to transverse collagen fibers. In this study we found that functional characteristics had a large impact on bone vascular orientation but more so in the humerus than in the femur. The effect of functional characteristics was smaller than the effect of phylogeny, and the purely functional component (part b in Figure 3-1) was small or zero. Bone geometry measures were equally impacted by functional demands. Again the effect was less than the effect of phylogeny and was greater in the humerus than in the femur. Also, much of the effect of function on bone geometry was a compound effect with phylogenetics.

Physiology

Growth rate has been shown to have a clear effect on bone microstructure characteristics including vascular orientation(de Ricqlès et al. 1991; de Margerie et al. 2002; de Margerie et al. 2004). In mice, it is known that physiological factors, including diet, can impact bone geometry (Li et al. 1990). In this study we found that physiology has a large affect on vascular orientation and a smaller affect on bone geometry. In the femur, the "pure" physiological component of bone geometry and vascular orientation was 23%, and much larger than the pure component for either phylogeny or function. However, in this study and others, it was found that physiology is strongly associated with phylogeny and function and, in combination, yields greater effects (Cubo et al. 2008).

Shared Variance

At least two levels of shared variance can be hypothesized in the presented data. The first involves bone microstructure itself and the second involves our parameterization of independent variables. The performance of bone certainly cannot be fully explained by simple parameters. For example, the cross-sectional area and shape of bones predicts a general level of beam theory mechanics about the element, but internal structures, such as collagen fiber orientation, may build further mechanical properties in regions within the bone. Similarly, the survey of bone microstructure of the humeri and femora of six mustelids and a canid yield a novel and wide range of variation.

The bones in some of these species is dominated by avascular bone whereas others are heavily vascularized. The vascular orientation is not limited to any particular type, but instead grades from aligned orientations to seemingly random reticular orientations, within discrete regions of the same bone cross section. Future work must take into account this more complex view of bone microstructure in order to avoid the possibility of this variation confounding important signals in bone microstructure.

While both phylogeny and function had large affects on bone micro- and macro-structure, their individual "pure" affects were much smaller than that caused by physiological factors. Clearly, the shared variance between these three characteristics is of great importance in determining bone structure at all scales. The phylogenetic, functional, and physiological variables of species are not entirely independent. Phylogenetic effects cannot be orthogonal to function and physiology, and the latter two need not be orthogonal parameters to each other as well. The task of teasing the effects of these parameters may be impossible at present. Additional studies with different phylogenetic groups and different levels of relatedness would certainly aid in parsing these very complex relationships.

Literature Cited

Amprino, R. 1947. La structure du tissu osseux envisagée comme expression de différences dans la vitesse de l'accroissement. Archives of Biology 58:315-330.

Banci, V. 1981. Ecology and Behaviour of Wolverine in Yukon. Pp. 178. Department of Biological Sciences. Simon Fraser University, Burnaby, BC, Canada.

Chamay, A., and P. Tschantz. 1972. Mechanical influences in bone remodeling. Experimental research on Wolff's law Journal of Biomechanics 5:173-180.

Cubo, J., P. Legendre, A. d. Ricqlès, L. Montes, E. d. Margerie, J. Castanet, and Y. Desdevises. 2008. Phylogenetic, functional, and structural components of variation in bone growth rates of amniotes. Evolution & Development 10:217-227.

Cubo, J., F. Ponton, M. Laurin, E. de Margerie, and J. Castanet. 2005. Phylogenetic Signal in Bone Microstructure of Sauropsids. Systemactic Biology 54:562-574.

Davison, R. P., W. W. Mautz, H. H. Hayes, and J. B. Holter. 1978. The Efficiency of Food Utilization and Energy Requirements of Captive Female Fishers. The Journal of Wildlife Management 42:811-821.

de Boef, M., and H. C. E. Larsson. 2007. Bone Microstructure: quantifying bone vascular orientation. Canadian Journal of Zoology 85:63-70.

de Margerie, E. 2002. Laminar bone as an adaptation to torsional loads in flapping flight. Journal of Anatomy 201:521-526.

de Margerie, E., J. Cubo, and J. Castanet. 2002. Bone typology and growth rate: testing and quantifying 'Amprino's rule' in the mallard (*Anas platyrhynchos)*. Comptes Rendus Biologies 325:225-230.

de Margerie, E., J. Robin, D. Verrier, J. Cubo, R. Groscolas, and J. Castanet. 2004. Assessing a relationship between bone microstructure and growth rate: a fluorescent labelling study in the king penguin chick (*Aptenodytes patagonicus*). Journal of Experimental Biology 207:869-879.

de Margerie, E., S. Sanchez, J. Cubo, and J. Castanet. 2005. Torsional Resistance as a Principal Component of the Structural Design of Long Bones: Comparative Multivariate Evidence in Birds. The Anatomical Record Part A 282A:49-66.

de Ricqlès, A., F. Meunier, J. Castanet, and H. Francillon-Vieillot. 1991. Comparative microstructure of bone. Pp. 1-78 *in* B. Hall, ed. Bone. CRC Press.

Desdevises, Y., P. Legendre, L. Azouzi, and S. Morand. 2003. Quantifying phylogenetically structured environmental variation. Evolution 57:2647-2652.

Frost, H. M. 2003. A 2003 Update of Bone Physiology and Wolff's Law for Clinicians. The Angle Orthodontist 74:3-15.

Fulton, T. L., and C. Strobeck. 2006. Molecular phylogeny of the Arctoidea (Carnivora): Effect of missing data on supertree and supermatrix analyses of multiple gene data sets. Molecular Phylogenetics and Evolution 41:165-181.

Gittleman, J. L. 1986. Carnivore Brain Size, Behavioral Ecology, and Phylogeny. 1986 67:23-36.

Gittleman, J. L., and P. H. Harvey. 1982. Carnivore Home-Range Size, Metabolic Needs and Ecology. Behavioural Ecology and Sociobiology 10:57-63.

Habib, M. B., and C. B. Ruff. 2008. The effects of locomotion on the structural characteristics of avian limb bones. Zoological Journal of the Linnean Society 153:601-624.

Harris, J. E., and C. V. Ogan. 1997. Mesocarnivores of Northern California: Biology, Management, and Survey Techniques, Workshop Manual. The Wildlife Society, California North Coast Chapter, Arcata, CA.

Johnson, G. E. 1931. Hibernation in Mammals. The Quarterly Review of Biology 6:439-461.

Knudsen, K. L., and D. L. K. Jr. 1990. Temperature regulation and basal metabolic rate in the spotted skunk, *Spilogale putorius*. Comparative Biochemistry and Physiology 97A:27-33.

Lanyon, L. E., P. T. Magee, and D. G. Baggott. 1979. Relationship of function stress and strain to the processes of bone remodeling- Experimental study on the sheep radius. Journal of Biomechanics 12.

Li, K.-C., R. F. Zernicke, R. J. Barnard, and A. F.-Y. Li. 1990. Effects of a High Fat-Sucrose Diet on Cortical Bone Morphology
and Biomechanics. Calcified Tissue International 47:308-313.

Lieberman, D. E., O. M. Pearson, J. D. Polk, B. Demes, and A. W. Crompton. 2003. Optimization of bone growth and remodeling in response to loading in tapered mammalian limbs. The Journal of Experimental Biology 206.

Muñoz-Garcia, A., and J. B. Williams. 2005. Basal Metabolic Rate in Carnivores Is Associated with Diet after Controlling for Phylogeny. Physiologcial and Biochemical Zoology 78:1039-1056.

Pearson, O. M., and D. E. Lieberman. 2004. The Aging of Wolff's "Law": Ontogeny and Responses to Mechanical Loading in Cortical Bone. Yearbook of Physical Anthropology 47:63-99.

Ruff, C., B. Holt, and E. Trinkaus. 2006. Who's Afraid of the Big Bad Wolff?: "Wolff's Law" and Bone Functional Adaptation. American Journal of Physical Anthropology 129:484-489.

Wolff, J. 1892. Das Gesetz der Transformation der Knochen *in* A. Hirchwild., ed, Berlin

Woo, S. L., S. C. Kuei, D. Amiel, M. A. Gomez, W. C. Hayes, F. C. White, and W. H. Akeson. 1981. The effect of prolonged physical training on the properties of long bone:a study of Wolff's Law. The Journal of Bone and Joint Surgery 63:780-787.

Chapter 4

The structure-function relationship in bone microstructure: An experimental study in Helmeted GuineaFowl (*Numida meleagris)*

Bridging Text

This chapter is in manuscript format in preparation for its submission to a peer-reviewed journal. This chapter aims to evaluate the role that biomechanical function plays in the formation of bone microstructure. Using a single species in order to control for physiological and phylogenetic effects, an experimental study is done to measure strain and test for differences between two bones with highly different biomechanical functions.

Abstract

It has been well established that bone macrostructural morphology is strongly influenced by bone function. This relationship is evident not only in the how bones with different functions are structured but also in how bone structure adapts to changes in loading patterns. Several studies have found that this strong structure-function relationship extends to bone microstructural morphology as well. However, the precise relationship between the various microstructure morphologies and types (tensile, compressive or shear) and magnitudes of bone strain has not yet become clear. In this study, Helmeted GuineaFowl (*Numida meleagris*) were exposed to flight and running exercise during development. The types and magnitudes of strain experienced by the humerus and the tibiotarsus were quantified and compared to the bone microstructure found in these bones. It was found that while significant differences existed between skeletal elements and between exercised and control birds patterns in bone microstructure cannot be easily linked to the type of strain experienced.

Introduction

Wolff's law (1892) states that when bone is repeatedly loaded in the same way it will be remodeled to resist that loading most effectively. This is a relationship that has been well studied and applies to bone density and bone

shape at the macroscopic scale (Chamay and Tschantz 1972; Woo et al. 1981; de Ricqlès et al. 1991; Starck and Chinsamy 2002; Lieberman et al. 2003; Pearson and Lieberman 2004; Ruff et al. 2006; Habib and Ruff 2008). However, Wolff's law is less straightforward when considering bone structure at the microscopic scale. Bone microstructure is composed of vascular canals, osteocyte lacunae, and collagen fiber arrangement. Skedros and colleagues have found significant effects of mechanical use in some bone microstructural characteristics, such as degree of secondary reconstruction; but not others, such as density of osteocyte lacuna (2005; 2005; 2007). Whereas these previous studies looked only at magnitude and frequency of load, recent studies by de Margerie and colleagues (2002; 2005) have found that type of loading (compressive, tensile, or torsional) may also be of importance. For example, in 2005, this group found several measures of bone microstructure to be strongly correlated with torsional strain in avian bone.

To our knowledge, no experimental work has examined the influence of particular exercise regimes and the resulting strains on bone microstructure. In this study we exposed test groups of Helmeted GuineaFowl (*Numida meleagris*) to daily flight or running treatments, took *in vivo* measures of bone strain experienced by their humeri and tibiotarsi, and examined the resulting bone microstructural and cross-sectional geometry characteristics. Three aspects of bone form and function are addressed:

1. How does bone microstructure and cross sectional geometry among bones with different functional demands in the same species?

2. What is the impact of repeated loading (exercise) on bone microstructure and cross-sectional geometry?

3. How does bone microstructure and cross-sectional geometry vary among bones exposed to different types and magnitudes of strain?

Vascular orientation and osteocyte density were measured as bone parameters . The cross-sectional geometry measures examined were cortical area, second moment of area and polar moment of inertia. Vascular orientation was measured quantitatively through the use of the radial index(RI) and longitudinal index(LI) developed by de Boef and Larsson (2007). These metrics quantify vascular orientation to be quantified in three dimensions from two-dimensional cross sections. Previous studies in birds have revealed a pattern, often referred to as laminar, that is visible in the vascular orientation in the humerus (de Margerie 2002; de Margerie et al. 2005). In these bones vascular canals are oriented within the plane of section and parallel to the periosteal surface. It was suggested that this pattern of vascular orientation is a signal of the torsional loading that occurs during flight (Swartz et al. 1992; Biewener and Dial 1995). It was also found that the tibiotarsus, which is generally considered to undergo mainly compressive

stresses, has vasculature oriented mainly parallel to the long axis of the bone, a pattern often described as longitudinal.

Although previous studies have found little to no evidence to suggest that strain magnitude or frequency affects density of osteocyte cells (Skedros 2005; Skedros et al. 2005), it is known that osteocyte cells act as mechanoreceptors in the bone (Cullinane 2002) and therefore it seems likely that their density would be associated with the characteristics of the strain experienced by the bone. Therefore, osteocyte density was measured by counting the number of osteocyte lacuna in the bone section divided by that section's area.

Beam theory of bone biomechanics predicts that cross-sectional area and shape occupy important roles in bone function. The most used measures of these parameters are the cortical area, second moment of area (I) and the polar moment of inertia (J). Cortical area has already been shown to increase in response to exercise in experimental animals (Woo et al. 1981; Lieberman et al. 2003) and we predict a similar result with our experimental birds. The second moment of area measures the bone's resistance to bending and the polar moment of inertia provides a measure of its resistance to torsion. It is expected that due to the high levels of torsion experienced by the humerus during flight (Swartz et al. 1992; Biewener and Dial 1995), J will be higher in the humerus than in the tibiotarsus, and that it will increase in the flight

exercised bird humeri over that of the the controls. All of these three measures were made.

Materials and Methods

Animals and Exercise Regime

Twenty-four (24) Helmeted Guineafowl (*Numida meleagris*) keets of the larger French strain were obtained from a hatchery at two days of age. The birds were housed in an indoor, unheated, free-range enclosure with access to heat from a heat lamp and given water and food *ad libitum.* Within this enclosure, the birds were able to walk freely but in a limited and small area. There were no areas within the enclosure onto which the birds could fly, and thus it is assumed that the birds did not fly while within the enclosure. No flight or persistent running was observed in any of the birds while in their enclosure.

When the birds were able to fly (at the age of 5 weeks), they were randomly assigned into one of three groups of eight birds and marked using leg bands. One group of birds was trained to locomote steadily on a motorized treadmill (Woodway Treadmills, Waukesha, WI) at a speed of 1.5 m s^{-1}. They were exercised in this way for 30 minutes per day for the entire exercise period. A second group of birds was trained to fly between two wooden platforms (0.9m long, 0.3m wide) that were spaced 6 m apart. The

birds were trained to fly back and forth repeatedly between the platforms for 1 hour per day with rest periods between each flight of no more than 30 seconds. The flying group experienced a longer period of exercise because of the unavoidable interruptions in wing loading caused by the periods on the platforms between flights. The third group of eight guinea fowl served as a control and remained within the enclosure that all three groups shared when animals were not being exercised. Over the course of the study, one of the birds in the flight-exercise group became ill and, although, subsequently recovered, it was removed from the study as it had missed three consecutive days of exercise. Additionally, one of the birds in the control group was noted to have a mild deformation in its feet that appeared to be related to injury early in life. It was excluded from all tibiotarsus measures but was included for humerus measures.

Bone strain measures were collected for the humerus in the flight-exercise group, the tibiotarsus in the running-exercise group and in both the humerus and the tibiotarsus in the control group. These measures were taken at the end of the exercise period, but, due to the time required for surgery and data recording, these measures could be taken on a maximum of two birds per day. In order to prevent changes in bone structure or strain measures due to inactivity, birds that had not yet undergone surgery continued to be exercised. Therefore, the exercise period ranged from 5 weeks to 7 weeks in each group.

Surgical Procedures

Birds were anesthetized using a mixed subcutaneous injection of xylazine (1mg kg^{-1}) and ketamine (4 mg kg^{-1}). After induction, the birds were prepped for sterile surgery and maintained on 0.5-1.0% isoflurane using a closed system anesthesia machine (Matrx, Orchard Park, NY, USA) while breathing rate was carefully monitored.

Bone strain measures were taken at their midshafts because this is where the highest stresses occur *in vivo* (Lanyon et al. 1979). For implantation of strain gauges on the tibiotarsus, feathers were removed from the entire right leg and the right latero-dorsal surface of the animal just dorsal to the same leg. A small incision was made just lateral to the synsacrum of the animal and sterilized strain gauges with attached lead wires (36-gauge, etched Teflon insulated) were passed subcutaneously along the leg to the medial surface of the tibiotarsus. Muscles were reflected to allow exposure to the cranial, caudal and medial surfaces of the tibiotarsus (Figure 4-1a). because no muscles attach to the bone at these sites, muscles were minimally damaged during the procedure. The tibiotarsus length was measured from its axis of rotation at the knee to that at the ankle using digital calipers. The exact mid-diaphysis was then measured from the ankle before proceeding to bond the strain gauges to the bone. Once exposed, the periosteum of the bone was removed and the bone was lightly scraped to facilitate bonding of the strain gauge to the bone.

The surface of the bone was cleaned with methyl-ethyl-ketone and allowed to dry thoroughly before the strain gauge was bonded to the bone using a cyanoacrylate adhesive. All incisions were then sutured. Exposed lead wires attached to a pre-soldered epoxy-mounted connector were sutured to the skin in order to prevent strain on the wires and were covered with vetrap and elastic bandaging tape. An intramuscular injection of flunixin (4 mg kg^{-1}) was given both post surgery and the following morning to relieve soreness.

Bonding to the humerus followed similar procedures. Feathers were removed from the dorsal surface of the right shoulder and along all surfaces of the humerus; however, it was not required to remove feathers necessary for flight. The initial incision was made just lateral to the vertebral column and lead wires and strain gauges were passed subcutaneously along the dorsal surface of the humerus. The second incision was made on the dorsal surface of the humerus allowing for attachment of strain gauges to the dorsal, cranial and caudal surfaces of the bone (Figure 4-1b). As with the tibiotarsus, there are no muscle attachments at these sites minimizing muscle damage during the surgery. The location, orientation and bonding of the strain gauges were similar on the humerus to the tibiotarsus. Incisions were sutured and the connector secured as in the tibiotarsus.

Strain Gauges

For each skeletal element three strain gauges were used. In all cases two of these were single element gauges (FLA-2-11; Tokyo Sokki Kenkyujo Co.) and one was a rosette three element gauge (FRA-1-11; Tokyo Sokki Kenkyujo Co.). The rosette gauge contains three strain gauges which are oriented at 45 degrees to each other. By aligning the central of the three gauges to the long axis of the bone, it is possible to determine the maximum (tensile) principal strain, minimum (compressive) strain and their angles (Φ). For both the tibiotarsus and the humerus it was found that, due to size constraints, it was only possible to affix two single-element and one rosette three-element gauges. In order to determine the strain orientation on all three surfaces for each skeletal element, the location of the rosette strain gauge was rotated among the three locations on each individuals (Table 4-1).

Strain Data Recordings

Following surgery the animals were allowed to recover overnight and strain recordings were made the following day. The connector attached to the strain gauge lead wires was connected to a 5.5m shielded cable that was secured with surgical tape to the back of the animal. This in turn was connected to a bridge amplifier (Vishay 2120; Micromeasurements) which allowed for the sampling of raw strain signals by an A/D converter (Axon instruments). Calibration recordings were also collected using a 1000 με shunt-calibration on the bridge amplifier. Recordings were viewed using the

Axoscope for Windows acquisition software (Axon CNS molecular devices) at 2.5 kHz. Strain measures for the tibiotarsus were recorded while animals ran at the exercise speed of 1.5m s^{-1}. Strain measures for the humerus were recorded while animals made short flight from the ground to one of the platforms used during exercise. Occasionally strain measures could not be made from one or more of the strain gauges due to inevitable difficulties that can arise during surgery, recovery or data recording. A summary of sample sizes for all recorded strain measures is included in Table 4-1. Following *in vivo* strain measures, all birds were euthanized by lethal injection of sodium pentobarbital (120 mg/kg).

Strain Data Analysis

Raw strain data were filtered using a 4th order zero phase lag butterworth filter with 125Hz cutoff frequency in forward and backward direction, resulting in an 8th order filter in order to minimize signal noise. Filtered data was then zeroed and calibrated to convert voltages to microstrain using the calibration recordings. This was all done using custom MATLAB programs (The Mathworks, Inc., Natick, MA, USA) written by Ty Hedrick and M.D.

When both single element gauges and the central gauge of the rosette were available, it was possible to determine the distribution of strain parallel to the long axis of the bone (also known as longitudinal strain) (Biewener

1992) assuming that bone is linearly elastic and isotropic in this plane (Carter 1978). In the tibiotarsus this was done during peak strain which occurs at roughly 25% of stance (Figure 4-2). The humerus is loaded during both the upstroke and downstroke in the loading cycle and thus longitudinal strain was determined for the peak strain that occurs at both of these times (Figure 4-3). The resulting maps of longitudinal bone strain across a transverse cross-section of the bone were visualized using a custom MATLAB program (Main and Biewener 2004) (Figure 4-4).

When all three channels on the rosette strain gauge were available, it was possible to determine the maximum (tensile) and minimum (compressive) principal strains and the angle of the maximum strain to the bone's longitudinal axis. This gives a representation of the degree of torsion occurring during loading which is not possible to determine using longitudinal strain alone. Using these three values it is then possible to determine the shear strains experienced by the bone (Carter 1978).

Bone Geometry Measures

Both tibiotarsi and humeri were carefully dissected immediately following euthanasia for morphological and histological analysis. All muscle and connective tissues were removed manually and the bones were allowed to dry in a fume hood for at least one week. The location and alignment of the strain gauges were measured relative to the bone midshaft and longitudinal

axis respectively. Copper wire (20 gauge) was adhered to the bone superior to the strain gauges to aid in identification once sectioned. One strand was adhered to the cranial and medial (dorsal in the humerus) surfaces, while two strands were adhered to the caudal surfaces to facilitate bone section orientation. Bones with attached wires were then embedded in an epoxy resin (Bono-Mar-Hyde Crop.) and sectioned transversely at the midshaft using a diamond-coated annular saw (Microslice II; Cambridge Instruments, Ltd.). The resulting ~280μm thick sections were bonded to a glass slide using permount and covered with a glass coverslip.

These sections were viewed under 40x magnification under a compound light microscope (Nikon Optiphot, Japan) and photographed using a digital camera (QICAM Fast 1394, QImaging, Surrey, BC, Canada). The resulting photos did not contain a full cross section of the bone, so several overlapping photos were taken of each sample and manually combined in Adobe Photoshop (Adobe Systems Inc., USA).

From these magnified cross-sections, measures of cross-sectional area, cranial-caudal and medial (dorsal)-lateral (ventral) second moments of area (I_{CC} and I_{ML}/I_{DV}) (Figure 4-5) and polar moment of inertia (F) were calculated in Image J (National Institutes of Health, USA) using a custom macro. The second moments of area are an estimation of the bone's ability to resist bending

along the axis in question. The polar moment of inertia is an estimation of the bone's ability to resist torsion.

Bone Microstructure Measures

The orientation of the vasculature was measured using the radial index (RI) and longitudinal index (LI) (de Boef and Larsson 2007). The first gives a quantitative measure of each vascular canal's orientation within the plane of section while the second gives a measure of orientation in the plane perpendicular to the plane of section. These indices are in gradians which, for RI, gives a value of 100 for a vascular canal oriented perpendicular to the periosteal surface and a value of 0 for a vascular canal oriented parallel to it. Similarly, LI gives a value of 100 for a vascular canal oriented perpendicular to the plane of section and a value of 0 for a vascular canal oriented parallel to the plane of section. These two indices were measured for every vascular canal in each bone section using a custom program in MATLAB.

The density of osteocytes was measured for the cranial, caudal, medial and lateral (dorsal and ventral in the humerus) quadrants of each bone. Images of each were imported into Image J and osteocyte lacunae were counted using the analyze particles function.

Statistical Analyses

When describing the strain data in tables or in the text, means and standard deviations represent strain measures from all birds based on individual means from a minimum of 3 to a maximum of 5 loading cycles. Comparisons of strain measures between skeletal elements were analyzed using t-test. Comparisons of osteocyte density and polar moment of inertia (J) among the different exercise conditions and skeletal elements were analyzed using two-way analysis of variance (ANOVA). Comparisons of the radial index (RI) and longitudinal index (LI) and of the two second moment of areas (I_{CC} and I_{ML}/I_{DV}) among the different exercise conditions and skeletal elements were analyzed using multivariate analysis of variance (MANOVA). Standard diagnostic tests were run to ensure that the data did not violate any of the assumptions of the tests, and any outliers (maximum of 2) were removed. Least-squares regressions were used to examine patterns of RI and LI *versus* longitudinal strain. All statistical analyses were completed using R (R_Development_Core_Team 2009).

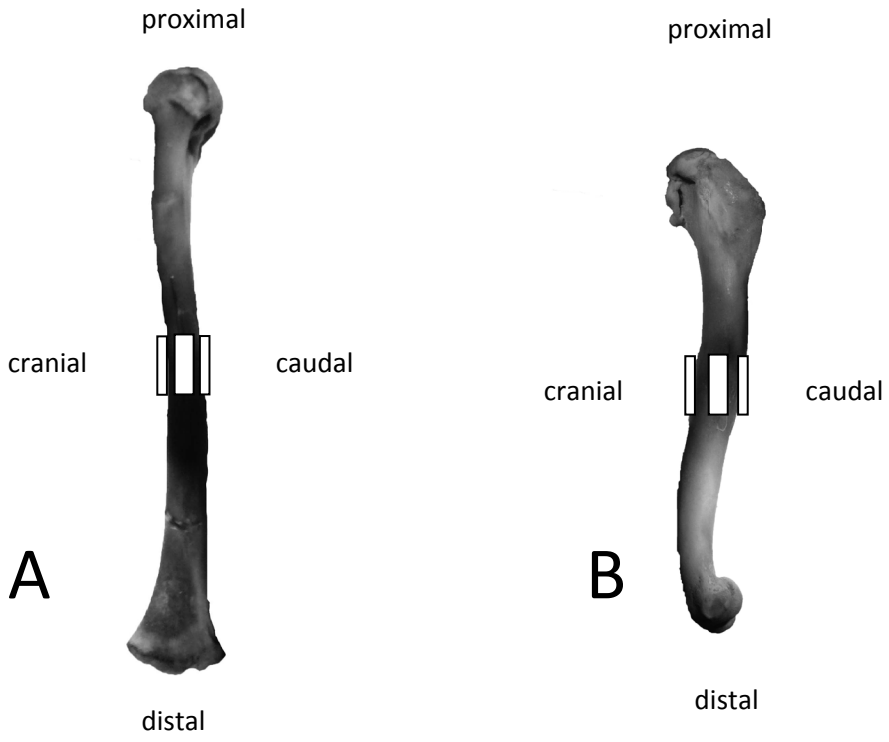

FIGURE 4-1: (A) A medial view of the right tibiotarsus in the Helmeted Guineafowl and (B) a dorsal view of the right humerus in the Helmeted Guineafowl showing the location of the three strain gauges that were affixed to the bone. For both skeletal elements two of the three gauges were single element gauges while the third was a three-gauge rosette. The location of the rosette was rotated between different individuals.

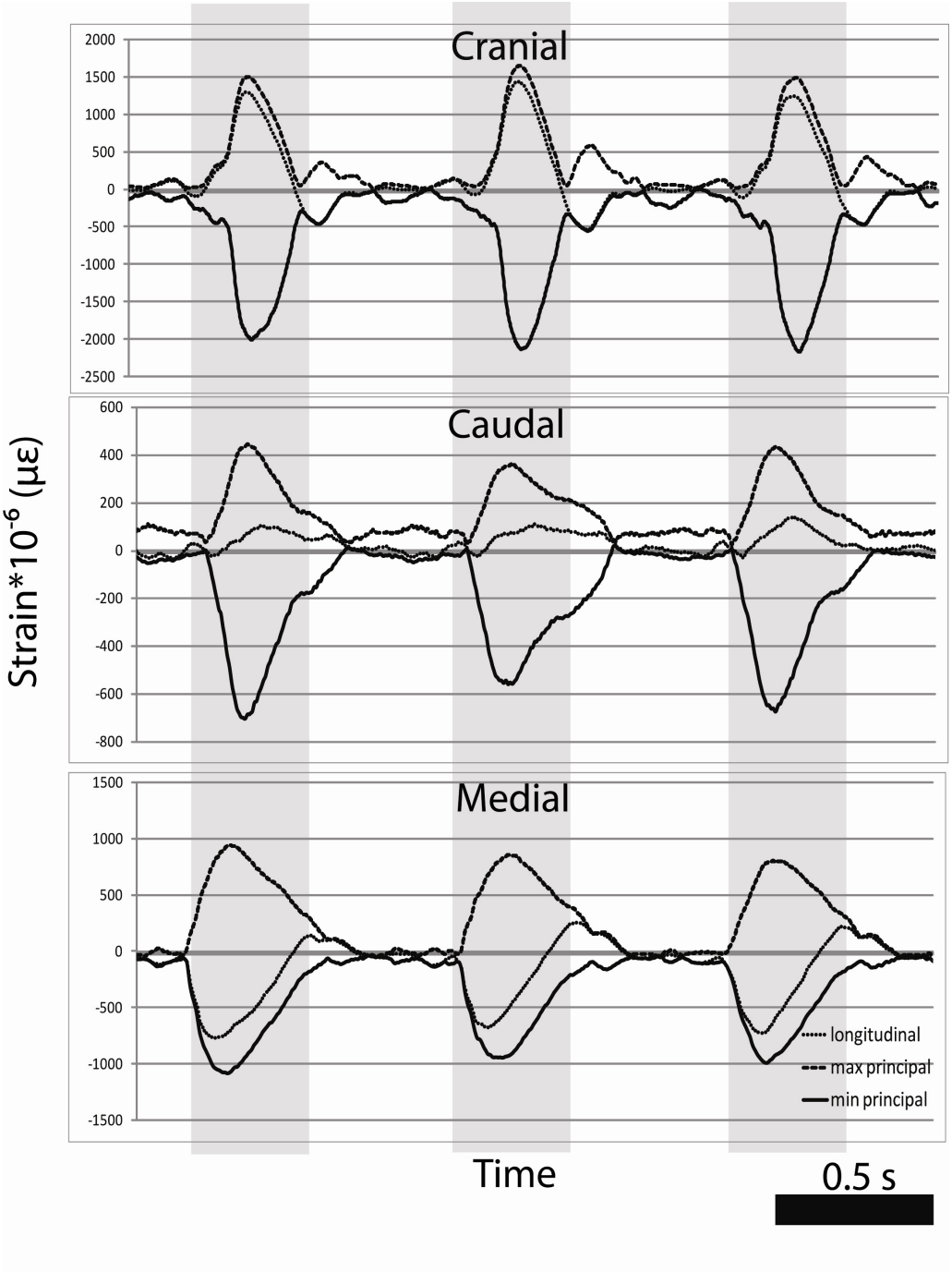

Figure 4-2. Representative strain traces for longitudinal, maximum(tensile) and minimum(compressive) principal strains in the tibiotarsus on the (A) cranial, (B)caudal and (C)medial surfaces at a running speed of 1.5m s^{-1}. Shaded areas represent times when the foot is in contact with the ground.

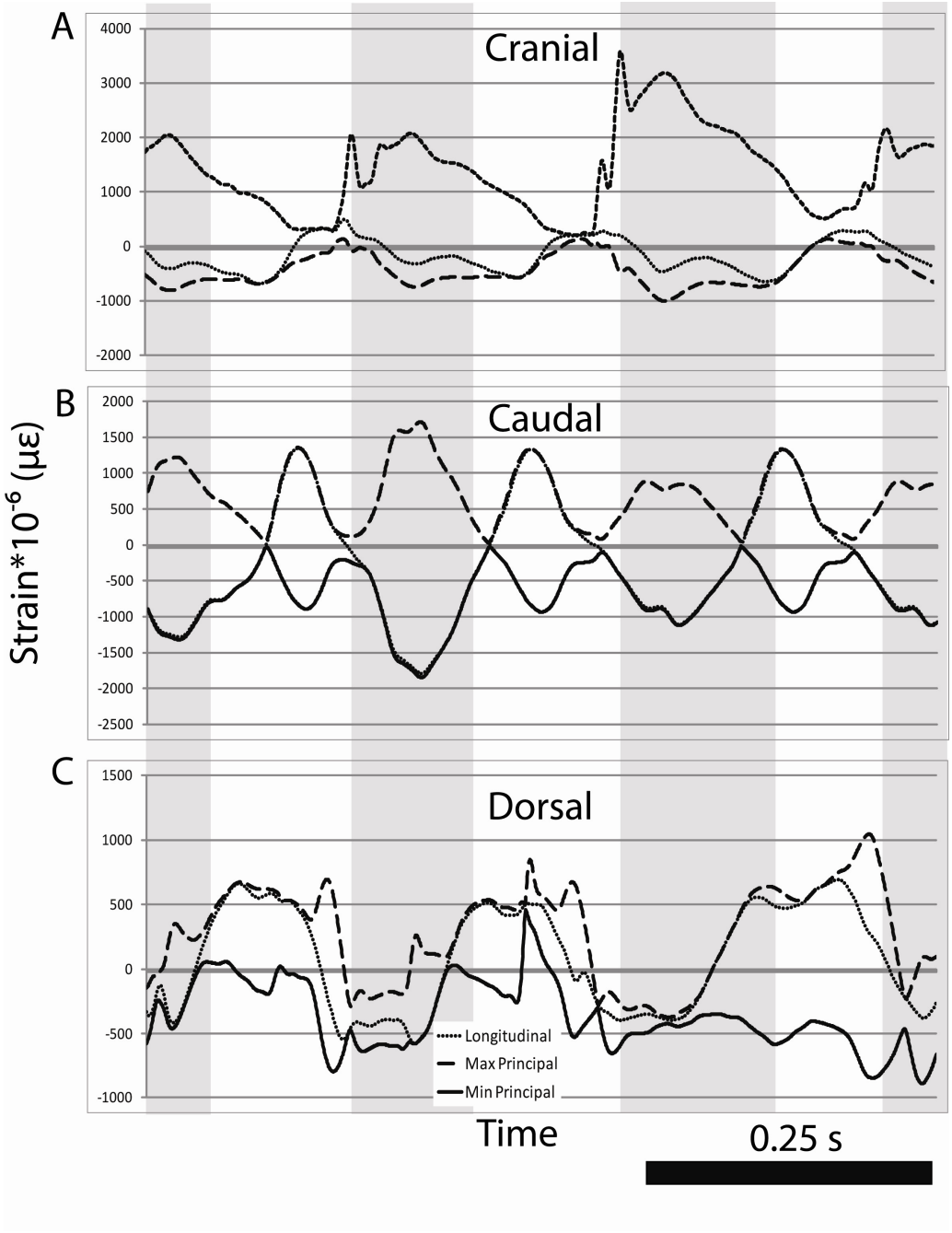

Figure 4-3. Representative strain traces for longitudinal, maximum(tensile) and minimum(compressive) principal strains in the humerus on the (A) cranial, (B)caudal and (C)dorsal surfaces. Shaded areas represent downstroke.

Results

Bone Strain Data

Representative strain traces of the tibiotarsus showing both longitudinal strain and maximum and minimum principal strains on the cranial, caudal and medial surfaces are shown in Figure 4-2. Colour representations of the distribution of the longitudinal strains in this bone are shown in Figure 4-4B.

As these figures show, the tibiotarsus experiences peak strain during the first half of stance. On the cranial midshaft surface this strain was tensile, with a maximum principal strain of 1746 ±928 με which was oriented -17°± 9 away from the longitudinal axis and thus toward the lateral side of the bone (Fig 6). The minimum principal strain was -447±131με. On the caudal midshaft surface, longitudinal strain was also tensile but much lower in magnitude. The maximum principal strain was 367 ± 121 με and was oriented -13°± 19 away from the longitudinal axis and thus toward the medial surface of the bone. The minimum principal strain at this site was -474± 194 με. The medial surface experienced very high compressive strain during stance with a minimum principal strain of -2733±330 με and a maximum principal strain of 690±330με at an angle of 86°±12 relative to the longitudinal axis and thus oriented toward the cranial surface of the bone.

All three surfaces of the humerus experience both tension and compression during a loading cycle as evidenced by the nearly inverted strain pattern shown between upstroke and downstroke (Figure 4-4). During downstroke the cranial surface is loaded mainly in compression while the caudal surface is loaded in tension. During upstroke the situation reverses, and the caudal surface is loaded in compression while the cranial surface is loaded in tension. The dorsal surface, which is situated near the neutral axes for both upstroke and downstroke, experiences both tensile and compressive strain. On the cranial surface, peak maximum principal strains of 1746±835 με and peak minimum principal strains of -1138±466 με were recorded during upstroke and downstroke respectively. The maximum principal strain angle relative to the longitudinal axis ranged from 60° to -44° as the bird moved through a full wingstroke (Figure 4-7). On the caudal surface the peak maximum principal strain during downstroke and peak minimum principal strain during downstroke were 1330 ± 35με and -1187±188με respectively. The maximum principal strain angle ranged from 46° to -44°. The dorsal surface experienced both tensile and compressive strains during both upstroke and downstroke. Peak maximum and minimum principal strains were 1781±248με and -1520±504με respectively while the maximum principal strain angle varied between 54° and -43°.

In both bones, principal strains were oriented at an angle to the long axis of the bone and thus experienced torsion, or twisting of the bone. This results in the bone experiencing shear strains; however, the complete reversal in strain pattern experienced by the humerus suggests a much greater shear strain. Also, as the humerus experienced strain at an angle closer to 45 degrees to the long axis than the tibiotarsus the humerus experienced a greater degree of shear strain.

Bone Microstructure Measures

Osteocyte densities measured for cranial, caudal, medial and lateral regions of the tibiotarsus and cranial, caudal, ventral and dorsal regions of the humerus are presented in Figure 4-8.

The cranial regions of the tibiotarsus and humerus had osteocyte densities of 1326±232 mm^{-2} and 1332±167 mm^{-2} in the control group and 1663±823 mm^{-2} and 1242±260 mm^{-2} in the exercised groups respectively. The caudal regions of the tibiotarsus and humerus had osteocyte densities of 1534±372 mm^{-2} and 1913±979 mm^{-2} in the control group and 2200±1136 mm^{-2} and 1418±304 mm^{-2} in the exercised groups respectively. The medial regions of the tibiotarsus and ventral regions of the humerus had osteocyte densities of 1590±149 mm^{-2} and 1160±300 mm^{-2} in the control group and 2236±1530 mm^{-2} and 1348±367 mm^{-2} in the exercised groups respectively. The lateral regions

of the tibiotarsus and dorsal regions of the humerus had osteocyte densities of 1308±665 mm^{-2} and 1269±419 mm^{-2} in the control group and 1948±1553 mm^{-2} and 1677±950 mm^{-2} in the exercised groups respectively. Osteocyte density showed significant difference between the different skeletal elements ($F_{(1,7)}$4.29, p=0.040) with the tibiotarsus showing on average higher osteocyte densities. There were also significant differences between the exercise and control groups ($F_{(1,7)}$4.14, p=0.044), with the exercise group showing on average higher osteocyte densities. There was also an interaction between skeletal element and experimental group ($F_{(1,7)}$4.00, p=0.48). Differences in osteocyte densities between the different regions of the bone were not significant ($F_{(1,7)}$1.19, p=0.31).

An image of transverse cross sections of a representative humerus and tibiotarsus are shown in Figure 4-5. Both show a great deal of vascularization with no secondary reconstruction. As these animals were all very young (athough adult sized) when sacrificed, it is possible that secondary reconstruction does occur later in life but had not yet taken place in these animals. The pattern of vascular orientation differed greatly between the skeletal elements. Vascular canals in the tibiotarsus were oriented along the longitudinal axis with very few oriented within the plane of section. Those that were oriented within the plane of section were in a reticulated pattern and there was no visibly consistent pattern of orientation relative to the periosteal

surface of the bone. Vascular canals appeared to increase in diameter toward the periosteal surface, although this was not measured or tested for. Vascular canals in the humerus were oriented mainly within the plane of section and parallel to the periosteal surface, a pattern often described as laminar(de Ricqlès et al. 1991). There were a number of short, radially-oriented vascular canals however which connected to those oriented laminarly. Vascular canal size did not seem to vary in this element.

Vascular canal orientation did not visibly appear to differ between exercised and control groups. However when the RI and LI were used to quantify vascular orientation, there were significant differences between these groups ($F_{(1,7)}$6.48, p=0.0052) (Figure 4-9). As expected, these same measures found a highly significant effect of skeletal element on vascular orientation ($F_{(1,7)}$92.00, p<0.001). There was also a significant effect of the interaction between skeletal element and exercise ($F_{(1,7)}$6.78, p=0.0423). When looking at the two measures of vascular orientation independently, it was found that there were significant relationships between RI and exercise($F_{(1,7)}$12.4, p=0.016), skeletal element($F_{(1,7)}$31.7,p<0.001), and the interaction between exercise and element ($F_{(1,7)}$5.08, p=0.032), with RI being higher in the tibiotarsus than in the humerus and in the exercised animals than in the controls. There were significant relationships between LI and skeletal element($F_{(1,7)}$145.3, p<0.001) and the interaction between element and

exercise ($F_{(1,7)}$7.73, p=0.098), with LI being higher in the tibiotarsus than in the humerus. There was not a significant relationship between LI and exercise($F_{(1,7)}$1.82, p=0.018). The high LI in the tibiotarsus is consistent with the qualitative observation of a large number of longitudinally-oriented vascular canals. The low RI and LI in the humerus is consistent with the qualitative observation of a large number of laminarly-oriented vascular canals(de Boef and Larsson 2007).

Relationships between longitudinal strain and vascular orientation were determined using the peak longitudinal strain values at the cross sectional positions for each RI and LI measurement and least squares regression. As can be predicted by visually comparing the vastly different pattern of longitudinal strains to the highly consistent pattern of vascular orientation, there was no relationship between longitudinal strain and vascular orientation for neither RI (slope 0.010, R^2<0.01) nor LI(slope≈0, R^2<0.001) (results not shown).

Bone Geometry Measures

The means and standard deviations of cortical area, polar moment of inertia(J), second moment of area on the cranial-caudal index(I_{CC}) and the second moment of area on the medial-lateral or dorsal-ventral axis($I_{ML/DV}$) are represented for each group in Figure 4-10. Also, the orientation of I_{cc} and $I_{ML/DV}$ are represented in Figure 4-5. A significant relationship between exercise and cortical area was found ($F_{(1,7)}$8.2230, p=0.008) with the cortical area in

exercised animals being lower than that of the control animals. Interestingly, the cortical area in the humeri and tibiotarsi were not significantly different from each other, and there was no effect of the interaction between skeletal element

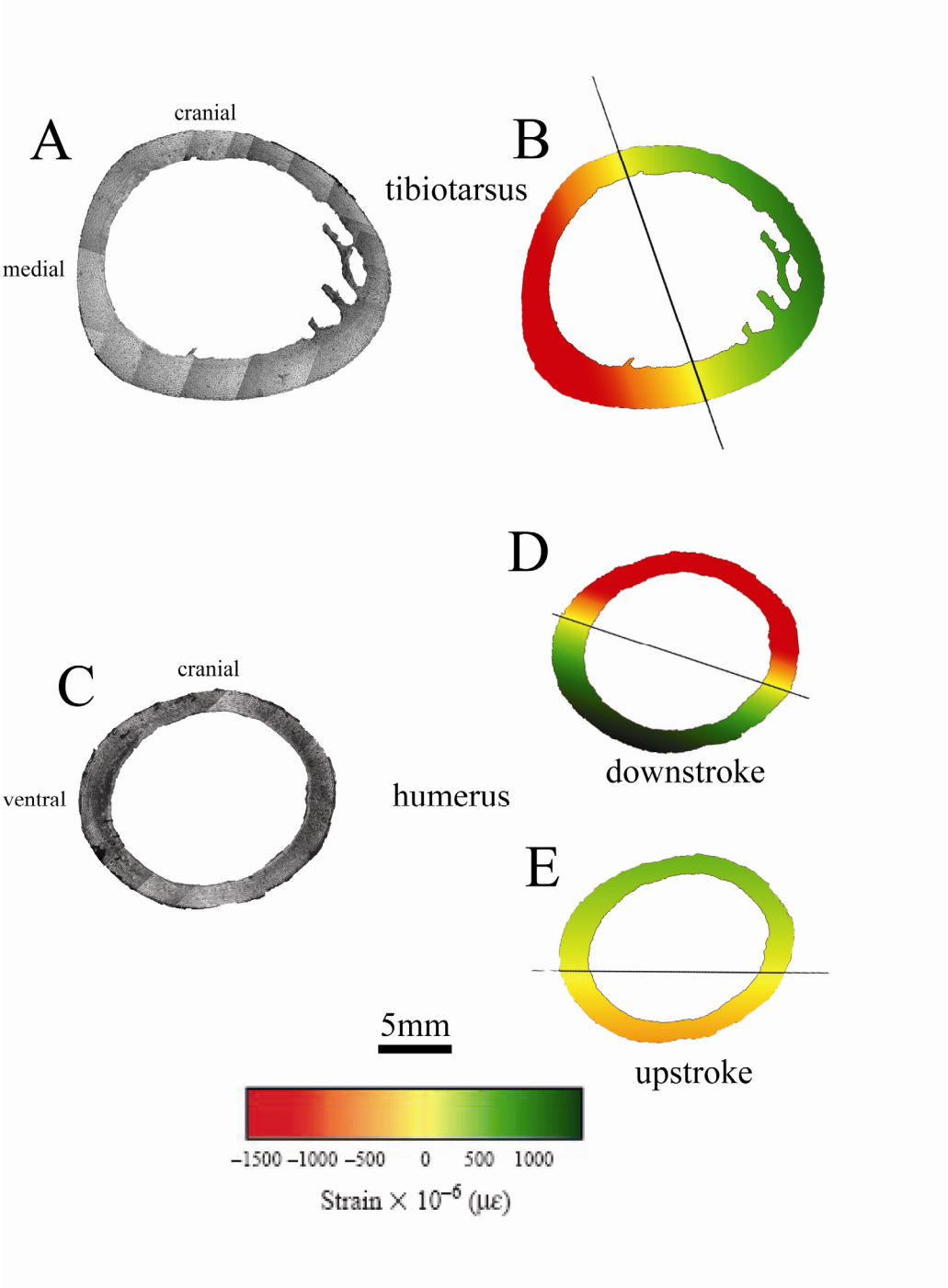

Figure 4-4. Representative transverse sections of the (A)tibiotarsus and (C)humerus and corresponding peak longitudinal strains measured during (B)stance, (D)downstroke and (E)upstroke.

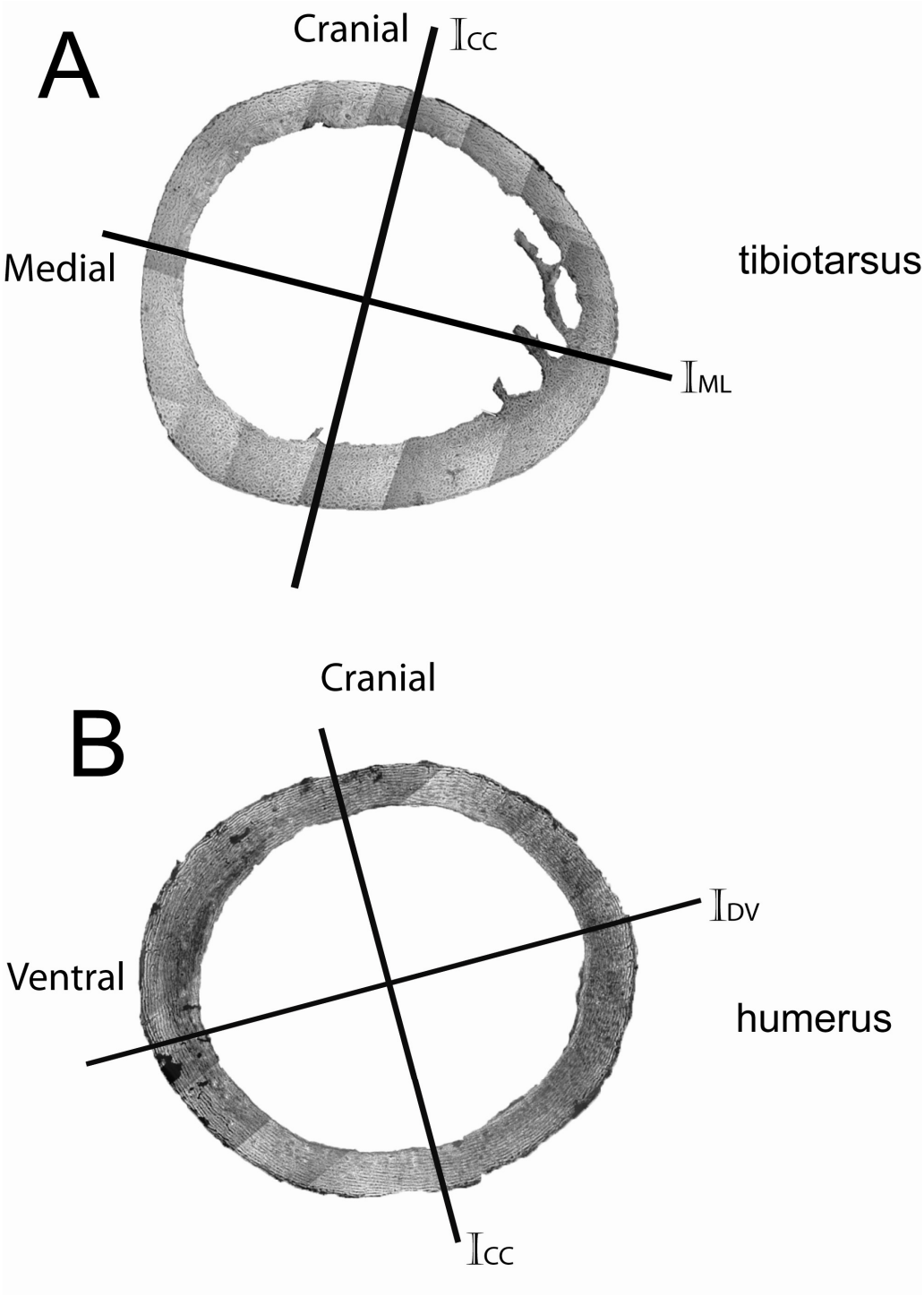

Figure 4-5. Representative transverse sections of the (A) tibiotarsus and (B) humerus showing the orientation of the peak second moment of area most closely associated with the cranial-caudal axis (I_{CC}), the medial-lateral axis(I_{ML}) and the dorsal-ventral axis(I_{DV})

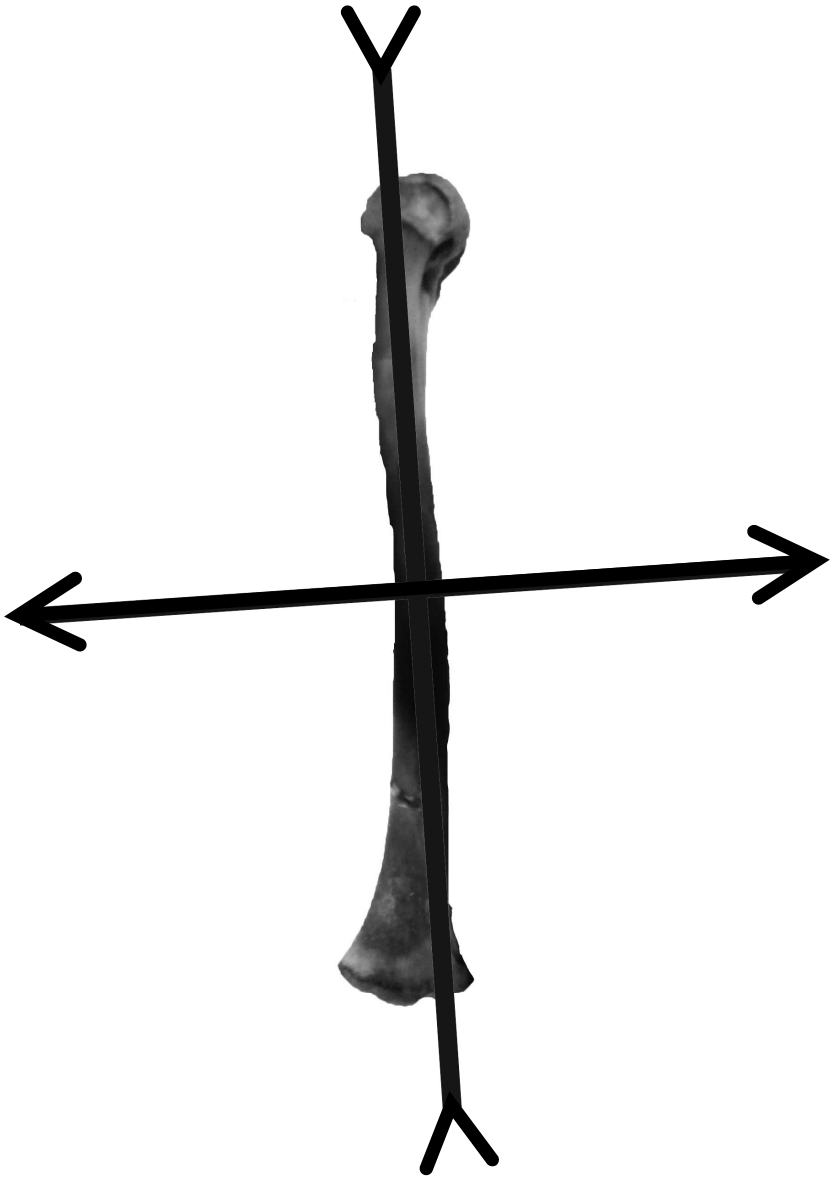

Figure 4-6. A medial view of the right tibiotarsus in the Helmeted Guineafowl showing mean principal strain angle on the medial surface.

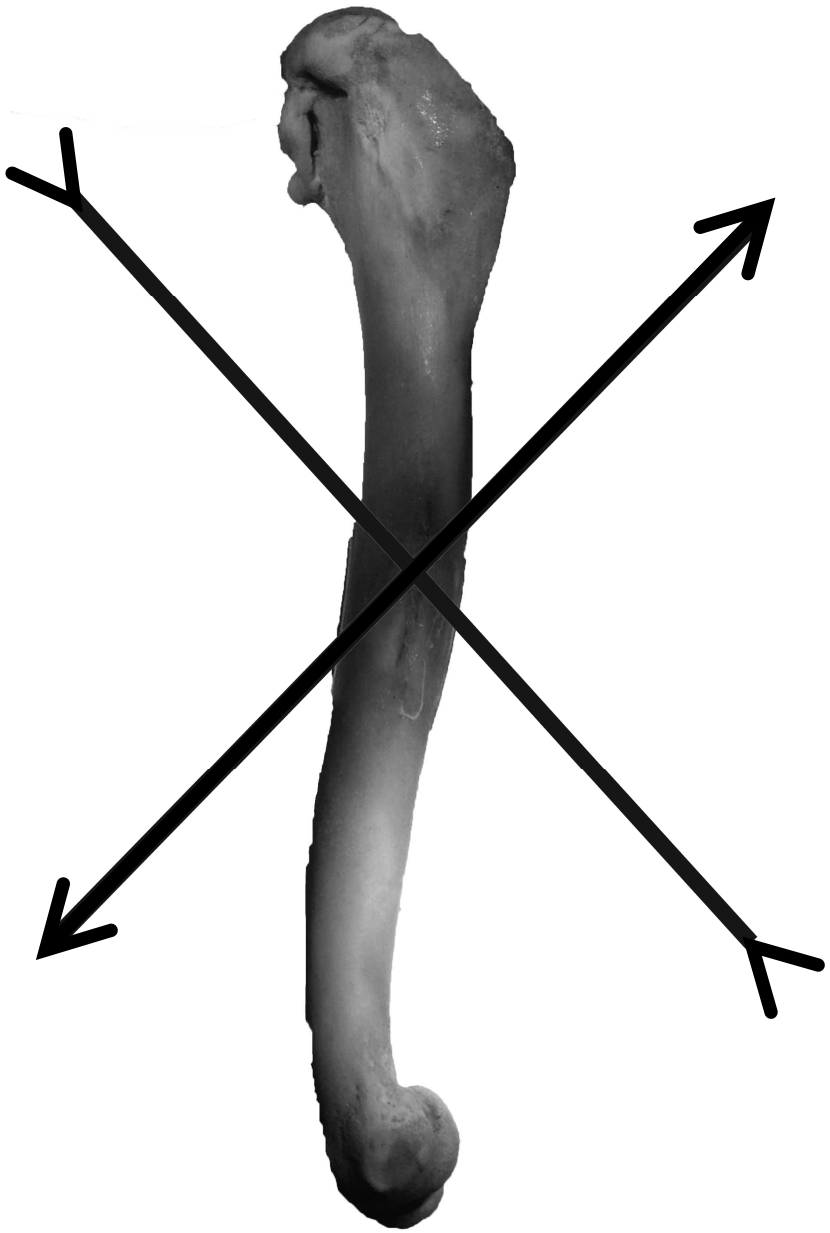

Figure 4-7. A dorsal view of the right humerus in the Helmeted Guineafowl showing the mean principal strain angles during upstroke and downstroke on the dorsal surface.

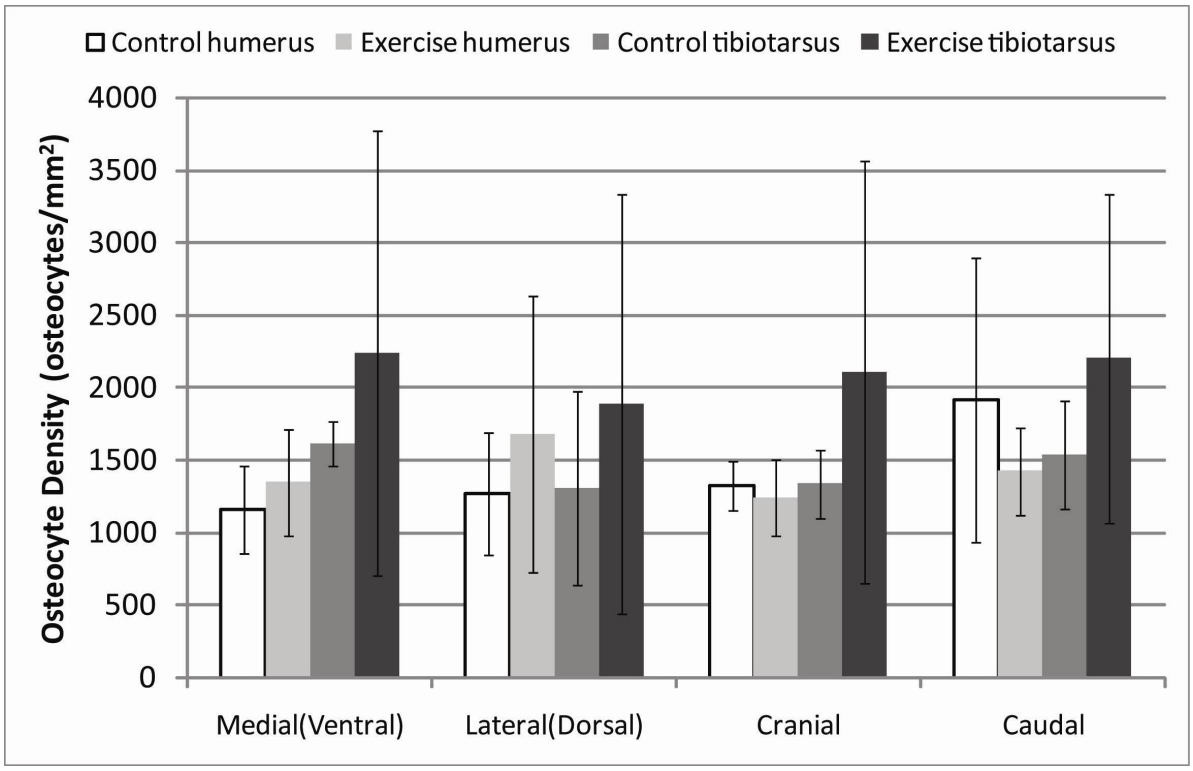

Figure 4-8. Mean osteocyte densities for different areas of the humerus and tibiotarsus in control and exercised Helmeted Guineafowl. Error bars represent standard deviations. There is a significant effect of exercise ($F_{(1,7)}$4.14, p=0.044), skeletal element ($F_{(1,7)}$4.29, p=0.040) and the interaction of exercise and skeletal element ($F_{(1,7)}$1.19,p=0.31). Differences between regions of the bone were not significant.

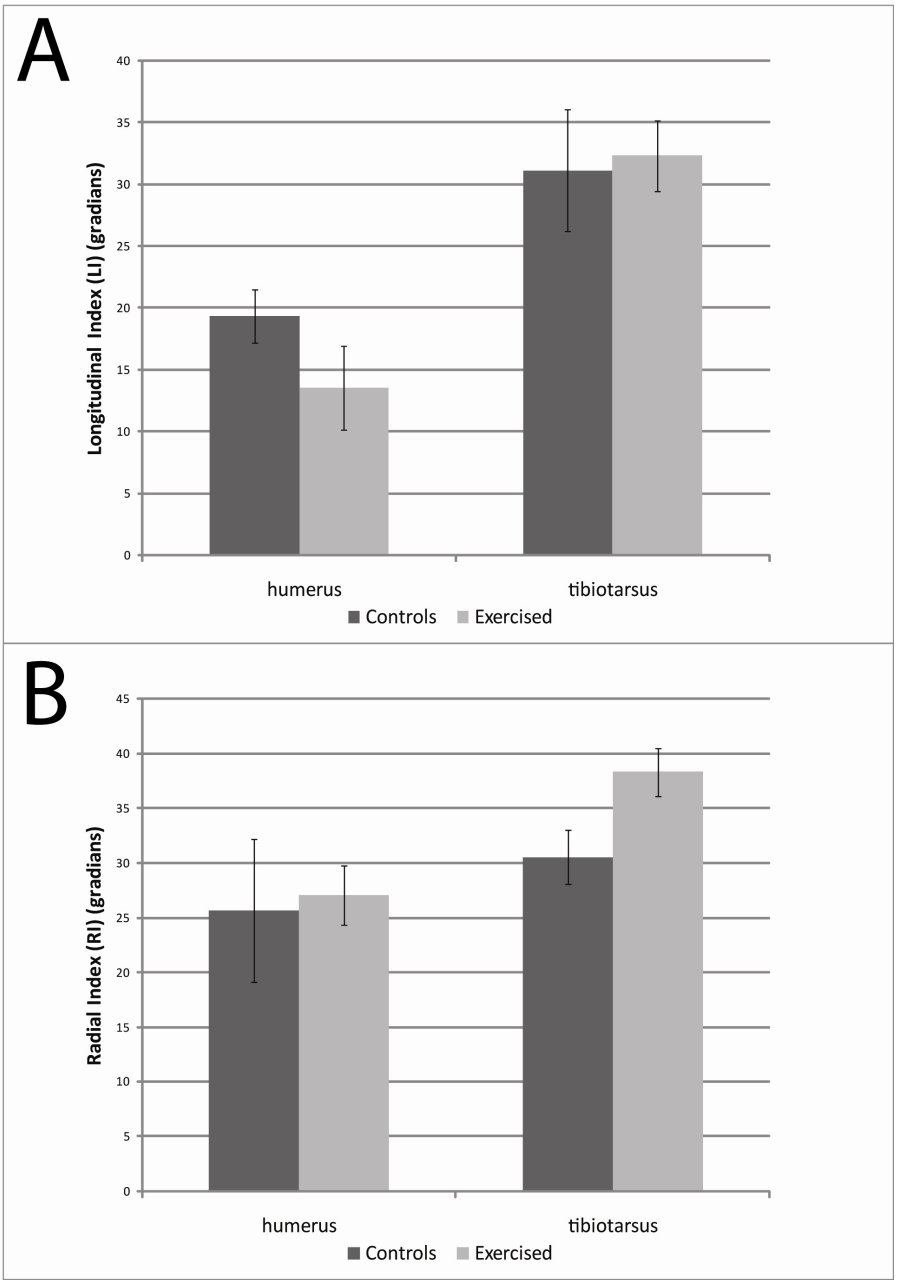

Figure 4-9. (A) The mean longitudinal index (LI) and radial index (RI) for all vascular canals in the humerus and tibiotarsus for control and exercised animals. Error bars represent standard deviations. When evaluated together the indices showed significant effects of exercise ($F_{(1,7)}$6.48,p=0.0052), skeletal element ($F_{(1,7)}$92.00, p<0.001) and interaction between exercise and skeletal element($F_{(1,7)}$6.78, p=0.0423).

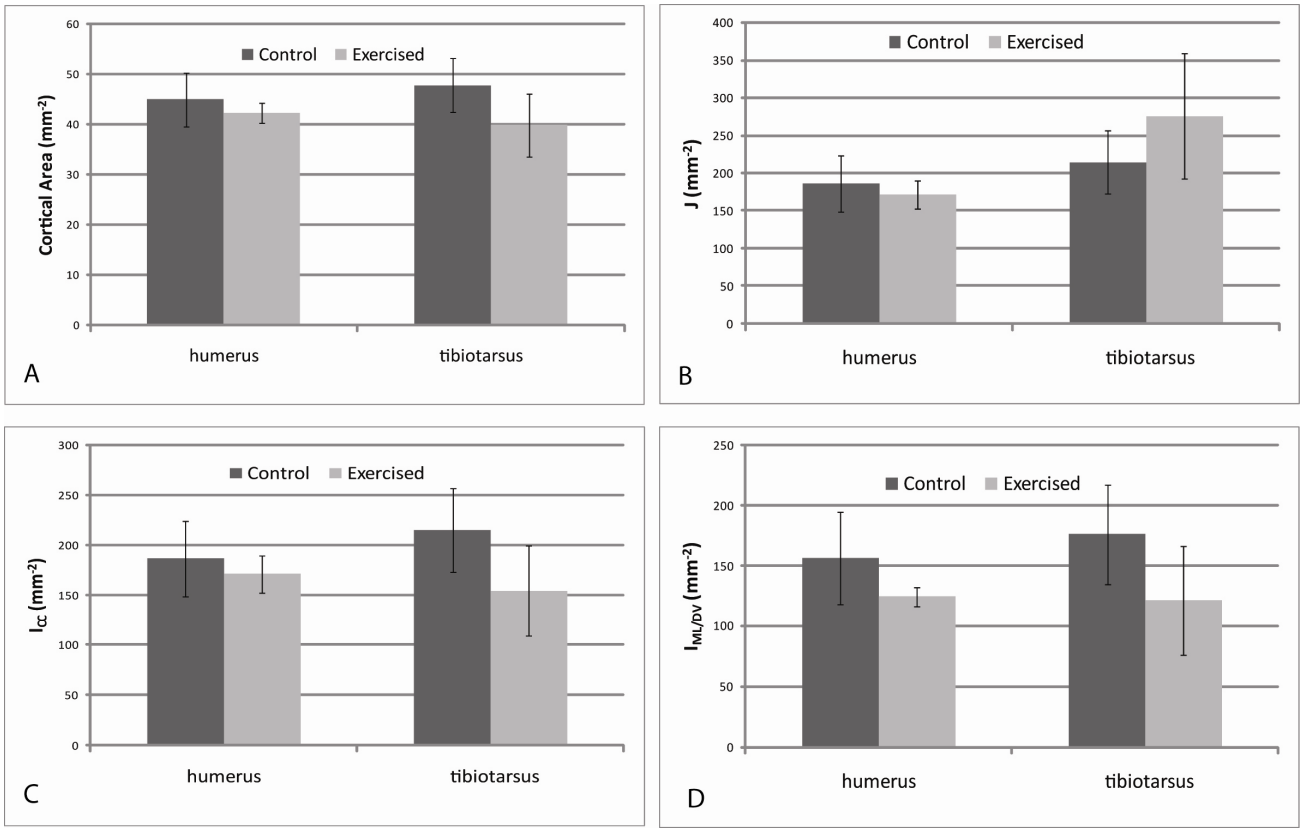

Figure 4-10. Mean cross sectional geometry measures. Error bars represent standard deviations(A)There was a significant effect of exercise on bone cortical area ($F_{(1,7)}$8.22, p=0.008) with exercised animals slowing less cortical area than control animals. (B) A significant relationship between exercise and polar moment of inertia (J) was found ($F_{(1,7)}$7.61,p=0.01) with exercised animals showing lower values for this metric. The second moment of areas along the (C)cranial-caudal and (D)medial-lateral/dorsal-ventral axes were significantly different between exercise and control groups ($F_{(1,7)}$5.14,p=0.013).

Group	Element	Longitudinal Strain	Principal Strain (cranial)	Principal Strain (caudal)	Principal Strain (medial or dorsal)	Bone microstructure measures	Bone Geometry measures
control	humerus	3	2	2	2	7	7
exercised	humerus	5	1	1	2	7	7
control	tibiotarsus	3	3	1	1	8	8
exercised	tibiotarsus	3	2	2	2	8	8

Table 4-1. Sample sizes for all measures. Sample sizes for bone strain measures were lower than bone microstructure and bone geometry measures due to normal difficulties in obtaining clear strain signals.

and exercise on this metric. A significant relationship between exercise and J was also found ($F_{(1,7)}$ 7.6104, p=0.010), with J being lower in exercised animals than in control animals. Again there was neither a significant relationship between skeletal element and J nor between the interaction of skeletal element and exercise and J. The second moment of areas along the cranial-caudal axis (I_{cc}) and the medial-lateral axis (tibiotarsus) or dorsal-ventral (humerus) axis ($I_{ML/DV}$) showed significant difference between exercise and control groups ($F_{(1,7)}$5.14, p=0.013). There was not a significant relationship between these measures and skeletal element or the interaction between skeletal element and exercise.

Discussion

Bone Strain

The strain pattern experienced by the tibiotarsus was in agreement with previously reported results from similar birds (Biewener et al. 1986) with high tensile strain on cranial and low tensile strain on caudal surfaces. The bone experienced some torsion during loading, as the maximum strain was not in line with the long axis of the bone. The strain pattern experienced by the humerus is also similar to what has been previously reported for birds (Biewener and Dial 1995). However, when we compare the strain experienced by the humerus to that experience by the tibiotarsus it is evident that the bones are required to withstand very different loading patterns. Any given region of the tibiotarsus experiences a similar type (compression, tension or shear) of strain throughout the loading cycle. It is simply the magnitude of the strain that differs, with peak strains occurring during footfall and the bone being effectively unloaded during swing. In contrast, any given surface of the humerus will experience multiple or even all types (compression, tension or shear) of strain throughout a wingstroke. Also, there is very little time during which any portion of the humerus is unloaded. Finally, loading cycles in the humerus are much shorter than in the tibiotarsus leading to a much higher strain-rate in the former. High strain-rate has been found to influence compressive strength of bone (Carter and Hayes 1976) and degree of adaptive

remodeling (O'Connor et al. 1982). These differences between the tibiotarsus and the humerus suggest that differences in the organization of bone tissue within these bones may be related to their vastly different mechanical requirements.

Bone Microstructure Measures

Osteocytes are bone mechanoreceptors (Cullinane 2002; Ehrlich and Lanyon 2002) and thus it was hypothesized that their densities would change as a function of bone strain type or magnitude. Considering the bone strain pattern observed, it would be expected that osteocyte density would differ within the tibiotarsus, which experiences differing strains and strain magnitudes on different regions of the bone. Osteocyte density within the humerus could be expected to vary little as all regions of the bone experience several types of strain at similar magnitudes. However, osteocyte densities did not differ between the different regions of the bones in either the tibiotarsus or the humerus. This is similar to what has been found in mammals in previous studies (Skedros 2005; Skedros et al. 2005). In contrast, a significant difference was found in osteocyte densities between these two skeletal elements. While this is not unexpected considering their very different strain patterns, it is surprising that it is the tibiotarsus that has a higher density in spite of the reduced magnitude of the strain it experiences. It is less surprising that the exercised animals had higher osteocyte densities than the control animals. It

appears that it may be loading cycles rather than simply magnitude of loading that causes the increase in osteocyte density. All animals were able to spend time walking and foraging even while not exercising and thus the tibiotarsus was loaded in all groups regularly. In contrast, only the animals in the flying exercise group loaded their humeri and thus overall the humeri experienced much fewer loading cycles than the tibiotarsus among all groups.

Vascular orientation differed greatly between the humerus and tibiotarsus and the pattern found in Helmeted GuineaFowl is consistent with the other avian species examined to date (de Margerie et al. 2005). Exercise, skeletal element and the interaction between these two factors was found to have a significant effect on the vascular orientation as measured by the RI and LI. In previous studies the highly laminar orientation of the vasculature in the humerus has been thought to be associated with the torsion experienced by this bone (de Margerie 2002; de Margerie et al. 2005). The data presented here supports that hypothesis as torsion in the humerus was found to be much greater than that in the tibiotarsus. However, the differences in strain experienced by the tibiotarsus and the humerus are much more complex than simply an increase in torsion. The humerus experiences both compression and tension on all regions of its midshaft as the bird moves from upstroke to downstroke. Strain patterns in the tibiotarsus remain much more consistent as it moves through a loading cycle. It is perhaps also the much more complex

strain pattern exhibited by the humerus that has led to the highly laminar orientation of its vascular canals. A third factor may also play a role. As was discussed above, the loading cycle of a wing-stroke occurs much more quickly than the loading cycle of a step, even during running. This results in a much higher strain rate in the humerus than in the tibiotarsus. It is possible that strain rate may also have an effect on vascular orientation as it has been shown to have an effect on patterns of bone remodeling.

When a linear regression was done to test for the relationship between peak longitudinal strain at points on a transverse cross section of the bones and the orientation of the vasculature at those same points, no relationship was found. While such a relationship would be highly convenient for those wishing to reconstruct bone strain patterns from the fossils of extinct species, this unfortunately is not possible. Bones are three dimensional units and the pattern of strain they experience is also three dimensional. It seems likely that the vascular orientation at any given point along a cross section is a function not only of the longitudinal strain experienced at that point but also the strain in adjacent regions. This is particularly true because vascular canals themselves are three dimensional and the orientation we are able to observe in a cross section is also a function of the orientation of the canal above and below the cross section. Therefore, as useful as it would be, it seems that

mapping longitudinal strain patterns onto cross sections of bones using vascular orientation is not possible.

Bone is complex tissue with multiple factors determining its resistance to stresses. Gross morphology contributes to bone properties best described by beam theory. Beam theory is parameterized from the cross sectional area, shape, and often internal medullary surface of bones. The material properties of bone matrix itself are determined by the hydroxyapatite lattice with collagen fibers and the cross-woven orientation of the fiber sheets. However, an intermediate realm of bone biomechanics has been little explored and this involves its microstructure – composed of vascular canals and osteocyte lacunae.

Osteocyte lacunae may provide a dynamic response to stresses as discussed above. This response is principally through the repair of microfractures and local bone deposition. However, the biomechanical properties of vascular canals within bone have been little discussed. An obvious property of these canals is to supply nutrients and gas exchange for the osteocytes. Thus, bones with relatively high numbers of microfractures, and associated high densities of osteocytes, should have relatively high densities of vascular canals. Bone under intense stresses, such as the tibiotarsus and humerus of Guinea Fowl, tend to make up substantial proportions of the entire bone (see Figure 4-5). The bone tissue associated

with vascular canals is visually the largest component of the entire bone cortical cross-section. The dominance of vascular canals within bone should make them and their orientation a significant component of the mechanical properties of bone. While trabeculae spanning the medullary cavity in mammalian femoral heads have long been shown to follow the force vectors acting about that region, vascular canals may be playing similar roles within cortical bone. However, while trabeculae are composed of bony struts, vascular canals are liquid filled tubes. The mechanical properties of tubes allow them to resist larger compressive and tensile forces than solid columns of equivalent mass. The tube walls are composed of sheets of cross woven bone matrix (Clark 1990) and provide further resistance to compressive, tensile, and bending forces. The liquid filling each tube offers even greater resistance to buckling given the relatively high pressure within the closed vascular system. We propose that these properties of vascular canals within bone may play an important and overlooked role in the biomechanical properties of bone.

The humeri of birds have been documented elsewhere and here to experience high degrees of torsion. Similarly, we and others have also documented a nearly uniform laminar orientation of vascular canals within this bone. It seems that the canals are indeed oriented within the planes of torsion. Similarly, the tibiotarsus of birds experiences primarily compressive

and tensile stresses. The nearly uniform longitudinal vascular orientation of this bone is also in line with these forces. While limited, this dataset does provide insight into a potential biomechanical role of bone microstructure. The orientation and abundance of vascular canals within bone may provide a novel intermediate biomechanical property of bone.

Bone Geometry Measures

Exercise had a significant effect on bone cortical area. Birds that were exercised had on average lower cortical areas. While this may seem counter intuitive , and is in fact opposite to what has been found in sheep (Lieberman et al. 2003), it has been found that daily exercise can decrease muscle mass in birds (Swaddle and Biewener 2000) as a method of increasing locomotor efficiency. It seems likely that exercise has had a similar effect in this study and either bone mass itself (and therefore bone cortical area) was reduced to increase efficiency or else muscle mass was reduced which caused a corresponding decrease in bone mass.

Exercise had a similar effect on the polar moment of inertia, with exercised animals showing a lower value for this metric as well. As with cortical area, this is counter to what has been found in sheep (Lieberman et al. 2003). As polar moment of inertia is related to radius to the fourth power, it seems the same effect that caused cortical area to decrease could also cause

this decrease in moment of inertia. If this is the case, then this effect of decreasing mass to increase efficiency must be overpowering any developmental plasticity that would cause the bones to increase their moment of inertia in response to the repeated loading.

The second moment of area measures for the cranial-caudal (I_{CC}) and medial-lateral/dorsal-ventral ($I_{ML/DV}$) axes showed significant differences between exercise and control groups but not between the tibiotarsus and humerus. As with the moment of inertia, the effect of decreasing mass to increase efficiency could also cause this decrease in the second moment of area.

Conclusions

As was found in previous studies, the humerus experiences a great deal of torsion during flight (Swartz et al. 1992; de Margerie 2002; de Margerie et al. 2005). However, we found the tibiotarsus also experiences torsion, although to a much lesser degree. Patterns of vascular orientation that are attributed to torsional loading from flight may also be related to the higher magnitude of strain, the greater variety of strain (compression, tension and shear) and higher strain rate experienced by the humerus. Further studies to tease apart these components are necessary if we are to use vascular orientation to predict strain patterns and/or bone function. Additionally

patterns in vascular orientation were found to be significantly affected by exercise, indicating a degree of plasticity in the bones that would cause additional difficulty in using vascular orientation to make predictions about differences in bone function between species but would aid in its use for predicting differences between individuals. Differences in vascular orientation were not perceptible in a qualitative sense, however, and it is imperative that they be quantified.

Osteocyte density was found to be higher on average in exercised animals than in the controls. Bone that experiences increased loading cycles also experience fatigue damage in the form of microcracks. In order to prevent fatigue failure, this microdamage must be detected and repaired through remodeling (Carter 1984). Osteocytes function, in part, as mechanoreceptors in the bone (Cullinane 2002; Ehrlich and Lanyon 2002; Pearson and Lieberman 2004). It is therefore logical that as a bone experiences increased loading cycles, as the exercised guinea fowl in this study did, the bone would benefit from increased osteocyte density.

This study elucidates some of the relationships between the function of a bone and its microstructural and geometric characteristics. Many predictions of the association between bone microstructure and its function proved intractable, perhaps due to a more complex relationship between bone and forces acting upon it. It is clear that additional studies correlating *in vivo*

bone strain measures with these and other parameters will be necessary to bring such relationships into focus.

Literature Cited

Biewener, A. A. 1992. In vivo measurement of bone strain and tendon force. Pp. 123-147 *in* A. A. Biewener, ed. Biomechanics:Structures and Systems. A Practical Approach. Oxford University Press, Oxford.

Biewener, A. A., and K. P. Dial. 1995. In Vivo Strain in the Humerus of Pigeons (*Columba livia)* During Flight. Journal of Morphology 225:61-75.

Biewener, A. A., S. M. Swartz, and J. E. A. Bertram. 1986. Bone Modeling During Growth: Dynamic Strain Equilibrium in the Chick Tibiotarsus. Calcified Tissue International 39:390-395.

Carter, D. R. 1978. Anisotropic analysis of strain rosette information from cortical bone. Journal of Biomechanics 11:199-202.

Carter, D. R. 1984. Mechanical loading histories and cortical bone remodeling. Calcified Tissue International 36:19-24.

Carter, D. R., and W. C. Hayes. 1976. Bone compressive strength: the influence of density and strain rate. Science 194:1174-1176.

Chamay, A., and P. Tschantz. 1972. Mechanical influences in bone remodeling. Experimental research on Wolff's law Journal of Biomechanics 5:173-180.

Clark, J. M. 1990. The structure of vascular channels in the subchondral plate. Journal of Anatomy 171:105-115.

Cullinane, D. M. 2002. The role of osteocytes in bone regulation: Mineral homeostasis versus mechanoreception. Journal of Musculoskeletal and Neuronal Interaction 2:242-244.

de Boef, M., and H. C. E. Larsson. 2007. Bone Microstructure: quantifying bone vascular orientation. Canadian Journal of Zoology 85:63-70.

de Margerie, E. 2002. Laminar bone as an adaptation to torsional loads in flapping flight. Journal of Anatomy 201:521-526.

de Margerie, E., S. Sanchez, J. Cubo, and J. Castanet. 2005. Torsional Resistance as a Principal Component of the Structural Design of Long Bones: Comparative Multivariate Evidence in Birds. The Anatomical Record Part A 282A:49-66.

de Ricqlès, A., F. Meunier, J. Castanet, and H. Francillon-Vieillot. 1991. Comparative microstructure of bone. Pp. 1-78 *in* B. Hall, ed. Bone. CRC Press.

Ehrlich, P. J., and L. E. Lanyon. 2002. Mechanical Strain and Bone Cell Function: A Review. Osteoporosis International 13:688-700.

Habib, M. B., and C. B. Ruff. 2008. The effects of locomotion on the structural characteristics of avian limb bones. Zoological Journal of the Linnean Society 153:601-624.

Lanyon, L. E., P. T. Magee, and D. G. Baggott. 1979. Relationship of function stress and strain to the processes of bone remodeling- Experimental study on the sheep radius. Journal of Biomechanics 12.

Lieberman, D. E., O. M. Pearson, J. D. Polk, B. Demes, and A. W. Crompton. 2003. Optimization of bone growth and remodeling in response to loading in tapered mammalian limbs. The Journal of Experimental Biology 206.

Main, R. P., and A. A. Biewener. 2004. Ontogenetic patterns of limb loading, in vivo bone strains and growth in the goat radius. The Journal of Experimental Biology 207:2577-2588.

O'Connor, J. A., L. E. Lanyon, and H. MacFie. 1982. The influence of strain rate on adaptive bone remodelling. Journal of Biomechanics 15:767-781.

Pearson, O. M., and D. E. Lieberman. 2004. The Aging of Wolff's "Law": Ontogeny and Responses to Mechanical Loading in Cortical Bone. Yearbook of Physical Anthropology 47:63-99.

R_Development_Core_Team. 2009. R: A Language and Environment for Statistical Computing *in* R. F. f. S. Computing, ed, Vienna, Austria.

Ruff, C., B. Holt, and E. Trinkaus. 2006. Who's Afraid of the Big Bad Wolff?: "Wolff's Law" and Bone Functional Adaptation. American Journal of Physical Anthropology 129:484-489.

Skedros, J. 2005. Osteocyte lacuna population densities in sheep, elk and horse calcanei. Cells Tissues Organs 181:23-27.

Skedros, J. G., T. R. Grunander, and M. W. Hamrick. 2005. Spatial distribution of osteocyte lacunae in equine radii and third metacarpals:

Considerations for cellular communication, microdamage detection and metabolism. Cells Tissues Organs 180:215-236.

Skedros, J. G., S. M. Sorenson, and N. H. Jenson. 2007. Are distributions of secondary osteon variants useful for interpreting load history in mammalian bones? Cells Tissues Organs 185:285-307.

Starck, J., and A. Chinsamy. 2002. Bone microstructure and developmental plasticity in birds and other dinosaurs. Journal of Morphology 254:232-246.

Swaddle, J. P., and A. A. Biewener. 2000. Exercise and reduced muscle mass in starlings. Nature 406:585-586.

Swartz, S. M., M. B. Bennett, and D. R. Carrier. 1992. Wing bone stresses in free flying bats and the evolution of skeletal design for flight. Nature 359.

Wolff, J. 1892. Das Gesetz der Transformation der Knochen *in* A. Hirchwild., ed, Berlin

Woo, S. L., S. C. Kuei, D. Amiel, M. A. Gomez, W. C. Hayes, F. C. White, and W. H. Akeson. 1981. The effect of prolonged physical training on the properties of long bone:a study of Wolff's Law. The Journal of Bone and Joint Surgery 63:780-787.

CONCLUSIONS AND FUTURE RESEARCH

The effects of physiology, function and phylogeny on bone microstructure are strong and significant. The variance partitioning analyses done in chapter 3 identified each as a significant contributor to the variance found in both bone microstructure and bone geometry metrics. However, it was also found that the interactions between these three variables contribute much more to the variance in these measures than any one does independently. Thus, if bone microstructure is to be used to estimate any one of physiology, function or phylogeny, as has been done in the past, it must be done with some independent control for the other two factors.

For example, physiological effects on bone microstructural properties are not consistent between species as was determined in chapter 2. Bone growth marks, while common in the three species examined here, do not number one-to-one with organismal age. These organisms tended to produce more than one growth mark per year of age. However, some individuals produced no growth marks at all. While the use of growth marks for aging ectothermic species is common and well supported, this work suggests that its use should be limited in endothermic species. Specifically such uses should be limited to species for which a controlled study of bone-age to known-age has been done.

The variable effects of function on bone were demonstrated more specifically in Chapter 4. The microstructural patterns found in the humerus

and tibiotarsus of the GuineaFowl studied here are similar to patterns found in the other avian species studied to date. However, previous studies have attributed these patterns to differences in torsional loading between the humerus and tibiotarsus. Here it is demonstrated that the tibiotarsus also experiences torsional loads, albeit to a lesser degree than the humerus. Also, it is noted that the humerus experiences a greater magnitude of strain and a wider range of strain types with all portions of the bone experiences tension, compression and torsion. Additionally, the humerus experiences greater strain-rate as each loading cycle (wingstroke) occurs much more quickly than a loading cycle in the tibiotarsus (a step).

In considering the major findings in all chapters a few patterns emerge. It can be noted that in both the carnivorans and the GuineaFowl areas which are known to experience high bending stresses or those that are postulated to do so are dominated by vascular canals with longitudinal orientations. Examples of this are seen in the GuineaFowl tibiotarsus and the protuberances on the humeri and femora in the mammals. Also, the previously suggested hypothesis that a laminar arrangement of vascular canals is associated with high torsional loads is supported by findings of this pattern in both the GuineaFowl humerus and central portions of the mammalian cortical bone.

The effects of phylogeny, function and physiology on bone microstructure are just beginning to be elucidated. The use of bone microstructure in paleontological and ecological studies can be a highly valuable tool. However, its use is dependent on a

good understanding of what bone microstructure patterns reflect. Such an understanding will only come with additional observational and experimental studies in modern species from all taxonomic groups.

Appendix 1: Taxa and skeletal elements used in Chapter 1

Amphibia

Dutuitosaurus ouazzouii – femur (Steyer *et al.* 2004)

Amniota

Synapsida

Diictodon feliceps – femur; humerus ; radius, tibia, ulna (Ray and Chinsamy 2004)

Diapsida

Ornithischia

Psittacosaurus mongoliensis – tibia (Erickson and Tumanova 2000)

Saurischia

Sauropodomorpha

Janenschia rubusta – femur (Sander 2000)

Barosaurus africanus – femur; humerus (Sander 2000)

Brachiosaurus brancai – humerus (Sander 2000)

Dicraeosaurus hansemanni - femur (Sander 2000)

Theropoda

Coelophysis (Padian *et al.* 2001)

Troodon (Padian *et al.* 2001)

Hesperornis (Padian *et al.* 2001)

Tyrannosaurus rex – femur; fibula; tibia (Horner and Padian 2004)

Aves

Confuciusornis (Padian *et al.* 2001)

Dromaius novaehollandiae - digit 3, phalanx 1; humerus; (Castanet *et al.* 2000)

Struthio camelus – femur; tibiotarsus (Castanet *et al.* 2000)

Enantiornithes (Padian *et al.* 2001)

Dinornis (Padian *et al.* 2001)

Anas platyrhynchos – humerus; radius; tibiotarsus; ulna (de Margerie *et al.* 2002)

Confuciusornis sanctus - femur; metatarsus; phalanx; radius; tibia; ulna (de Ricqles *et al.* 2003)

Aptenodytes patagonicus - femur; humerus; radius; tibiotarsus (de Margerie *et al.* 2004)

specimen	species	element	length (mm)	tooth age (years)	bone age (years)
362	fox	femur	123.6	0.5	2.0
363	fox	femur	114.5	1.5	3.0
363	fox	humerus	126.6	1.5	4.0
364	fox	femur	118.5	1.5	4.0
364	fox	humerus	128.4	1.5	3.0
365	fox	femur	119.0	0.5	1.0
365	fox	humerus	130.4	0.5	2.0
366	fox	femur	123.5	0.5	1.0
366	fox	humerus	127.4	0.5	2.0
367	fox	femur	121.9	0.5	2.0
367	fox	humerus	135.5	0.5	2.0
368	fox	femur	129.7	1.5	4.0
368	fox	humerus	131.2	1.5	4.0
369	fox	femur	126.8	1.5	3.0
369	fox	humerus	137.5	1.5	4.0
370	fox	femur	129.4	0.5	3.0
370	fox	humerus	NA	0.5	1.0
371	fox	femur	118.4	0.5	2.0
371	fox	humerus	133.7	0.5	2.0
373	fox	femur	127.4	0.5	1.0
373	fox	humerus	130.9	0.5	2.0
402	fox	femur	138.9	0.5	2.0
403	fox	femur	131.1	0.5	2.0
403	fox	humerus	137.4	0.5	3.0
404	fox	femur	129.7	0.5	2.0
404	fox	humerus	129.8	0.5	2.0
405	fox	femur	123.8	0.5	2.0
405	fox	humerus	134.0	0.5	2.0
406	fox	femur	127.4	0.5	2.0
406	fox	humerus	130.3	0.5	2.0
407	fox	femur	121.8	0.5	2.0
407	fox	humerus	NA	0.5	2.0
21	raccoon	femur	86.1	1.5	3.0
23	raccoon	femur	119.7	0.5	2.0
24	raccoon	femur	123.3	6.5	7.0
25	raccoon	femur	115.6	1.5	3.0
28	raccoon	femur	99.6	1.5	4.0
30	raccoon	femur	102.0	0.5	1.0

31	raccoon	femur	97.2	0.5	0.0
32	raccoon	humerus	93.1	1.5	3.0
33	raccoon	humerus	65.4	0.5	1.0
34	raccoon	humerus	87.0	0.5	2.0
35	raccoon	humerus	NA	0.5	2.0
36	raccoon	humerus	NA	0.5	0.0
902	raccoon	humerus	98.9	0.5	1.0
903	raccoon	femur	89.2	0.5	1.0
903	raccoon	humerus	96.8	0.5	1.0
904	raccoon	femur	87.7	0.5	2.0
904	raccoon	humerus	105.3	0.5	2.0
905	raccoon	femur	96.3	0.5	1.0
905	raccoon	humerus	115.7	0.5	1.0
906	raccoon	femur	98.1	2.5	5.0
906	raccoon	humerus	92.0	2.5	4.0
907	raccoon	femur	84.7	0.5	3.0
907	raccoon	humerus	97.5	0.5	2.0
908	raccoon	femur	87.3	0.5	2.0
908	raccoon	humerus	101.8	0.5	2.0
909	raccoon	femur	103.8	1.5	4.0
909	raccoon	humerus	124.7	1.5	4.0
910	raccoon	femur	105.0	1.5	3.0
910	raccoon	humerus	129.6	1.5	3.0
911	raccoon	femur	NA	2.5	6.0
911	raccoon	humerus	125.8	2.5	5.0
912	raccoon	femur	104.2	3.5	8.0
700	skunk	femur	60.7	0.5	1.0
700	skunk	humerus	58.1	0.5	1.0
701	skunk	femur	54.7	1.5	1.0
701	skunk	humerus	56.9	1.5	1.0
702	skunk	femur	59.0	1.5	1.0
702	skunk	humerus	67.4	1.5	1.0
703	skunk	femur	59.1	0.5	1.0
703	skunk	humerus	73.4	0.5	1.0
704	skunk	femur	64.1	0.5	0.0
704	skunk	humerus	77.9	0.5	0.0
705	skunk	femur	66.1	2.5	5.0
705	skunk	humerus	60.6	2.5	5.0
706	skunk	femur	54.9	0.5	2.0
706	skunk	humerus	56.2	0.5	2.0

707	skunk	femur	53.7	0.5	1.0
707	skunk	humerus	74.6	0.5	1.0
708	skunk	femur	65.1	0.5	1.0
708	skunk	humerus	NA	0.5	2.0
709	skunk	femur	54.6	0.5	2.0
709	skunk	humerus	68.6	0.5	1.0
710	skunk	femur	58.4	1.5	4.0
710	skunk	humerus	71.2	1.5	4.0
711	skunk	femur	60.6	1.5	3.0
711	skunk	humerus	67.0	1.5	4.0
712	skunk	femur	56.0	0.5	3.0
712	skunk	humerus	71.2	0.5	3.0
713	skunk	femur	60.8	0.5	3.0
713	skunk	humerus	57.6	0.5	2.0
714	skunk	femur	55.0	0.5	2.0
714	skunk	humerus	69.2	0.5	2.0
715	skunk	femur	60.2	0.5	1.0
715	skunk	humerus	70.8	0.5	2.0
716	skunk	femur	60.3	1.5	3.0
716	skunk	humerus	65.0	1.5	3.0
717	skunk	femur	55.8	1.5	4.0
717	skunk	humerus	67.4	1.5	4.0
718	skunk	femur	57.6	1.5	3.0
718	skunk	humerus	62.5	1.5	4.0
719	skunk	femur	52.2	0.5	2.0
719	skunk	humerus	73.0	0.5	1.0
720	skunk	femur	63.1	0.5	1.0
720	skunk	humerus	62.2	0.5	2.0
721	skunk	femur	58.4	0.5	2.0
721	skunk	humerus	66.6	0.5	1.0
722	skunk	femur	58.2	0.5	1.0
722	skunk	humerus	68.8	0.5	1.0
723	skunk	femur	60.1	2.5	4.0
723	skunk	humerus	69.6	2.5	5.0

Individual	element	lateralization	length	sex	RI	LI	OD	BMR	hibernate
Gulo_gulo_1	humerus	L	143.96	NA	43.8898	28.9331	9323.6438	197.25881	N
Gulo_gulo_1	femur	L	146.78	NA	35.335	24.0328	10008.3541	197.25881	N
Gulo_gulo_10	humerus	L	144.76	NA	43.6588	30.5119	19883.3101	197.25881	N
Gulo_gulo_10	femur	L	150.27	NA	36.8027	27.2866	19304.1449	197.25881	N
Gulo_gulo_11	humerus	L	136.01	NA	39.8434	30.0345	2390.7719	197.25881	N
Gulo_gulo_11	femur	L	143.7	NA	36.7071	27.4015	4159.6226	197.25881	N
Gulo_gulo_12	humerus	R	145.95	NA	41.5122	29.4929	6779.8512	197.25881	N
Gulo_gulo_12	femur	R	152.49	NA	37.4318	28.1798	4380.7993	197.25881	N
Gulo_gulo_13	humerus	L	124.29	NA	46.5874	27.871	1154.3989	197.25881	N
Gulo_gulo_13	femur	L	128.37	NA	44.8395	16.9124	310.1731	197.25881	N
Gulo_gulo_14	humerus	L	144.7	NA	40.8059	29.2548	14378.8133	197.25881	N
Gulo_gulo_14	femur	L	152.37	NA	35.0125	29.9791	15666.3889	197.25881	N
Gulo_gulo_15	humerus	L	122.59	NA	44.7108	27.8017	843.7245	197.25881	N
Gulo_gulo_15	femur	L	129.49	NA	37.8707	29.2412	6631.2799	197.25881	N
Gulo_gulo_16	humerus	R	121.8	NA	46.0762	28.8031	3038.8908	197.25881	N
Gulo_gulo_16	femur	R	127.44	NA	36.4774	24.8002	23635.524	197.25881	N
Gulo_gulo_17	humerus	R	142.95	NA	44.1603	29.1708	6180.3875	197.25881	N
Gulo_gulo_17	femur	R	145.29	NA	37.7949	27.8341	6776.6389	197.25881	N
Gulo_gulo_18	humerus	L	120.36	NA	41.4249	29.4018	7504.799	197.25881	N
Gulo_gulo_18	femur	L	126.23	NA	38.0186	27.1291	1305.5282	197.25881	N
Gulo_gulo_19	humerus	L	127.82	NA	43.2588	28.2569	2029.2556	197.25881	N
Gulo_gulo_19	femur	L	134.59	NA	38.7156	28.7604	13821.6706	197.25881	N
Gulo_gulo_2	humerus	L	140.16	NA	40.2303	29.7966	7501.8919	197.25881	N
Gulo_gulo_2	femur	L	144.91	NA	36.2632	26.7279	10561.5181	197.25881	N
Gulo_gulo_20	humerus	L	122.22	NA	42.4095	28.575	4002.1044	197.25881	N
Gulo_gulo_20	femur	L	129.48	NA	36.0177	26.969	15423.3443	197.25881	N
Gulo_gulo_21	humerus	L	145.96	NA	41.2271	29.7071	12949.5808	197.25881	N

Individual	element	lateralization	length	sex	RI	LI	OD	BMR	hibernate
Gulo_gulo_21	femur	L	158.23	NA	38.7062	29.9163	3023.9093	197.25881	N
Gulo_gulo_22	humerus	L	144.17	NA	43.478	28.0899	2624.9879	197.25881	N
Gulo_gulo_22	femur	L	151.38	NA	36.5867	27.2171	25682.8898	197.25881	N
Gulo_gulo_23	humerus	L	144.03	NA	43.0352	28.4723	3363.3462	197.25881	N
Gulo_gulo_23	femur	L	151.38	NA	33.3606	24.5712	26131.5244	197.25881	N
Gulo_gulo_24	humerus	L	126.51	NA	40.7018	29.4413	1694.156	197.25881	N
Gulo_gulo_24	femur	L	129.77	NA	35.8516	30.4527	7775.2985	197.25881	N
Gulo_gulo_25	humerus	R	128.24	NA	41.5466	30.6115	1791.9632	197.25881	N
Gulo_gulo_25	femur	R	135.87	NA	35.1602	28.4915	11273.9972	197.25881	N
Gulo_gulo_3	humerus	R	133.75	NA	33.9	31.3	1467.0305	197.25881	N
Gulo_gulo_3	femur	R	138.63	NA	33.9	33.8	1377.9161	197.25881	N
Gulo_gulo_4	humerus	L	140.16	NA	43.6933	28.0345	6769.9255	197.25881	N
Gulo_gulo_4	femur	L	145.83	NA	37.0332	26.3221	14394.9126	197.25881	N
Gulo_gulo_5	humerus	L	125.98	NA	44.0108	28.6371	1915.2884	197.25881	N
Gulo_gulo_5	femur	L	134.42	NA	36.5303	29.0667	35783.6723	197.25881	N
Gulo_gulo_6	humerus	L	143.69	NA	43.5423	28.7442	4810.2739	197.25881	N
Gulo_gulo_6	femur	L	150.67	NA	36.6442	28.283	18704.5126	197.25881	N
Gulo_gulo_7	humerus	L	140.44	NA	40.9266	30.1008	13854.7016	197.25881	N
Gulo_gulo_7	femur	L	144.04	NA	40.1924	29.3997	744.5925	197.25881	N
Gulo_gulo_8	humerus	L	137.39	NA	42.1772	30.8218	9837.6906	197.25881	N
Gulo_gulo_8	femur	L	143.83	NA	31.7111	28.1697	25608.173	197.25881	N
Gulo_gulo_9	humerus	R	145.34	NA	48	28.4	1064.7802	197.25881	N
Gulo_gulo_9	femur	L	149.98	NA	29.6893	32.0446	624.9413	197.25881	N
Martes_americana_1	humerus	R	65.26	M	39.5887	22.2048	11975.2602	317.28324	N
Martes_americana_1	femur	R	72.85	M	43.6247	29.7648	11209.9994	317.28324	N
Martes_americana_10	humerus	R	56.89	M	37.3826	20.6553	999.4621	317.28324	N
Martes_americana_10	femur	R	63.92	M	47.1067	27.28	619.324	317.28324	N

Individual	element	lateralization	length	sex	RI	LI	OD	BMR	hibernate
Martes_americana_11	humerus	R	56.47	M	41.0245	21.8918	1901.1735	317.28324	N
Martes_americana_11	femur	R	62.37	M	38.535	34.7	331.1768	317.28324	N
Martes_americana_12	humerus	R	56.95	M	39.3679	22.5716	20.5015	317.28324	N
Martes_americana_12	femur	R	63.04	M	42.4813	20.4227	660.9911	317.28324	N
Martes_americana_13	humerus	R	58.77	M	41.7156	21.8574	28906.642	317.28324	N
Martes_americana_13	femur	R	64.7	M	42.8028	27.3725	1873.5742	317.28324	N
Martes_americana_14	humerus	R	57.13	M	45.2686	20.8301	6137.9521	317.28324	N
Martes_americana_14	femur	R	62.53	M	42.2791	28.5124	383.9417	317.28324	N
Martes_americana_15	humerus	R	55.58	M	41.6813	22.076	3825.5333	317.28324	N
Martes_americana_15	femur	R	61.82	M	42.8289	27.6253	23389.4922	317.28324	N
Martes_americana_16	humerus	L	58.93	M	39.1222	21.3321	5398.0735	317.28324	N
Martes_americana_16	femur	L	63.93	M	43.8293	30.4479	791.9	317.28324	N
Martes_americana_17	humerus	R	58.37	M	41.6172	20.8065	2907.2636	317.28324	N
Martes_americana_17	femur	R	64.7	M	45.9821	26.8427	7420.0745	317.28324	N
Martes_americana_18	humerus	R	65.55	M	39.1029	23.1624	69.3144	317.28324	N
Martes_americana_18	femur	R	72.7	M	43.1862	28.9698	1873.475	317.28324	N
Martes_americana_19	humerus	R	57.5	F	41.4704	21.5321	20460.5399	317.28324	N
Martes_americana_19	femur	R	64.47	F	43.9714	25.9849	2437.3715	317.28324	N
Martes_americana_2	humerus	L	64.39	M	42.3704	20.5977	1995.114	317.28324	N
Martes_americana_2	femur	L	69.7	M	42.8421	26.4423	7530.1748	317.28324	N
Martes_americana_20	humerus	R	57.42	F	38.7184	20.7084	5007.0863	317.28324	N
Martes_americana_20	femur	R	63.71	F	43.7022	25.0812	9980.176	317.28324	N
Martes_americana_21	humerus	R	57.13	F	42.3231	21.9819	1161.0324	317.28324	N
Martes_americana_21	femur	R	63.69	F	43.5198	28.7271	5804.2739	317.28324	N
Martes_americana_22	humerus	R	56.85	F	42.9546	22.8289	6918.687	317.28324	N
Martes_americana_22	femur	R	64.33	F	44.1739	24.8365	2714.2397	317.28324	N
Martes_americana_23	humerus	R	59.15	F	43.5675	21.9478	8407.4159	317.28324	N

Individual	element	lateralization	length	sex	RI	LI	OD	BMR	hibernate
Martes_americana_23	femur	R	65.69	F	44.5512	25.0105	2649.0082	317.28324	N
Martes_americana_24	humerus	R	54.06	F	43.316	22.1069	569.7416	317.28324	N
Martes_americana_24	femur	R	61.41	F	42.7723	26.3245	8637.767	317.28324	N
Martes_americana_25	humerus	R	57.14	F	40.1155	21.5524	4822.5044	317.28324	N
Martes_americana_25	femur	R	61.57	F	42.2478	24.6553	14868.7345	317.28324	N
Martes_americana_26	humerus	R	57.53	F	41.9099	21.3388	3835.4847	317.28324	N
Martes_americana_26	femur	R	64.41	F	43.0395	28.5228	9525.4886	317.28324	N
Martes_americana_27	humerus	L	62.2	F	40.0478	23.1839	312.0239	317.28324	N
Martes_americana_27	femur	L	69.93	F	44.1667	26.9436	301.7	317.28324	N
Martes_americana_3	humerus	R	65.9	M	41.9958	21.6306	1547.5162	317.28324	N
Martes_americana_3	femur	R	72.55	M	41.5254	29.191	8420.824	317.28324	N
Martes_americana_4	humerus	R	66.3	M	40.4754	22.0848	6345.8477	317.28324	N
Martes_americana_4	femur	R	72.05	M	42.0323	27.1424	113.1522	317.28324	N
Martes_americana_5	humerus	R	66.37	M	40.4127	20.4244	8428.2888	317.28324	N
Martes_americana_5	femur	R	73.55	M	40.6495	26.8329	21388.2657	317.28324	N
Martes_americana_6	humerus	R	57.07	M	40.1226	20.6958	2960.3511	317.28324	N
Martes_americana_6	femur	R	64.31	M	42.1594	28.4906	5767.7965	317.28324	N
Martes_americana_7	humerus	L	64.24	M	42.6319	22.0972	15020.5625	317.28324	N
Martes_americana_7	femur	L	69.74	M	42.0183	29.2286	12097.1922	317.28324	N
Martes_americana_8	humerus	R	58.07	M	40.877	21.4621	3816.833	317.28324	N
Martes_americana_8	femur	R	63.37	M	45.2713	26.3902	3530.4949	317.28324	N
Martes_americana_9	humerus	R	57.2	M	46.3148	20.5625	362.7596	317.28324	N
Martes_americana_9	femur	R	63.41	M	43.8103	24.6363	5972.1819	317.28324	N
Martes_pennanti_1	humerus	R	98.43	NA	45.4747	13.9295	10561.8461	517.4	N
Martes_pennanti_1	femur	R	107.98	NA	45.0279	20.584	1143.1406	517.4	N
Martes_pennanti_10	humerus	R	99.87	M	47.7332	13.7954	21511.8905	517.4	N
Martes_pennanti_10	femur	R	109.61	M	50.1787	15.2172	27813.4283	517.4	N

Individual	element	lateralization	length	sex	RI	LI	OD	BMR	hibernate
Martes_pennanti_11	humerus	R	97.43	M	44.1267	14.2541	316.3103	517.4	N
Martes_pennanti_11	femur	R	107.24	M	50.8783	16.107	30986.2577	517.4	N
Martes_pennanti_12	humerus	R	101.17	M	49.2944	14.4426	15395.7627	517.4	N
Martes_pennanti_12	femur	R	110.88	M	49.7157	13.5463	26231.4635	517.4	N
Martes_pennanti_13	humerus	R	88.07	F	48.2781	13.908	8043.0125	517.4	N
Martes_pennanti_13	femur	R	95.46	F	55.7616	14.6264	267.5228	517.4	N
Martes_pennanti_14	humerus	L	86.87	F	45.1386	13.5847	16626.578	517.4	N
Martes_pennanti_14	femur	L	93.55	F	50.1979	14.9171	2836.0613	517.4	N
Martes_pennanti_15	humerus	L	84.04	F	45.8886	14.5594	15921.8474	517.4	N
Martes_pennanti_15	femur	L	93.73	F	49.9706	15.3075	2606.4047	517.4	N
Martes_pennanti_16	humerus	R	86.2	F	48.593	14.1971	9858.3615	517.4	N
Martes_pennanti_16	femur	R	94.85	F	48.6887	18.0126	5356.7331	517.4	N
Martes_pennanti_17	humerus	R	101.45	M	47.3115	13.9308	26004.3063	517.4	N
Martes_pennanti_17	femur	R	109.13	M	49.438	17.6717	19226.8281	517.4	N
Martes_pennanti_18	humerus	R	86.14	F	47.3182	14.1283	21344.2518	517.4	N
Martes_pennanti_19	humerus	R	85.52	F	46.1338	13.9525	6093.2197	517.4	N
Martes_pennanti_2	humerus	R	88.31	F	46.0198	13.0627	5216.9712	517.4	N
Martes_pennanti_2	femur	R	96.79	F	50.0122	17.95	13775.3553	517.4	N
Martes_pennanti_3	humerus	R	102.1	M	44.8801	13.4516	851.2528	517.4	N
Martes_pennanti_3	femur	R	111.65	M	46.2451	16.814	5970.1777	517.4	N
Martes_pennanti_4	humerus	R	97.82	M	46.1886	14.1346	3763.7311	517.4	N
Martes_pennanti_4	femur	R	105.49	M	49.9811	13.4671	154.1601	517.4	N
Martes_pennanti_5	humerus	R	86.44	F	48.2448	13.5422	7886.1151	517.4	N
Martes_pennanti_5	femur	R	97.08	F	51.0322	17.9345	7437.3152	517.4	N
Martes_pennanti_6	humerus	L	98.87	F	49.9805	13.3784	11453.1938	517.4	N
Martes_pennanti_6	femur	L	104.78	F	50.4484	15.562	25990.5648	517.4	N
Martes_pennanti_7	humerus	R	99.9	M	51.3619	13.7766	808.3818	517.4	N

Individual	element	lateralization	length	sex	RI	LI	OD	BMR	hibernate
Martes_pennanti_7	femur	R	108.12	M	49.2886	14.7336	1793.6929	517.4	N
Martes_pennanti_8	humerus	R	85.68	F	47.0979	13.7443	18417.7647	517.4	N
Martes_pennanti_8	femur	R	92.5	F	49.1844	17.3032	16476.9526	517.4	N
Martes_pennanti_9	humerus	L	87.3	F	46.4309	13.3554	5682.5239	517.4	N
Martes_pennanti_9	femur	L	94.48	F	48.4866	16.2808	17160.3395	517.4	N
Mephitis_mephitis_1	humerus	L	58.06	M	54.9235	21.2323	1077.9616	279	Y
Mephitis_mephitis_1	femur	R	60.65	M	58.5932	25.5681	15091.7015	279	Y
Mephitis_mephitis_10	humerus	R	68.59	M	52.869	18.853	23122.3618	279	Y
Mephitis_mephitis_10	femur	R	54.62	M	58.9068	29.1643	22436.5966	279	Y
Mephitis_mephitis_11	humerus	L	71.17	F	50.6458	19.7434	23114.1154	279	Y
Mephitis_mephitis_11	femur	R	58.37	F	57.707	24.7849	13130.874	279	Y
Mephitis_mephitis_12	humerus	R	66.99	F	52.7494	18.5801	16841.2359	279	Y
Mephitis_mephitis_12	femur	L	60.59	F	59.4899	21.5428	10347.1466	279	Y
Mephitis_mephitis_13	humerus	R	71.21	F	50.0624	19.7082	15765.5898	279	Y
Mephitis_mephitis_13	femur	R	55.97	F	60.6186	24.7334	12913.3324	279	Y
Mephitis_mephitis_14	humerus	R	57.55	F	53.086	20.4219	6202.7771	279	Y
Mephitis_mephitis_14	femur	R	60.77	F	59.4425	24.9518	7755.0989	279	Y
Mephitis_mephitis_15	humerus	R	69.19	F	48.4518	19.6675	14721.1275	279	Y
Mephitis_mephitis_15	femur	R	54.99	F	59.5318	23.0452	10368.9725	279	Y
Mephitis_mephitis_16	humerus	R	70.75	F	52.1431	19.5975	12562.2538	279	Y
Mephitis_mephitis_16	femur	R	60.16	F	59.377	24.4525	1026.9154	279	Y
Mephitis_mephitis_17	humerus	R	64.99	F	50.5824	19.8086	1083.4834	279	Y
Mephitis_mephitis_17	femur	R	60.3	F	59.5413	22.8809	15651.3815	279	Y
Mephitis_mephitis_18	humerus	R	67.37	F	50.521	20.5172	13066.6353	279	Y
Mephitis_mephitis_18	femur	R	55.83	F	60.1222	24.0483	18044.04	279	Y
Mephitis_mephitis_19	humerus	R	62.54	F	51.9394	20.7206	1105.2738	279	Y
Mephitis_mephitis_19	femur	R	57.56	F	59.5485	24.8007	7464.6346	279	Y

Individual	element	lateralization	length	sex	RI	LI	OD	BMR	hibernate
Mephitis_mephitis_2	humerus	L	56.89	M	54.6737	18.9577	214.4406	279	Y
Mephitis_mephitis_2	femur	R	54.68	M	58.625	23.9938	3352.8779	279	Y
Mephitis_mephitis_20	humerus	R	73	F	51.1902	18.5561	11259.6681	279	Y
Mephitis_mephitis_20	femur	R	52.19	F	58.3318	15.8531	715.3992	279	Y
Mephitis_mephitis_21	humerus	R	62.22	F	53.1948	19.6329	23924.5606	279	Y
Mephitis_mephitis_21	femur	R	63.14	F	60.0182	26.257	22148.3294	279	Y
Mephitis_mephitis_22	humerus	R	66.63	M	51.5422	19.9685	12705.0177	279	Y
Mephitis_mephitis_22	femur	R	58.42	M	59.8155	25.4646	19467.8149	279	Y
Mephitis_mephitis_23	humerus	R	68.75	F	53.2603	19.2221	9183.6676	279	Y
Mephitis_mephitis_23	femur	R	58.21	F	59.5071	19.019	4862.3033	279	Y
Mephitis_mephitis_24	humerus	R	69.63	F	50.9779	21.6367	8681.3131	279	Y
Mephitis_mephitis_24	femur	R	60.08	F	59.6286	24.5478	1220.7012	279	Y
Mephitis_mephitis_3	humerus	R	67.43	M	45.5226	18.1695	324.9912	279	Y
Mephitis_mephitis_3	femur	R	59.04	M	59.3883	25.6292	7416.1655	279	Y
Mephitis_mephitis_4	humerus	R	73.4	M	52.0877	19.5135	13115.4463	279	Y
Mephitis_mephitis_4	femur	R	59.07	M	59.6895	25.4713	11813.1297	279	Y
Mephitis_mephitis_5	humerus	R	77.9	M	49.4229	19.8019	11963.8077	279	Y
Mephitis_mephitis_5	femur	R	64.08	M	61.0202	30.099	368.6629	279	Y
Mephitis_mephitis_6	humerus	R	60.57	M	52.1872	20.43	12467.9494	279	Y
Mephitis_mephitis_6	femur	L	66.06	M	59.3944	22.3207	19044.1789	279	Y
Mephitis_mephitis_7	humerus	R	56.18	M	48.6021	19.9961	10827.6813	279	Y
Mephitis_mephitis_7	femur	R	54.92	M	58.845	26.0753	1153.9447	279	Y
Mephitis_mephitis_8	humerus	R	74.64	M	52.5176	19.2014	11704.7949	279	Y
Mephitis_mephitis_8	femur	R	53.73	M	57.9861	25.5417	18001.128	279	Y
Mephitis_mephitis_9	femur	R	65.1	M	60.4345	24.2159	14176.861	279	Y
Mustela_erminea_1	femur	R	29.08	NA	82.067	12.7407	107.6949	862.27192	N
Mustela_erminea_10	humerus	R	30.34	M	61.5782	10.6472	29673.4206	957.51634	N

Individual	element	lateralization	length	sex	RI	LI	OD	BMR	hibernate
Mustela_erminea_10	femur	R	32.56	M	75.112	11.1859	19526.891	862.27192	N
Mustela_erminea_11	humerus	R	29.08	M	59.5909	11.2997	2081.8911	957.51634	N
Mustela_erminea_12	humerus	R	30.17	M	62.8369	12.6068	17361.9423	957.51634	N
Mustela_erminea_12	femur	R	31.86	M	78.8275	10.3121	861.2011	862.27192	N
Mustela_erminea_13	humerus	R	28.61	M	56.1947	11.0658	24815.6946	957.51634	N
Mustela_erminea_13	femur	R	30.6	M	76.6697	10.8287	9195.7136	862.27192	N
Mustela_erminea_14	humerus	R	30.76	M	63.5124	12.0002	5653.7405	957.51634	N
Mustela_erminea_14	femur	R	33.15	M	77.5966	10.0967	13033.9156	862.27192	N
Mustela_erminea_15	humerus	R	31.31	M	61.8301	11.3897	13508.6203	957.51634	N
Mustela_erminea_15	femur	R	33.4	M	77.0599	10.214	4237.7785	862.27192	N
Mustela_erminea_16	humerus	R	28.86	M	61.9234	11.1501	9564.304	957.51634	N
Mustela_erminea_16	femur	R	29.03	M	75.7739	12.4948	14475.7276	862.27192	N
Mustela_erminea_17	humerus	R	34.38	M	63.9996	11.3077	18178.9856	957.51634	N
Mustela_erminea_18	humerus	R	29.82	M	60.7535	11.9442	10550.5745	957.51634	N
Mustela_erminea_18	femur	R	31.2	M	77.6922	10.0684	5124.5282	862.27192	N
Mustela_erminea_19	humerus	R	31.47	M	61.0622	12.5354	3128.484	957.51634	N
Mustela_erminea_19	femur	R	32.63	M	75.2149	11.1293	23348.1946	862.27192	N
Mustela_erminea_2	femur	R	30.45	M	78.0114	10.095	2659.9424	862.27192	N
Mustela_erminea_20	humerus	R	28.11	M	58.5813	12.2377	508.9713	957.51634	N
Mustela_erminea_20	femur	R	29.69	M	78.2922	10.1486	18125.2505	862.27192	N
Mustela_erminea_21	femur	R	31.76	M	77.9149	9.9493	9793.1427	862.27192	N
Mustela_erminea_22	humerus	R	29.16	M	59.818	12.1048	17037.373	957.51634	N
Mustela_erminea_22	femur	R	31.5	M	75.4428	10.931	19105.5341	862.27192	N
Mustela_erminea_23	humerus	R	28.76	M	61.9653	10.7977	1130.7142	957.51634	N
Mustela_erminea_23	femur	R	29.85	M	76.4313	12.0266	428.4306	862.27192	N
Mustela_erminea_24	humerus	R	29.41	M	60.1721	12.367	8448.3042	957.51634	N
Mustela_erminea_25	humerus	R	28.57	M	58.4438	12.4303	8168.0046	957.51634	N

Individual	element	lateralization	length	sex	RI	LI	OD	BMR	hibernate
Mustela_erminea_26	humerus	R	27.94	M	63.6925	12.6822	7360.577	957.51634	N
Mustela_erminea_26	femur	R	32.58	M	77.2804	11.4618	3332.0715	862.27192	N
Mustela_erminea_4	humerus	R	29.22	M	61.3417	12.3454	18289.1152	957.51634	N
Mustela_erminea_4	femur	R	29.45	M	78.3239	9.1798	10747.0034	862.27192	N
Mustela_erminea_5	humerus	L	29.55	M	60.7501	12.3561	5931.3679	957.51634	N
Mustela_erminea_5	femur	R	30.89	M	78.5761	12.0563	17203.8758	862.27192	N
Mustela_erminea_6	humerus	R	33.15	M	64.137	12.1007	4794.9994	957.51634	N
Mustela_erminea_6	femur	R	33.88	M	75.1399	10.6986	6368.2674	862.27192	N
Mustela_erminea_7	humerus	R	32.94	M	65.4173	12.7645	1160.6001	957.51634	N
Mustela_erminea_8	humerus	R	29.94	M	60.2128	12.0857	6361.7872	957.51634	N
Mustela_erminea_8	femur	R	31.79	M	77.3264	11.3776	17898.4425	862.27192	N
Mustela_erminea_9	humerus	R	31.48	M	73.9384	9.8463	1774.0249	957.51634	N
Mustela_erminea_9	femur	R	33.5	M	79.2168	9.4856	1046.6932	862.27192	N
Procyon_lotor_1	femur	L	86.07	F	52.9044	21.3977	230.7749	153.13183	Y
Procyon_lotor_10	humerus	L	86.97	M	59.0746	13.8358	9044.4699	153.13183	Y
Procyon_lotor_13	humerus	R	98.87	M	61.8595	13.2672	722.8684	153.13183	Y
Procyon_lotor_14	humerus	L	96.78	M	57.6958	14.6088	3391.1924	153.13183	Y
Procyon_lotor_14	femur	L	89.22	M	53.7216	22.6814	6340	153.13183	Y
Procyon_lotor_15	humerus	L	105.27	M	57.5575	13.4311	3461.7312	153.13183	Y
Procyon_lotor_15	femur	L	87.73	M	51.2561	19.7854	37527.6446	153.13183	Y
Procyon_lotor_16	humerus	L	115.66	M	54.4725	13.602	5975.1022	153.13183	Y
Procyon_lotor_16	femur	L	96.33	M	51.1862	18.4443	39102.0089	153.13183	Y
Procyon_lotor_17	humerus	L	91.97	F	56.953	13.9094	4508.0749	153.13183	Y
Procyon_lotor_17	femur	L	98.12	F	50.5196	19.1701	41766.1538	153.13183	Y
Procyon_lotor_18	humerus	L	97.45	F	55.9198	13.4577	2602.5071	153.13183	Y
Procyon_lotor_18	femur	L	84.73	F	51.9051	18.6405	25312.478	153.13183	Y
Procyon_lotor_19	humerus	R	101.78	F	54.8839	13.317	596.7521	153.13183	Y

Individual	element	lateralization	length	sex	RI	LI	OD	BMR	hibernate
Procyon_lotor_19	femur	L	87.28	F	53.0744	20.6222	43242.6869	153.13183	Y
Procyon_lotor_2	femur	L	119.68	M	53.4316	18.95	58811.5621	153.13183	Y
Procyon_lotor_20	humerus	L	124.68	F	54.0795	14.118	5391.087	153.13183	Y
Procyon_lotor_20	femur	L	103.76	F	50.9572	19.1522	44100.4088	153.13183	Y
Procyon_lotor_21	humerus	L	129.58	M	56.0421	13.1741	601.532	153.13183	Y
Procyon_lotor_21	femur	L	104.99	M	51.0471	20.3773	24128.0047	153.13183	Y
Procyon_lotor_22	humerus	R	125.79	NA	55.2048	13.3859	798.3	153.13183	Y
Procyon_lotor_23	femur	L	104.23	F	51.6786	18.7698	34242.7716	153.13183	Y
Procyon_lotor_3	femur	L	123.26	F	49.6469	19.3202	28735.2206	153.13183	Y
Procyon_lotor_4	femur	L	115.56	M	50.4258	17.8995	7881.4391	153.13183	Y
Procyon_lotor_5	femur	L	99.56	M	50.741	18.7586	31128.9408	153.13183	Y
Procyon_lotor_6	femur	L	102.01	F	54.173	18.9871	26936.2242	153.13183	Y
Procyon_lotor_7	femur	R	97.15	F	48.2715	13.2934	816.1417	153.13183	Y
Procyon_lotor_8	humerus	L	93.1	F	52.3485	13.862	24.9792	153.13183	Y
Procyon_lotor_9	humerus	L	65.39	M	52.7797	13.3215	4666.7192	153.13183	Y
Vulpes_vulpes_1	femur	L	123.58	M	44.0163	15.3076	331.5896	253.01587	Y
Vulpes_vulpes_10	humerus	R	133.65	M	39.1681	18.5579	1398.4638	253.01587	N
Vulpes_vulpes_10	femur	R	118.42	M	42.3211	17.3043	121.4289	253.01587	N
Vulpes_vulpes_11	humerus	R	130.85	M	36.2433	25.4117	1033.7795	253.01587	N
Vulpes_vulpes_11	femur	R	127.38	M	35.7419	21.3241	460.8286	253.01587	N
Vulpes_vulpes_12	femur	L	138.9	M	41.7743	17.3242	1938.3238	253.01587	N
Vulpes_vulpes_13	humerus	L	137.41	M	39.7761	18.0071	232.2958	253.01587	N
Vulpes_vulpes_13	femur	R	131.09	M	39.2988	17.3863	12970.5233	253.01587	N
Vulpes_vulpes_14	humerus	R	129.8	M	42.2597	14.8188	4181.5267	253.01587	N
Vulpes_vulpes_14	femur	L	129.71	M	43.3652	17.7364	558.379	253.01587	N
Vulpes_vulpes_15	humerus	L	134.04	M	36.9259	17.4485	414.9297	253.01587	N
Vulpes_vulpes_15	femur	L	123.81	M	41.281	16.9151	9304.6955	253.01587	N

Individual	element	lateralization	length	sex	RI	LI	OD	BMR	hibernate
Vulpes_vulpes_16	humerus	L	130.26	M	40.4099	17.079	25274.0472	253.01587	N
Vulpes_vulpes_16	femur	L	127.37	M	43.9241	16.6651	4545.8306	253.01587	N
Vulpes_vulpes_17	femur	R	121.76	F	39.4951	18.153	2057.4444	253.01587	N
Vulpes_vulpes_18	humerus	R	122.04	NA	46.2736	11.4704	743.3942	253.01587	N
Vulpes_vulpes_2	humerus	L	126.56	F	39.7169	17.5037	2453.272	253.01587	N
Vulpes_vulpes_2	femur	L	114.52	F	41.796	16.57	2338.4566	253.01587	N
Vulpes_vulpes_3	humerus	L	128.42	F	41.1586	17.9176	3280.1046	253.01587	N
Vulpes_vulpes_3	femur	L	118.51	F	41.2631	16.5888	1833.3135	253.01587	N
Vulpes_vulpes_4	humerus	R	130.44	F	40.1571	15.4716	9715.3436	253.01587	N
Vulpes_vulpes_4	femur	L	118.98	F	40.65	17.3983	5794.8002	253.01587	N
Vulpes_vulpes_5	humerus	R	127.38	M	39.9275	16.1936	243.6657	253.01587	N
Vulpes_vulpes_5	femur	R	123.48	M	39.0263	16.3315	574.4029	253.01587	N
Vulpes_vulpes_6	humerus	R	135.54	F	40.8521	16.7749	19770.4103	253.01587	N
Vulpes_vulpes_6	femur	R	121.92	F	41.5523	16.3475	5140.9567	253.01587	N
Vulpes_vulpes_7	humerus	L	131.18	M	42.7498	18.9808	9337.6507	253.01587	N
Vulpes_vulpes_7	femur	L	129.71	M	39.257	14.6119	5351.9818	253.01587	N
Vulpes_vulpes_8	humerus	L	137.5	F	36.7739	17.2022	18064.6875	253.01587	N
Vulpes_vulpes_8	femur	L	126.82	F	40.0268	16.5018	1255.2736	253.01587	N
Vulpes_vulpes_9	femur	R	129.37	M	40.9338	17.8454	1152.6366	253.01587	N

Individual	Imax	Imin	J	area	home range	climb
Gulo_gulo_1	1057.43	1056.823	2114.253	79.9217	207.5	N
Gulo_gulo_1	729.0222	539.6626	1268.685	70.4435	207.5	N
Gulo_gulo_10	941.3443	1345.644	2286.989	110.24	207.5	N
Gulo_gulo_10	803.5071	569.319	1372.826	71.725	207.5	N
Gulo_gulo_11	784.0973	827.5144	1611.612	92.9313	207.5	N
Gulo_gulo_11	656.0107	502.3015	1158.312	75.3752	207.5	N
Gulo_gulo_12	1061.645	710.0196	1771.665	89.6067	207.5	N
Gulo_gulo_12	751.6623	641.966	1393.628	71.0532	207.5	N
Gulo_gulo_13	710.1948	498.9215	1209.116	67.3564	207.5	N
Gulo_gulo_13	425.4311	329.6671	755.0982	65.2161	207.5	N
Gulo_gulo_14	1053.25	983.7684	2037.019	69.8664	207.5	N
Gulo_gulo_14	670.5283	653.933	1324.461	69.9869	207.5	N
Gulo_gulo_15	886.6327	851.1309	1737.764	75.4012	207.5	N
Gulo_gulo_15	698.1265	578.4158	1276.542	70.0116	207.5	N
Gulo_gulo_16	897.8619	1113.455	2011.316	63.2979	207.5	N
Gulo_gulo_16	681.6688	546.625	1228.294	73.4083	207.5	N
Gulo_gulo_17	1203.417	1004.37	2207.787	64.4297	207.5	N
Gulo_gulo_17	787.7775	596.1257	1383.903	70.4372	207.5	N
Gulo_gulo_18	723.2351	527.023	1250.258	68.4784	207.5	N
Gulo_gulo_18	764.9411	564.1494	1329.091	77.25	207.5	N
Gulo_gulo_19	1426.849	207.402	1634.251	84.5991	207.5	N
Gulo_gulo_19	595.9799	588.3805	1184.36	74.2654	207.5	N
Gulo_gulo_2	1140.55	1138.295	2278.845	71.8243	207.5	N
Gulo_gulo_2	658.524	589.1556	1247.68	73.1109	207.5	N
Gulo_gulo_20	1285.156	978.8199	2263.976	98.2161	207.5	N
Gulo_gulo_20	695.4234	493.4829	1188.906	73.5299	207.5	N
Gulo_gulo_21	1079.977	643.9536	1723.931	92.8427	207.5	N

Individual	Imax	Imin	J	area	home range	climb
Gulo_gulo_21	747.5576	672.8082	1420.366	72.161	207.5	N
Gulo_gulo_22	1134.977	1058.231	2193.208	72.8636	207.5	N
Gulo_gulo_22	627.2725	602.0437	1229.316	73.5157	207.5	N
Gulo_gulo_23	941.9029	1203.939	2145.842	54.5456	207.5	N
Gulo_gulo_23	704.2182	622.2716	1326.49	76.4967	207.5	N
Gulo_gulo_24	912.3009	650.4172	1562.718	80.7745	207.5	N
Gulo_gulo_24	691.7389	668.2219	1359.961	66.1103	207.5	N
Gulo_gulo_25	1221.492	1079.81	2301.301	70.2114	207.5	N
Gulo_gulo_25	744.1497	477.5144	1221.664	76.3494	207.5	N
Gulo_gulo_3	1049.958	653.5605	1703.518	76.2549	207.5	N
Gulo_gulo_3	645.4575	553.5401	1198.998	70.5037	207.5	N
Gulo_gulo_4	1333.006	834.2404	2167.246	95.2989	207.5	N
Gulo_gulo_4	678.1107	557.8457	1235.956	74.1307	207.5	N
Gulo_gulo_5	1267.076	994.4318	2261.508	72.5878	207.5	N
Gulo_gulo_5	747.821	511.3977	1259.219	70.9959	207.5	N
Gulo_gulo_6	787.8136	1284.807	2072.621	91.5373	207.5	N
Gulo_gulo_6	648.2427	564.9946	1213.237	73.465	207.5	N
Gulo_gulo_7	811.9389	1351.757	2163.696	95.4053	207.5	N
Gulo_gulo_7	671.7908	561.1616	1232.952	69.0428	207.5	N
Gulo_gulo_8	1265.142	781.1869	2046.329	55.5082	207.5	N
Gulo_gulo_8	731.4518	569.8267	1301.279	72.0499	207.5	N
Gulo_gulo_9	1662.386	1432.069	3094.456	90.9108	207.5	N
Gulo_gulo_9	1075.642	872.4619	1948.104	82.0442	207.5	N
Martes_americana_1	8.3485	7.0915	15.44	8.0637	15.15	Y
Martes_americana_1	12.9824	9.672	22.6544	7.7059	4.12	Y
Martes_americana_10	12.482	9.083	21.5649	7.4571	15.15	Y
Martes_americana_10	11.9734	9.2344	21.2079	7.6259	15.15	Y

Individual	Imax	Imin	J	area	home range	climb
Martes_americana_11	8.743	6.7026	15.4456	7.9331	15.15	Y
Martes_americana_11	11.9734	9.2344	21.2079	7.6259	15.15	Y
Martes_americana_12	8.8413	6.8803	15.7217	7.9387	15.15	Y
Martes_americana_12	14.1164	10.7373	24.8537	7.9869	15.15	Y
Martes_americana_13	8.4244	6.6964	15.1208	7.9125	15.15	Y
Martes_americana_13	13.0977	9.6279	22.7256	7.6006	15.15	Y
Martes_americana_14	8.6924	6.743	15.4354	7.6623	15.15	Y
Martes_americana_14	12.5225	9.663	22.1855	7.851	15.15	Y
Martes_americana_15	8.8102	6.6391	15.4493	8.1823	15.15	Y
Martes_americana_15	12.9984	9.6545	22.6529	7.8173	15.15	Y
Martes_americana_16	8.3795	6.6117	14.9911	8.6213	15.15	Y
Martes_americana_16	12.6437	9.7338	22.3775	7.6804	15.15	Y
Martes_americana_17	8.4499	6.6837	15.1335	7.8265	15.15	Y
Martes_americana_17	12.5901	9.5308	22.1209	7.6748	15.15	Y
Martes_americana_18	8.8134	6.5249	15.3383	7.8602	15.15	Y
Martes_americana_18	12.8771	9.6798	22.557	7.6486	15.15	Y
Martes_americana_19	8.6487	6.7729	15.4216	8.3967	15.15	Y
Martes_americana_19	13.0049	9.6194	22.6243	7.8746	15.15	Y
Martes_americana_2	8.6812	6.7438	15.425	7.3775	15.15	Y
Martes_americana_2	12.9222	9.6305	22.5528	7.5942	15.15	Y
Martes_americana_20	8.7601	6.7477	15.5078	8.0973	15.15	Y
Martes_americana_20	12.5135	9.7686	22.282	7.7166	15.15	Y
Martes_americana_21	8.9365	6.7229	15.6594	8.7554	15.15	Y
Martes_americana_21	12.2098	9.7919	22.0017	7.7298	15.15	Y
Martes_americana_22	8.7512	6.342	15.0932	7.3346	15.15	Y
Martes_americana_22	12.6835	9.7528	22.4363	7.5807	15.15	Y
Martes_americana_23	8.4847	6.6418	15.1265	7.627	15.15	Y

Individual	Imax	Imin	J	area	home range	climb
Martes_americana_23	12.8809	9.7312	22.6121	7.7921	15.15	Y
Martes_americana_24	8.8079	6.773	15.5809	7.7454	15.15	Y
Martes_americana_24	12.7273	9.5117	22.239	8.1119	15.15	Y
Martes_americana_25	8.615	6.7937	15.4087	9.0337	15.15	Y
Martes_americana_25	13.216	9.7424	22.9585	7.789	15.15	Y
Martes_americana_26	8.4786	6.7609	15.2395	8.2691	15.15	Y
Martes_americana_26	12.5918	9.6641	22.2559	7.5586	15.15	Y
Martes_americana_27	3.6689	3.114	6.7829	6.4779	15.15	Y
Martes_americana_27	12.9601	9.717	22.6771	7.7832	15.15	Y
Martes_americana_3	8.2945	6.5682	14.8627	8.2287	15.15	Y
Martes_americana_3	12.8815	9.7978	22.6792	7.828	15.15	Y
Martes_americana_4	8.801	6.8397	15.6408	8.0225	15.15	Y
Martes_americana_4	13.0276	9.6193	22.647	7.7823	15.15	Y
Martes_americana_5	8.8898	7.0204	15.9101	8.2926	15.15	Y
Martes_americana_5	13.1119	9.6273	22.7392	7.7028	15.15	Y
Martes_americana_6	8.9759	6.8325	15.8084	8.3424	15.15	Y
Martes_americana_6	12.7144	9.6876	22.402	7.87	15.15	Y
Martes_americana_7	8.9406	6.8664	15.807	8.0423	15.15	Y
Martes_americana_7	12.5972	9.611	22.2082	7.9623	15.15	Y
Martes_americana_8	8.4908	6.7482	15.239	8.2225	15.15	Y
Martes_americana_8	12.7742	9.7884	22.5626	7.6009	15.15	Y
Martes_americana_9	9.7895	7.9913	17.7808	10.3149	15.15	Y
Martes_americana_9	13.026	9.716	22.742	7.7465	15.15	Y
Martes_pennanti_1	201.0956	135.517	336.6126	2.2391	25.9	Y
Martes_pennanti_1	168.533	162.995	331.5281	27.9262	25.9	Y
Martes_pennanti_10	204.5028	138.268	342.7709	32.0736	25.9	Y
Martes_pennanti_10	158.5006	283.7547	442.2552	28.3755	25.9	Y

Individual	Imax	Imin	J	area	home range	climb
Martes_pennanti_11	236.6922	132.0118	368.7039	34.0461	25.9	Y
Martes_pennanti_11	147.7433	299.3963	447.1396	29.9396	25.9	Y
Martes_pennanti_12	211.4561	138.3717	349.8278	32.1495	25.9	Y
Martes_pennanti_12	165.0738	294.367	459.4408	29.4367	25.9	Y
Martes_pennanti_13	217.1621	140.7197	357.8818	32.4028	25.9	Y
Martes_pennanti_13	123.2447	122.1728	245.4174	24.6601	25.9	Y
Martes_pennanti_14	210.9379	138.8638	349.8018	32.7013	25.9	Y
Martes_pennanti_14	155.142	282.5414	437.6834	28.2541	25.9	Y
Martes_pennanti_15	207.1732	141.0304	348.2036	33.1578	25.9	Y
Martes_pennanti_15	166.5059	295.925	462.4309	29.5925	25.9	Y
Martes_pennanti_16	218.5229	140.8525	359.3754	32.9778	25.9	Y
Martes_pennanti_16	153.905	289.583	443.488	28.9583	25.9	Y
Martes_pennanti_17	214.3038	134.3455	348.6493	32.1632	25.9	Y
Martes_pennanti_17	153.5018	278.8295	432.3314	27.883	25.9	Y
Martes_pennanti_18	211.2035	130.2702	341.4737	33.5014	25.9	Y
Martes_pennanti_19	209.6269	131.4041	341.031	32.9048	25.9	Y
Martes_pennanti_2	212.0499	138.9604	351.0104	32.8425	25.9	Y
Martes_pennanti_2	161.4707	280.4929	441.9636	28.0493	25.9	Y
Martes_pennanti_3	182.3532	130.5474	312.9006	30.0015	25.9	Y
Martes_pennanti_3	166.1778	284.0261	450.204	28.4026	25.9	Y
Martes_pennanti_4	211.1884	139.4996	350.688	32.84	25.9	Y
Martes_pennanti_4	185.9954	178.6108	364.6062	33.5125	25.9	Y
Martes_pennanti_5	213.5758	137.7837	351.3596	33.6466	25.9	Y
Martes_pennanti_5	156.2109	294.2022	450.4131	29.4202	25.9	Y
Martes_pennanti_6	206.6789	138.8242	345.5032	32.985	25.9	Y
Martes_pennanti_6	152.7312	302.7919	455.5231	30.2792	25.9	Y
Martes_pennanti_7	209.6919	147.5811	357.273	34.4798	25.9	Y

Individual	Imax	Imin	J	area	home range	climb
Martes_pennanti_7	163.5257	288.5261	452.0518	28.8526	25.9	Y
Martes_pennanti_8	204.771	133.9429	338.714	32.8096	25.9	Y
Martes_pennanti_8	159.2309	285.2254	444.4563	28.5225	25.9	Y
Martes_pennanti_9	209.0319	141.4825	350.5144	32.6079	25.9	Y
Martes_pennanti_9	154.7625	291.6702	446.4327	29.167	25.9	Y
Mephitis_mephitis_1	124.3691	54.415	178.7841	31.258	0.04	N
Mephitis_mephitis_1	75.0305	50.7651	125.7956	26.1676	0.04	N
Mephitis_mephitis_10	113.6906	54.6979	168.3885	23.0561	0.04	N
Mephitis_mephitis_10	86.5943	54.7756	141.3699	22.991	0.04	N
Mephitis_mephitis_11	123.1807	49.185	172.3657	23.3788	0.04	N
Mephitis_mephitis_11	86.2811	47.9541	134.2352	23.9039	0.04	N
Mephitis_mephitis_12	104.0994	54.4018	158.5012	24.1214	0.04	N
Mephitis_mephitis_12	85.1328	55.0303	140.1631	25.8916	0.04	N
Mephitis_mephitis_13	124.8195	54.8802	179.6997	22.606	0.04	N
Mephitis_mephitis_13	74.1391	45.853	119.9921	24.5183	0.04	N
Mephitis_mephitis_14	117.99	54.1744	172.1643	23.1242	0.04	N
Mephitis_mephitis_14	76.9333	55.8759	132.8092	22.0033	0.04	N
Mephitis_mephitis_15	107.9688	50.2339	158.2027	23.2164	0.04	N
Mephitis_mephitis_15	83.9829	55.1479	139.1308	19.0009	0.04	N
Mephitis_mephitis_16	110.3661	52.1178	162.4839	24.383	0.04	N
Mephitis_mephitis_16	76.9986	56.7754	133.774	20.9005	0.04	N
Mephitis_mephitis_17	119.2886	54.3499	173.6385	25.0031	0.04	N
Mephitis_mephitis_17	78.5474	51.0846	129.6321	23.7186	0.04	N
Mephitis_mephitis_18	119.3727	48.6021	167.9748	24.7366	0.04	N
Mephitis_mephitis_18	83.9894	56.4692	140.4586	20.0368	0.04	N
Mephitis_mephitis_19	111.7494	51.1161	162.8655	24.326	0.04	N
Mephitis_mephitis_19	81.1843	49.591	130.7754	23.6071	0.04	N

Individual	Imax	Imin	J	area	home range	climb
Mephitis_mephitis_2	76.2373	44.3811	120.6184	18.5829	0.04	N
Mephitis_mephitis_2	82.336	54.3959	136.7318	26.8114	0.04	N
Mephitis_mephitis_20	115.1851	50.0521	165.2372	23.8602	0.04	N
Mephitis_mephitis_20	95.0914	60.0698	155.1612	23.2634	0.04	N
Mephitis_mephitis_21	126.6946	55.9347	182.6294	23.6554	0.04	N
Mephitis_mephitis_21	85.5756	57.331	142.9065	25.866	0.04	N
Mephitis_mephitis_22	115.1299	57.9917	173.1216	22.4058	0.04	N
Mephitis_mephitis_22	75.458	45.4684	120.9264	23.4784	0.04	N
Mephitis_mephitis_23	118.2033	55.1054	173.3087	23.267	0.04	N
Mephitis_mephitis_23	83.1174	54.9173	138.0347	23.2569	0.04	N
Mephitis_mephitis_24	122.9628	50.9846	173.9474	23.5832	0.04	N
Mephitis_mephitis_24	74.2256	50.9222	125.1479	23.925	0.04	N
Mephitis_mephitis_3	153.518	60.3826	213.9006	20.9058	0.04	N
Mephitis_mephitis_3	80.5095	52.4781	132.9876	19.9609	0.04	N
Mephitis_mephitis_4	125.0471	55.6366	180.6837	23.7822	0.04	N
Mephitis_mephitis_4	76.3445	57.6095	133.954	23.3689	0.04	N
Mephitis_mephitis_5	116.8857	53.49	170.3757	23.422	0.04	N
Mephitis_mephitis_5	88.5512	66.1394	154.6906	30.3045	0.04	N
Mephitis_mephitis_6	108.8853	48.5204	157.4056	22.9206	0.04	N
Mephitis_mephitis_6	81.0658	52.652	133.7178	22.503	0.04	N
Mephitis_mephitis_7	126.6691	48.4427	175.1118	23.8752	0.04	N
Mephitis_mephitis_7	59.6924	35.2714	94.9637	14.9727	0.04	N
Mephitis_mephitis_8	120.7389	54.3126	175.0514	23.6874	0.04	N
Mephitis_mephitis_8	84.7116	51.514	136.2255	25.6068	0.04	N
Mephitis_mephitis_9	84.3596	50.2825	134.6421	21.4835	0.04	N
Mustela_erminea_1	0.8229	0.6206	1.4435	1.7083	0.04	Y
Mustela_erminea_10	0.8064	0.4905	1.297	1.8369	0.04	Y

Individual	Imax	Imin	J	area	home range	climb
Mustela_erminea_10	1.343	0.7255	2.0685	2.2516	0.04	Y
Mustela_erminea_11	0.7428	0.527	1.2698	1.9484	0.04	Y
Mustela_erminea_12	0.7696	0.4932	1.2628	1.6951	0.04	Y
Mustela_erminea_12	1.2416	1.0776	2.3192	1.5832	0.04	Y
Mustela_erminea_13	0.8004	0.4474	1.2478	1.7074	0.04	Y
Mustela_erminea_13	0.5687	0.9933	1.562	2.287	0.04	Y
Mustela_erminea_14	0.6336	0.5101	1.1438	1.9036	0.04	Y
Mustela_erminea_14	1.0263	0.3811	1.4074	1.9861	0.04	Y
Mustela_erminea_15	0.7139	0.4908	1.2047	1.8616	0.04	Y
Mustela_erminea_15	0.9768	0.4119	1.3888	1.7221	0.04	Y
Mustela_erminea_16	0.7107	0.4801	1.1908	2.2138	0.04	Y
Mustela_erminea_16	1.5323	0.9909	2.5232	2.4875	0.04	Y
Mustela_erminea_17	0.6936	0.5413	1.2349	1.7844	0.04	Y
Mustela_erminea_18	0.7391	0.5644	1.3035	2.2875	0.04	Y
Mustela_erminea_18	0.7123	0.3763	1.0887	2.3648	0.04	Y
Mustela_erminea_19	0.8318	0.4704	1.3022	2.1451	0.04	Y
Mustela_erminea_19	0.7161	0.7309	1.447	2.4909	0.04	Y
Mustela_erminea_2	1.2545	0.9204	2.1749	2.3421	0.04	Y
Mustela_erminea_20	0.7469	0.4951	1.242	1.4466	0.04	Y
Mustela_erminea_20	1.233	0.7202	1.9532	1.1902	0.04	Y
Mustela_erminea_21	0.7809	0.5073	1.2882	2.9746	0.04	Y
Mustela_erminea_22	0.7111	0.5178	1.2289	1.724	0.04	Y
Mustela_erminea_22	1.8177	0.5217	2.3393	2.4103	0.04	Y
Mustela_erminea_23	0.7494	0.3979	1.1473	1.8024	0.04	Y
Mustela_erminea_23	1.3634	0.912	2.2755	2.3019	0.04	Y
Mustela_erminea_24	0.7064	0.53	1.2364	1.8418	0.04	Y
Mustela_erminea_25	0.7809	0.4996	1.2806	2.0093	0.04	Y

Individual	Imax	Imin	J	area	home range	climb
Mustela_erminea_26	0.7353	0.5013	1.2366	1.6939	0.04	Y
Mustela_erminea_26	0.7818	0.2073	0.9891	2.1214	0.04	Y
Mustela_erminea_4	0.7315	0.5173	1.2488	1.6588	0.04	Y
Mustela_erminea_4	1.426	0.7888	2.2148	2.1633	0.04	Y
Mustela_erminea_5	0.8163	0.4879	1.3042	1.8673	0.04	Y
Mustela_erminea_5	1.8155	0.919	2.7345	1.381	0.04	Y
Mustela_erminea_6	0.7147	0.526	1.2407	1.8119	0.04	Y
Mustela_erminea_6	0.1988	1.2055	1.4043	0.8572	0.04	Y
Mustela_erminea_7	0.6225	0.5819	1.2044	1.6047	0.04	Y
Mustela_erminea_8	0.682	0.5117	1.1936	2.0794	0.04	Y
Mustela_erminea_8	1.1878	1.1913	2.3791	1.5727	0.04	Y
Mustela_erminea_9	1.1357	0.6554	1.7912	2.2491	0.04	Y
Mustela_erminea_9	1.8229	1.2856	3.1085	2.5014	0.04	Y
Procyon_lotor_1	1007.22	594.6848	1601.905	58.1934	1.1	Y
Procyon_lotor_10	239.8221	112.3994	352.2215	35.8498	1.1	Y
Procyon_lotor_13	134.163	64.5549	198.7179	30.6744	1.1	Y
Procyon_lotor_14	202.4472	107.3738	309.821	36.1082	1.1	Y
Procyon_lotor_14	63.7678	44.3871	108.1549	15.7993	1.1	Y
Procyon_lotor_15	162.1015	110.0419	272.1434	36.4121	1.1	Y
Procyon_lotor_15	431.0126	254.8063	685.8189	38.6761	1.1	Y
Procyon_lotor_16	222.0576	87.3087	309.3663	33.7583	1.1	Y
Procyon_lotor_16	409.3261	299.5955	708.9217	39.4038	1.1	Y
Procyon_lotor_17	260.0107	88.0064	348.0171	35.7171	1.1	Y
Procyon_lotor_17	411.6569	251.965	663.622	36.3682	1.1	Y
Procyon_lotor_18	220.4612	104.765	325.2261	33.5296	1.1	Y
Procyon_lotor_18	454.7141	258.8735	713.5875	38.4272	1.1	Y
Procyon_lotor_19	223.4655	111.3782	334.8437	35.1546	1.1	Y

Individual	Imax	Imin	J	area	home range	climb
Procyon_lotor_19	453.0008	271.3097	724.3104	37.8464	1.1	Y
Procyon_lotor_2	409.9237	269.3916	679.3152	35.0546	1.1	Y
Procyon_lotor_20	218.259	88.8952	307.1543	36.2018	1.1	Y
Procyon_lotor_20	414.7903	253.039	667.8293	36.1125	1.1	Y
Procyon_lotor_21	223.7852	119.618	343.4032	38.2288	1.1	Y
Procyon_lotor_21	445.5142	247.3485	692.8627	37.4994	1.1	Y
Procyon_lotor_22	286.1131	122.2087	408.3218	44.2234	1.1	Y
Procyon_lotor_23	419.8863	241.5707	661.4571	36.3223	1.1	Y
Procyon_lotor_3	434.2323	247.5321	681.7644	36.5758	1.1	Y
Procyon_lotor_4	388.4836	268.3298	656.8133	37.8919	1.1	Y
Procyon_lotor_5	393.8246	270.0608	663.8854	35.3906	1.1	Y
Procyon_lotor_6	471.7915	242.2377	714.0291	39.7391	1.1	Y
Procyon_lotor_7	213.9731	129.4863	343.4594	39.8451	1.1	Y
Procyon_lotor_8	243.3197	106.9717	350.2914	37.1258	1.1	Y
Procyon_lotor_9	224.0255	154.1696	378.1951	28.1542	1.1	Y
Vulpes_vulpes_1	242.0432	168.1669	410.2101	33.3551	4.12	Y
Vulpes_vulpes_10	275.067	211.5172	486.5842	34.0172	4.12	N
Vulpes_vulpes_10	246.0772	173.5965	419.6736	30.8618	4.12	N
Vulpes_vulpes_11	265.3369	199.6006	464.9375	30.075	4.12	N
Vulpes_vulpes_11	275.0249	206.0469	481.0718	30.8351	4.12	N
Vulpes_vulpes_12	246.1586	172.0824	418.241	31.7105	4.12	N
Vulpes_vulpes_13	326.6007	257.8109	584.4116	37.8662	4.12	N
Vulpes_vulpes_13	246.4127	162.889	409.3017	30.2462	4.12	N
Vulpes_vulpes_14	273.7892	222.9519	496.741	34.2517	4.12	N
Vulpes_vulpes_14	247.8458	173.2323	421.0781	31.2027	4.12	N
Vulpes_vulpes_15	278.6672	222.2197	500.8869	34.6785	4.12	N
Vulpes_vulpes_15	244.484	181.4514	425.9354	31.3252	4.12	N

Individual	Imax	Imin	J	area	home range	climb
Vulpes_vulpes_16	276.5753	215.947	492.5223	35.5969	4.12	N
Vulpes_vulpes_16	243.4605	177.4858	420.9463	31.1154	4.12	N
Vulpes_vulpes_17	249.551	171.9831	421.5341	31.2118	4.12	N
Vulpes_vulpes_18	243.2589	178.4755	421.7344	34.539	4.12	N
Vulpes_vulpes_2	268.2292	207.3773	475.6066	33.6956	4.12	N
Vulpes_vulpes_2	243.0712	171.749	414.8202	31.0124	4.12	N
Vulpes_vulpes_3	270.7265	211.5934	482.3199	33.9119	4.12	N
Vulpes_vulpes_3	243.1482	175.2254	418.3736	31.4082	4.12	N
Vulpes_vulpes_4	272.7371	202.9016	475.6387	33.322	4.12	N
Vulpes_vulpes_4	246.4619	168.8687	415.3306	31.1333	4.12	N
Vulpes_vulpes_5	280.3674	215.8582	496.2257	33.9661	4.12	N
Vulpes_vulpes_5	242.0952	173.219	415.3142	31.0702	4.12	N
Vulpes_vulpes_6	274.2152	203.6609	477.8761	33.9059	4.12	N
Vulpes_vulpes_6	242.1608	177.9817	420.1425	31.3241	4.12	N
Vulpes_vulpes_7	287.9279	207.8315	495.7594	35.2937	4.12	N
Vulpes_vulpes_7	235.0566	169.2377	404.2944	31.8451	4.12	N
Vulpes_vulpes_8	278.9045	211.0794	489.9839	34.6704	4.12	N
Vulpes_vulpes_8	242.7923	174.7437	417.536	30.2045	4.12	N
Vulpes_vulpes_9	248.2919	172.7371	421.029	31.5543	4.12	N